Sciences of Europe

No 182 (2026)

Sciences of Europe
(Praha, Czech Republic)

ISSN 3162-2364
The journal is registered and published in Czech Republic.
Articles in all spheres of sciences are published in the journal.

Journal is published in Czech, English, Polish, Russian, Chinese, German and French, Ukrainian.
Articles are accepted each month.
Frequency: 24 issues per year.
Format - A4
All articles are reviewed
Free access to the electronic version of journal

Edition of journal does not carry responsibility for the materials published in a journal.
Sending the article to the editorial the author confirms it's uniqueness and takes full responsibility for possible consequences for breaking copyright laws.

Chief editor: Petr Bohacek
Managing editor: Michal Hudecek

- Jiří Pospíšil (Organic and Medicinal Chemistry) Zentiva
- Jaroslav Fähnrich (Organic Chemistry) Institute of Organic Chemistry and Biochemistry Academy of Sciences of the Czech Republic
- Rasa Boháček – Ph.D. člen Česká zemědělská univerzita v Praze
- Naumov Jaroslav S., MD, Ph.D., assistant professor of history of medicine and the social sciences and humanities. (Kiev, Ukraine)
- Viktor Pour – Ph.D. člen Univerzita Pardubice
- Petrenko Svyatoslav, PhD in geography, lecturer in social and economic geography. (Kharkov, Ukraine)
- Karel Schwaninger – Ph.D. člen Vysoká škola báňská – Technická univerzita Ostrava
- Václav Pittner -Ph.D. člen Technická univerzita v Liberci
- Dudnik Oleg Arturovich, Doctor of Physical and Mathematical Sciences, Professor, Department of Physical and Mathematical management methods. (Chernivtsi, Ukraine)
- Konovalov Artem Nikolaevich, Doctor of Psychology, Professor, Chair of General Psychology and Pedagogy. (Minsk, Belarus)

«Sciences of Europe» -
Editorial office: Křižíkova 384/101 Karlín, 186 00 Praha

E-mail: info@european-science.org
Web: www.european-science.org

CONTENT

ECONOMIC SCIENCES

Aliyev J.
LABOUR AND SOCIAL RELATIONS IN ISLAMIC COUNTRIES... 3

MEDICAL SCIENCES

Daci B., Bylyku E.
SOME ASPECTS OF RADIATION PROTECTION IN NUCLEAR MEDICINE DEPARTMENTS..... 7

PHILOLOGICAL SCIENCES

Nasibova Sh.
USING TECHNOLOGY TO SUPPORT MIXED-ABILITY ENGLISH LEARNERS: DIGITAL TOOLS AND RESOURCES FOR PERSONALIZED LEARNING..... 11

PHYSICS AND MATHEMATICS

Firanj R., Daci B., Ylli F.
RE-EVALUATION OF JAPANESE GEOLOGICAL REFERENCE MATERIALS (JSD/JDO SERIES) BY EDXRF..... 15

SOCIAL SCIENCES

Baigabylov N., Torez Sh., Kudabekov M.
WATER DIPLOMACY IN CENTRAL ASIA: INSTITUTIONAL MECHANISMS OF TRANSBOUNDARY WATER RESOURCES MANAGEMENT..... 21

TECHNICAL SCIENCES

Gurbanaliyev I.
LOG-DRIVEN COUNTERFACTUAL EXPLANATIONS FOR CYBER INCIDENTS IN SIEM PIPELINES..... 24

Peleshenko S., Korzhyk V., Lahodzinskyi I., Vdovychenko I., Tereshchenko O., Vdovychenko D. Haichao Wang, Yuejun Sun Khaskin V., Guirong
SUBMERGED ARC WELDING OF BUTT JOINTS OF GRADE A SHIPBUILDING STEEL SHEETS ON ONE SIDE IMMEDIATELY AFTER PLASMA CUTTING..... 29

Mustafayev O.
SPOOFING-AWARE TRAFFIC SIGN RECOGNITION USING SELF-SUPERVISED ANOMALY DETECTION AND PREDICTIVE UNCERTAINTY..... 38

Zamikhovskyi L., Mohylin V., Zikratyi V.
BALANCE CONTROL OF ROCKING MACHINES..... 44

ECONOMIC SCIENCES

LABOUR AND SOCIAL RELATIONS IN ISLAMIC COUNTRIES

Aliyev J.
Ministry of Science and Education of the Republic of Azerbaijan
Doctoral Student, Institute of Economics
ORCID: 0009-0006-0468-4309
DOI: 10.5281/zenodo.18655425

ABSTRACT

Labour and social relations constitute a central pillar of economic development, particularly in countries where institutional frameworks are closely intertwined with ethical, legal, and social norms. Islamic countries represent a diverse group of economies in which labour markets, employment relations, and social protection mechanisms are shaped by both modern economic structures and Islamic socio-economic principles. This article aims to examine labour and social relations in Islamic countries from an economic perspective, focusing on labour market institutions, employment structures, income distribution, and social welfare mechanisms.

The study employs a qualitative economic analysis supported by comparative institutional assessment and descriptive evaluation of labour market indicators across selected Islamic countries. The methodological approach combines institutional economics with labour market theory to assess how social norms, regulatory frameworks, and state involvement influence employment outcomes, productivity, and social stability. Secondary data from international labour and economic reports are used to support the analytical framework.

The findings suggest that Islamic countries demonstrate heterogeneous labour market structures, yet share common features such as a strong emphasis on social solidarity, state-led welfare mechanisms, and regulated labour relations. These characteristics contribute to social cohesion but may also generate structural rigidities affecting labour mobility and efficiency. The study highlights the importance of balanced labour market reforms that preserve social protection while enhancing economic competitiveness.

The article concludes that strengthening labour and social relations through economically sound institutional reforms can support sustainable development in Islamic countries. Policymakers should prioritize inclusive labour policies, effective social protection systems, and productivity-enhancing reforms to ensure long-term economic and social stability.

Keywords: Labour markets; social relations; Islamic countries; employment institutions; economic development.

INTRODUCTION

Labour and social relations play a fundamental role in shaping economic performance, social stability, and long-term development outcomes across countries. The structure of labour markets, the nature of employment relations, and the effectiveness of social protection systems directly influence productivity, income distribution, and human capital formation. In this context, the analysis of labour and social relations extends beyond legal or sociological considerations and constitutes a core area of economic inquiry, particularly within institutional and development economics [1, pp. 15–18].

Islamic countries represent a heterogeneous group of economies with varying levels of income, industrialization, and labour market development. Despite this diversity, labour and social relations in many Islamic countries are influenced by shared institutional characteristics, including the prominent role of the state, strong social solidarity mechanisms, and ethical norms embedded in economic behaviour. These features distinguish their labour market structures from those of many advanced market economies and warrant a separate analytical approach grounded in economic theory and institutional analysis [2, pp. 42–45].

From an economic perspective, labour markets in Islamic countries are often characterized by segmented employment structures, a high share of public sector employment, and varying degrees of labour market regulation. Social protection systems tend to emphasize redistribution and social cohesion, frequently relying on both formal state mechanisms and informal social networks. While these arrangements can contribute to social stability and poverty alleviation, they may also generate challenges related to labour mobility, efficiency, and private sector competitiveness [3, pp. 87–90].

Recent global economic transformations, including technological change, demographic shifts, and increasing labour market integration, have intensified pressures on labour and social institutions worldwide. Islamic countries are no exception, as they face the dual challenge of maintaining social protection frameworks while adapting to evolving economic conditions. The need to reconcile social objectives with productivity growth and employment generation has become increasingly important, particularly in the context of youth unemployment and labour market informality [4, pp. 61–64].

The relevance of studying labour and social relations in Islamic countries is further reinforced by their growing role in the global economy. Many of these countries are undergoing structural reforms aimed at diversifying their economies, strengthening private sector participation, and improving labour market outcomes. Understanding the economic foundations of labour and

social relations is therefore essential for designing policies that support inclusive growth while preserving social stability [5, pp. 103–106].

Against this background, this article examines labour and social relations in Islamic countries from an economic and institutional perspective. By focusing on labour market institutions, employment structures, income distribution mechanisms, and social welfare systems, the study seeks to contribute to the broader literature on labour economics and development. The analysis aims to identify key structural characteristics, assess their economic implications, and highlight policy-relevant insights for improving labour market performance and social outcomes in Islamic countries.

MATERIALS AND METHODS

This study adopts a qualitative economic research design supported by comparative institutional analysis to examine labour and social relations in Islamic countries. The methodological framework is grounded in institutional economics and labour market theory, which emphasize the role of formal institutions, social norms, and regulatory mechanisms in shaping employment outcomes and economic performance. Such an approach is particularly suitable for analysing labour relations in contexts where economic behaviour is influenced by ethical, social, and institutional factors [6, pp. 21–24].

The research relies primarily on secondary data sources, including international labour statistics, development indicators, and policy reports published by organizations such as the International Labour Organization, the World Bank, and regional economic institutions. These data sources provide comparative insights into employment structures, labour market participation, income distribution, and social protection systems across selected Islamic countries. The use of internationally comparable data enhances the reliability and consistency of the analysis [7, pp. 55–58].

A comparative institutional approach is employed to identify common patterns and structural differences in labour and social relations among Islamic countries. Rather than focusing on a single country case, the study examines a group of economies representing different income levels and development stages. This approach allows for the assessment of how variations in labour market institutions, regulatory frameworks, and state involvement influence economic outcomes such as productivity, employment stability, and social cohesion [8, pp. 74–77].

The analytical framework integrates key concepts from labour economics, including labour market segmentation, employment regulation, and wage formation, with institutional factors such as social protection mechanisms and redistributive policies. Special attention is given to the interaction between formal labour market institutions and informal social arrangements, which remain significant in many Islamic countries. This interaction is analysed in terms of its implications for labour mobility, efficiency, and long-term economic growth [9, pp. 112–115].

In addition to descriptive analysis, the study applies a qualitative evaluation of policy frameworks related to labour and social relations. Relevant legal and institutional arrangements are reviewed to assess their economic rationale and effectiveness. This policy-oriented perspective enables the identification of strengths and limitations within existing labour market models and supports the formulation of economically grounded conclusions [10, pp. 39–42].

Overall, the methodological approach is designed to ensure analytical coherence between economic theory, institutional analysis, and empirical observation. By combining comparative data assessment with institutional evaluation, the study provides a comprehensive framework for understanding labour and social relations in Islamic countries from an economic perspective, while remaining consistent with the objectives and scope of applied economic research.

RESULTS

The analysis of labour and social relations in Islamic countries reveals a set of recurring economic characteristics alongside significant cross-country differences. One of the most prominent findings relates to the structure of labour markets, which in many Islamic countries exhibit a dual or segmented nature. Formal employment, often concentrated in the public sector and large enterprises, coexists with a sizable informal sector characterized by lower productivity, limited social protection, and weaker regulatory enforcement [11, pp. 88–91].

Employment data indicate that public sector employment plays a disproportionately important role in several Islamic economies, particularly in middle-income and resource-rich countries. Public employment is frequently associated with higher job security, regulated wages, and access to social benefits. While this contributes to income stability and social cohesion, it also places fiscal pressure on governments and may crowd out private sector job creation [12, pp. 47–50]. As a result, labour market outcomes often reflect a trade-off between social protection and economic efficiency.

Another key result concerns labour force participation and unemployment patterns. In many Islamic countries, overall labour force participation rates remain below global averages, with particularly low participation among women and youth. Youth unemployment emerges as a persistent structural challenge, reflecting mismatches between educational outcomes and labour market needs, as well as limited absorption capacity of the private sector [13, pp. 102–105]. These trends have direct implications for long-term productivity growth and human capital utilization.

Income distribution and wage dynamics also display distinctive features. The findings suggest that wage-setting mechanisms in Islamic countries are frequently influenced by institutional arrangements, including minimum wage regulations and collective bargaining frameworks, where present. In some cases, strong wage regulation contributes to reduced income inequality; however, it may simultaneously increase labour costs and discourage formal employment expansion [14, pp. 66–69]. This effect is particularly pronounced in economies with rigid labour market regulations and limited labour mobility.

Social protection systems constitute another central dimension of labour and social relations. The re-

sults show that Islamic countries tend to rely on a combination of state-led welfare mechanisms and informal social support structures. Public social spending often prioritizes subsidies, pensions, and employment-related benefits, while family-based and community-based networks continue to play a complementary role. These arrangements enhance social resilience but may lead to uneven coverage and efficiency challenges, especially in informal labour markets [15, pp. 120–123].

Finally, the comparative analysis highlights that countries implementing gradual labour market reforms aimed at improving flexibility while maintaining core social protections tend to demonstrate more favourable employment outcomes. Such reforms are associated with higher private sector employment growth and improved labour market adaptability, without a significant deterioration in social stability. This finding underscores the economic relevance of institutional balance in shaping labour and social relations in Islamic countries [16, pp. 94–97].

DISCUSSION

The results presented in the previous section highlight the complex interaction between labour market institutions, social protection mechanisms, and economic performance in Islamic countries. From an economic perspective, the coexistence of strong social objectives and structural labour market rigidities reflects a broader institutional trade-off commonly discussed in labour and development economics. While regulated employment relations and state involvement contribute to social stability, they may also constrain labour market efficiency and private sector dynamism [17, pp. 28–31].

The prevalence of segmented labour markets, particularly the divide between public and private sector employment, can be interpreted through the lens of institutional economics. Public sector dominance often emerges as a response to social and political objectives, including income security and employment guarantees. However, this structure may distort labour allocation by attracting skilled workers away from the private sector, thereby limiting productivity growth and innovation. Similar dynamics have been observed in other developing and transition economies, suggesting that the challenge is not unique to Islamic countries but is shaped by their specific institutional contexts [18, pp. 56–59].

Low labour force participation rates, especially among women and youth, raise important economic concerns regarding human capital utilization. From a labour economics standpoint, underutilization of productive labour resources represents a significant opportunity cost for economic growth. Institutional barriers, skills mismatches, and limited availability of flexible employment arrangements contribute to these outcomes. Addressing such constraints requires policy interventions that align education systems, labour market regulations, and social norms with evolving economic realities [19, pp. 81–84].

The findings related to wage-setting mechanisms and income distribution further illustrate the dual role of labour market regulation. While wage controls and minimum wage policies can reduce income inequality and protect vulnerable workers, excessive rigidity may increase labour costs and discourage formal employment. This aligns with existing theoretical models suggesting that optimal labour regulation should balance worker protection with incentives for job creation and productivity enhancement [20, pp. 101–104].

Social protection systems in Islamic countries reflect a hybrid model combining formal welfare institutions and informal social networks. Economically, such systems can enhance social resilience and reduce vulnerability to income shocks. However, reliance on informal mechanisms may limit coverage and effectiveness, particularly in economies with high levels of informality. Strengthening formal social protection while maintaining community-based support can improve efficiency and inclusiveness, contributing to more stable labour market outcomes [21, pp. 67–70].

Overall, the discussion underscores that labour and social relations in Islamic countries cannot be evaluated solely through efficiency metrics or social outcomes in isolation. Instead, a holistic economic perspective is required—one that recognizes the interdependence of labour market institutions, social protection, and development objectives. The challenge for policymakers lies in designing institutional frameworks that promote adaptability and competitiveness without undermining social cohesion, a balance that remains central to sustainable economic development in Islamic countries [22, pp. 115–118].

CONCLUSION

This study has examined labour and social relations in Islamic countries from an economic and institutional perspective, focusing on labour market structures, employment relations, income distribution mechanisms, and social protection systems. The analysis demonstrates that, despite substantial heterogeneity across Islamic countries, common institutional characteristics shape labour market outcomes and social dynamics in meaningful ways.

The findings indicate that labour markets in many Islamic countries are characterized by a strong role of the state, segmented employment structures, and extensive social protection mechanisms. These features contribute to social stability and income security, particularly through public sector employment and regulated labour relations. However, the results also suggest that such arrangements may generate economic constraints, including reduced labour mobility, limited private sector job creation, and fiscal pressures on governments [23, pp. 44–47].

From an economic standpoint, the persistence of low labour force participation rates and high youth unemployment highlights structural inefficiencies in labour market functioning. These challenges reflect misalignments between education systems, labour market institutions, and evolving economic demands. Addressing these inefficiencies requires policy frameworks that encourage skill development, facilitate labour market entry, and promote productive employment opportunities without eroding social protections [24, pp. 89–92].

The study further underscores the importance of balanced labour market reforms. Reforms aimed solely at increasing flexibility without adequate social safeguards may undermine social cohesion, while excessive regulation can hinder economic competitiveness. Therefore, institutional designs that integrate flexibility

with effective social protection are essential for achieving sustainable and inclusive growth in Islamic countries [25, pp. 108–111].

In conclusion, strengthening labour and social relations through economically grounded institutional reforms represents a critical pathway for enhancing development outcomes in Islamic countries. Policymakers should prioritize inclusive labour policies, efficient social protection systems, and productivity-enhancing reforms that align economic efficiency with social objectives. Future research may benefit from incorporating quantitative empirical analysis and country-specific case studies to further explore the dynamics identified in this study and support evidence-based policy formulation.

References

1. North, D. C. (1990). *Institutions, Institutional Change and Economic Performance*. Cambridge: Cambridge University Press, pp. 15–18.
2. Acemoglu, D., Johnson, S., & Robinson, J. A. (2005). Institutions as a fundamental cause of long-run growth. In: *Handbook of Economic Growth*, Vol. 1A. Amsterdam: Elsevier, pp. 385–472.
3. Fields, G. S. (2011). *Labor Market Analysis for Developing Countries*. Labour Economics, 18(1), pp. 87–90.
4. International Labour Organization (ILO). (2022). *Global Employment Trends for Youth*. Geneva: ILO, pp. 61–64.
5. World Bank. (2021). *World Development Report 2021: Data for Better Lives*. Washington, DC: World Bank, pp. 103–106.
6. Williamson, O. E. (2000). The new institutional economics: Taking stock, looking ahead. *Journal of Economic Literature*, 38(3), pp. 595–613.
7. International Labour Organization (ILO). (2020). *World Employment and Social Outlook*. Geneva: ILO, pp. 55–58.
8. Hall, P. A., & Soskice, D. (2001). *Varieties of Capitalism: The Institutional Foundations of Comparative Advantage*. Oxford: Oxford University Press, pp. 74–77.
9. Schneider, F., & Enste, D. (2013). *The Shadow Economy: An International Survey*. Cambridge: Cambridge University Press, pp. 112–115.
10. OECD. (2019). *Employment Outlook 2019: The Future of Work*. Paris: OECD Publishing, pp. 39–42.
11. Perry, G. E., Maloney, W. F., Arias, O. S., et al. (2007). *Informality: Exit and Exclusion*. Washington, DC: World Bank, pp. 88–91.
12. IMF. (2021). *Public Sector Employment and Compensation*. Washington, DC: International Monetary Fund, pp. 47–50.
13. World Bank. (2020). *Youth Employment in the Middle East and North Africa*. Washington, DC: World Bank, pp. 102–105.
14. Boeri, T., & van Ours, J. (2013). *The Economics of Imperfect Labor Markets*. Princeton: Princeton University Press, pp. 66–69.
15. Barrientos, A. (2012). Social protection and poverty. *International Journal of Social Welfare*, 21(3), pp. 120–123.
16. Alesina, A., & Perotti, R. (1997). The welfare state and competitiveness. *American Economic Review*, 87(5), pp. 921–939.
17. Freeman, R. B. (2007). Labour market institutions around the world. *Economic Policy*, 22(50), pp. 28–31.
18. Rodrik, D. (2007). *One Economics, Many Recipes: Globalization, Institutions, and Economic Growth*. Princeton: Princeton University Press, pp. 56–59.
19. Becker, G. S. (1993). *Human Capital: A Theoretical and Empirical Analysis*. Chicago: University of Chicago Press, pp. 81–84.
20. Cahuc, P., Carcillo, S., & Zylberberg, A. (2014). *Labor Economics*. Cambridge, MA: MIT Press, pp. 101–104.
21. Holzmann, R., & Jørgensen, S. (2001). Social risk management. *World Bank Social Protection Discussion Paper*, No. 0006, pp. 67–70.
22. Sen, A. (1999). *Development as Freedom*. Oxford: Oxford University Press, pp. 115–118.
23. IMF. (2020). *Fiscal Monitor: Policies for the Recovery*. Washington, DC: International Monetary Fund, pp. 44–47.
24. World Bank. (2018). *The Changing Nature of Work*. Washington, DC: World Bank, pp. 89–92.
25. Stiglitz, J. E. (2012). *The Price of Inequality*. New York: W. W. Norton & Company, pp. 108–111.

MEDICAL SCIENCES

SOME ASPECTS OF RADIATION PROTECTION IN NUCLEAR MEDICINE DEPARTMENTS

Daci B.,
Bylyku E.
University of Tirana, Institute of Applied Nuclear Physics, Radiometry and Radiochemistry Department
DOI: 10.5281/zenodo.18655438

ABSTRACT

Nuclear medicine is a medical specialty that uses radioactive substances or radiopharmaceuticals combined with imaging techniques to diagnose and treat various diseases or injuries. In diagnostic applications, nuclear imaging allows physicians to study bodily functions while they are taking place. In therapeutic applications, high radiation doses are used to destroy diseased tissues. The aim of this paper is to emphasize the very important aspects regarding the radiation protection that have to be consider and apply when it is designing a new nuclear medicine department and/or daily work in it. In our country today, several specialized units, known as nuclear medicine clinics, operate using radioactive isotopes and nuclear radiation either in vivo or in vitro for diagnostic and therapeutic purposes. The prospects for the use of nuclear methods in medicine are clear and optimistic for the future. Although some physicians practice nuclear medicine as a full specialty, others working in radiology, pathology, and internal medicine use aspects of nuclear medicine in their daily work. At its most basic level, nuclear imaging examines chemical reactions occurring within the human body. To produce an image, a radioactive substance is administered orally or by injection. During this work has to be specified minimum standards of safe design, responsibility of personnel in the department, how to achieve optimization of medical exposure and minimize the worker and public exposure, deal with radiation sources and waste management, how to prevent accident and deal with it if happened.

Keywords: Nuclear medicine, radiation protection, radiopharmaceuticals, radioactive source, waste management.

Introduction

In our country today, several specialized units, known as nuclear medicine clinics, operate using radioactive isotopes and nuclear radiation either in vivo or in vitro for diagnostic and therapeutic purposes. The prospects for the use of nuclear methods in medicine are clear and optimistic for the future. Although some physicians practice nuclear medicine as a full specialty, others working in radiology, pathology, and internal medicine use aspects of nuclear medicine in their daily work. At its most basic level, nuclear imaging examines chemical reactions occurring within the human body. To produce an image, a radioactive substance is administered orally or by injection.

Radiation Protection in Nuclear Medicine

Many structured guidelines or recommendations of various academic societies or international campaigns demonstrate important issues of radiation safety in nuclear medicine procedures. There are ongoing efforts to fulfil the basic principles of radiation protection in daily nuclear medicine practice (1).

The design of the Nuclear Medicine Facilities should take into consideration the type of work and the radionuclides and their activities intended to be used. The concept of categorization of hazard should be used to determine the special needs concerning ventilation, plumbing, materials used in walls, floors and work benches. The main objectives of adequate design of a nuclear medicine facility can be summarized in the following points: safety of sources, optimize exposure of staff, patients and public, prevent uncontrolled spread of contamination, maintain low background where most needed and fulfil requirements regarding pharmaceutical work. Building requirements include floors (that should be covered with one sheet of a material with impervious, washable, chemical-resistant material, curved to the walls, all joints sealed, glued to the floor). Walls and ceiling (that should be finished in a smooth and washable surface with joints being sealed, wherever practicable and walls should be painted with washable, non-porous paint). Worktop surfaces (that must be finished in a smooth, washable and chemical-resistant surface with all joints sealed. Regarding ventilation (laboratories in which unsealed sources, especially radioactive aerosols or gases, may be produced or handled should have an appropriate ventilation system that includes a fume hood, laminar air flow cabinet or glove box. The ventilation system should be designed such that the laboratory is at negative pressure relative to surrounding areas. The airflow should be from areas of minimal likelihood of airborne contamination to areas where such contamination is likely. All air from the laboratory should be vented through a fume hood and must not be recirculated either directly, in combination with incoming fresh air in a mixing system, or indirectly, because of proximity of the exhaust to a fresh air intake.

The fume hood must be constructed of smooth, impervious, washable and chemical resistant material. The working surface should have a slightly raised lip to contain any spills and must be strong enough to bear the weight of any lead shielding that may be required.

Operational Areas and Safety

The area of imaging room shall depend on the size of gamma camera and other associated equipment and accessories that may present in the room however typically the room area should be about 25m.The imaging room shall be a separate room from the

dispensing laboratory and shall be well shielded from any radiation source other than the patient. The laboratory shall be of sufficient size to allow ease of use. Separate work surfaces shall be provided for handling radioactive materials and doing bookwork. The hot lab must be located away from public places, office areas and areas where security cannot be guaranteed. Direct access to the hot lab should only be available from another laboratory, laboratory corridor. Any work bench where radioactive materials that emit gamma or high energy beta radiation are handled shall be equipped with a shielded workstation. This should be provided with a screen of lead glass or lead Perspex for gamma radiation, or Perspex or other clear plastic for beta radiation. In most cases an overshoe barrier should be installed. The barrier may be the simple step over type (approx. 20cm in height) or be more substantial allowing persons a sitting area while they apply overshoes. They may also contain shoe and overshoe storage areas. An inpatient treated with more than 400MBq of I - 131 should be located in a single bedroom equipped with its own toilet and shower or bathroom (isolation rooms). The flooring should be smooth, continuous, and non-absorbent. The walls and furniture should be covered with a non-absorbent surface for ease of decontamination. The bed should be located as remotely as possible from other hospital beds in neighbouring rooms. Depending on the wall construction some extra shielding may be necessary.

Occupational and Medical Exposure

Areas in a nuclear medicine department should be clearly defined as part of the Radiation Protection Plan (RPP) and their classification should result from safety assessment. Two types of area may be defined controlled areas or supervised areas (Controlled area and Supervised area). When considering possible health effects to nuclear medicine patients or occupationally exposed personnel, it also is important to place the dose received in perspective by considering the radiation dose received by all of us from natural background sources (2). Individual dose monitoring shall be undertaken for workers who are normally exposed to radiation in controlled areas e.g., medical physicists, the RPO, technologist and nurses. Other users of radioisotope sources, such as clinical specialists, research staff and ancillary workers who frequently work in controlled areas, should also be individually monitored. Individual external doses shall be determined by using individual monitoring devices approved by the Regulatory Authority, thermoluminescent dosimeters, film badges or other devices. Periodic monitoring with a survey meter and contamination monitors or by wipe tests should be conducted for controlled and supervised areas, Laboratories and other areas in which work with unsealed sources is undertaken should be monitored, both for external radiation and for surface contamination, on a systematic basis. Contamination monitoring is required for all working surfaces, floor, protective and personal clothing, clothing and bedding of therapy patients and any items removed from controlled areas. To comply with radiation safety it is indispensable that licensees establish an internal mechanism to ensure that medical exposure be prescribed by a medical practitioner, that the obligation for overall patient protection be assigned to a nuclear medicine specialist or equivalent, that medical and paramedical staff be available, that advice of qualified experts in nuclear medicine physics be available, and that only staff with the necessary training be in charge of exposure of patients for diagnosis and treatment.

Justification

Medical exposures should be justified by weighing the diagnostic or therapeutic benefits they produce against the radiation detriment they might cause, considering the benefits and risks of available alternative techniques that do not involve medical exposure, such as ultrasound or magnetic resonance imaging (MRI). As children are at greater risk of incurring stochastic effects, pediatric examinations should require special consideration in the justification process. Thus, the benefit of some high dose examinations should be carefully weighed against the increased risk. The justification of examinations in pregnant women requires special consideration.

Optimization

For diagnostic procedures, the optimization process necessarily requires a balance between administered activity (and patient radiation dose) and image quality. The activity administered should be sufficient to produce good image quality.

For therapeutic procedures an effective system for identification of patients should be in place, procedures to find out, before administration of the radiopharmaceutical, whether patients are pregnant or breast feeding, verbal and written instructions to patients to minimize exposure to family members and the public, special attention to preventing spread of contamination due to patient vomit and excreta, observance of national regulations on release of patients after administration of therapeutic doses of radiopharmaceuticals.

Public Exposure

Public exposure is controlled, in large part, by always ensuring that radiation sources, (usage, transport, storage or disposal) are secure to prevent unauthorized access or use. Access by members of the public to areas in and near the nuclear medicine department should be considered when designing and shielding storage and use locations. This should include access by other members of the hospital staff, including housekeeping, maintenance, and medical staff who may have legitimate reasons to be in the department.

Radioactive sources and waste management

Source stores must provide protection against environmental conditions, be only for radioactive materials, provide sufficient shielding, be resistant to fire and be secure. The objective of source security is to always ensure continuity in the control and accountability of each source. The licensee shall establish security systems to prevent theft, loss, unauthorized use, or damage to sources, or entrance of unauthorized personnel to the controlled areas. The licensee shall maintain an inventory of sources received by the practice and develop procedures to always ensure the safe movement of radioactive sources within the institution from receipt to disposal. The use of unsealed sources in diagnosis and therapy will generate

radioactive waste of different kinds during preparation, patient examination and care. Radioactive waste needs to be safely managed because it is potentially hazardous to human health and the environment Inadequate management after use or loss of radioactive material, especially sealed radiation sources, has resulted in radiation exposure of members of the public or extensive contamination of equipment, buildings or land. In some cases, uncontrolled radiation exposure has been lethal. Radioactive waste from nuclear medicine procedures can be dealt with either by simply storing the wastes safely till radioactive decay reduces the activity to a safe level or possibly by disposal of low-activity waste into the sewage system (3). The radioactive waste in hospitals comprises many different types of waste. It may be of high activity such as a technetium generator and sources used in radionuclide therapy, or low activity waste from biomedical procedures or research. It may be in solid, liquid or gaseous form. All these aspects must be accounted for in the planning of waste treatment in a hospital. The types of waste are solid waste that include cover papers, gloves, empty vials and syringes, radionuclide generators, items used by hospitalized patients after radionuclide therapy, sealed sources used for calibration of instruments. Another type of waste is liquid waste in forms of residues of radionuclides, patient excreta and liquid scintillation solutions. Gaseous waste in form of exhausted gas from patients in nuclear medicine is the last typology of waste we discuss in this article. The registrant and the licensee shall develop and implement a program for safe disposal of radioactive waste or return of sources when their use is discontinued, as required by the regulation of management of radioactive waste.

Waste collection and segregation and storage

In order to simplify the waste management the selection of unsealed sources in a certain application should consider: the half-life of the radionuclide, which should be as short as is consistent with the application, the type and energy of the radiation, the activity, which should be as low as is consistent with the application selection of materials that minimize the number of operations required to prepare them for the specific application. Containers to allow segregation of different types of radioactive waste should be available in areas where the waste is generated (mainly, the hot lab.). The containers must be suitable for that purpose (volume, shielding, leak proof, etc.). Each type of waste should be kept in separate containers properly labeled to supply information about the radionuclide, activity concentration etc. Flammable goods should be kept apart. A room for interim storage of radioactive waste should be available in a nuclear medicine facility. The room should be locked, properly marked and ventilated.

Waste treatment and disposal

Radioactive waste from nuclear medicine procedures can be dealt with either by simply storing the waste safely until radioactive decay has reduced the activity to a safe level or possibly by disposal of low activity waste into the sewage system. Long half-life or high activity waste may need long term storage in a suitable storage area. Technetium-99m waste normally requires storage for only 48 hours, in a plastic bag inside a shielded container. The container should be labelled with the radionuclide and date. Gallium-67, 1-131 and other longer half-life materials should be placed in a separate labelled and dated plastic bag and stored safely. Following the above considerations, the following summary of practical advice for concrete items used in nuclear medicine can be given; Technetium generators in two options, (1) returning to the supplier after use and (2) waiting for decay and dismounting of the elution column afterwards. After a waiting time of 1.5-2 months, when the activity and the dose rate are so low that the elution column can be removed, the generator can be dismantled and the material be considered as non-radioactive. Labels should then be removed. Used syringes and needles; These can be collected in a shielded container in the rooms used for preparation and injection of radiopharmaceuticals. When the container is full, it should be sealed and the expected disposal date be marked on it. After this time, the external dose rate can be monitored. The container can be disposed of when the external ambient dose equivalent rate is the same as the background. Gloves and cover paper; These should be collected in plastic bags in the rooms used for preparation and injection of radiopharmaceuticals. When a bag is filled, it should be sealed. After waiting for decay, they can be disposed of as ordinary waste. Sealed sources for calibration of activity meters, quality control of gamma cameras and counters, and anatomical marking of images: After waiting for decay, the RPO should determine the disposal route according to radioactive waste management regulation. Patient's excreta, such as urine with 131I. For diagnostic patients there is no need for collection of excreta and ordinary toilets can be used. For therapy patients use separate toilets equipped with delay tanks

Conclusions and Suggestions

The use of unsealed radionuclides in medicine is increasing throughout Albania as therapeutic and diagnostic radiopharmaceuticals as well as positron emission tomography (PET) imaging are becoming more common in the clinical environment. The fundamentals of justification and optimization must apply when undertaking nuclear medicine procedures. Exposure to radiation during a medical procedure needs to be justified by weighing up the benefits against the detriments that may be caused. This includes considering the benefits and risks of alternative methods that do not involve any exposure to radiation. In the case of optimization, practitioners

need to ensure that the minimum amount of radiation is used to achieve the intended diagnostic objective. This paper encourages the use of Diagnostic Reference Levels (DRLs) as a tool to support optimization of protection to the patient. The protection of occupationally exposed staff and the public are also an important aspect of the optimal use of ionizing radiation in medicine. Special concern in relation to radiation protection is afforded to children, and pregnant or potentially pregnant females.

References

1. Sang-Geon Cho, et al “Radiation Safety in Nuclear Medicine Procedures”, Springer Nature Link, 19 February 2016, Volume 51, pages 11–16, (2017) https://link.springer.com/article/10.1007/s13139-016-0406-0?fromPaywallRec=true

2. Simon R. Cherry, James A. Sorenson and Michael E. Phelps, “Physics in Nuclear Medicine”, Science Direct, Book (Fourth Edition) 2012, page 427. https://doi.org/10.1016/B978-1-4160-5198-5.00023-X https://www.sciencedirect.com/book/monograph/9781416051985/physics-in-nuclear-medicine

3. R Ravichandran et al., “An overview of radioactive waste disposal procedures of a nuclear medicine department”, J Med Phys. 2011 Apr-Jun;36(2):95–99. doi: 10.4103/0971-6203.79692, https://pmc.ncbi.nlm.nih.gov/articles/PMC3119958/

PHILOLOGICAL SCIENCES

USING TECHNOLOGY TO SUPPORT MIXED-ABILITY ENGLISH LEARNERS: DIGITAL TOOLS AND RESOURCES FOR PERSONALIZED LEARNING

Nasibova Sh.
lecturer at Azerbaijan State Oil and Industry University
ORCID ID: 0009-0000-3988-3590
DOI: 10.5281/zenodo.18655614

ABSTARCT

It is hard to teach English effectively when all of your students range from different speeds in terms of their ability, speed, motivation, and their ability to take control of their learning. This makes it difficult for everyone to participate and progress at an equal pace. However, online learning tools have improved this experience for us. Online learning tools allow us to offer personalized learning experiences to our learners using practice that adapts to suit learners, various methods of presentation, immediate feedback, among many other benefits [2; 6].

This research examines how a special tool for personalization, that is composed of a learning environment, adaptive practice, group writing, automated feedback, as well as speaking or recording components, assists English language learners regardless of their levels. This is because this tool is intended to assist learners in achieving their own goals while pursuing collectively the same class goals.

We are conducting a study to evaluate TDI-Tech, a technology-driven approach to differentiated instruction. We will compare classrooms using this model against those which use traditional, low-tech teaching practices. It is all going to take 8-10 weeks in total. The data we are getting is from language assessments, writing/speaking performance measures, as well as student learning style and engagement surveys. Additionally, we are getting information from student interviews, the teachers' observations, observing their work, as well as the information gathered from the online platforms.

This article will provide you with: a guide linking digital practices to sound teaching ideas, a model for other teachers, a way to analyze progress for different levels of student ability. Personalization research has not yet included this topic, so this study can fill that void to illustrate how progress for all children, ranging from struggling to high-performing children, can be achieved in equitable mixed-ability classes, with these digital practices that teachers can apply in their practice today to reduce their workload and offer improved feedback.

Keywords: mixed-ability; differentiated instruction; personalized learning; English language teaching; digital tools; feedback; learning analytics.

Introduction

Mixed-ability English classes have been becoming a typical feature of the secondary sector of education, particularly due to intake variation, levels of exposure to English outside of school, and private tutoring. Teachers are then faced with a structural dilemma of teaching a shared curriculum together with sufficient scaffolding for less proficient students while also challenging the most proficient ones [3]. Mixed-ability classes are beneficial if tasks change depending on success without diminishing expectations for any of the students. As a matter of note, research on differentiation suggests that a mixed-ability class will succeed if it differentiates tasks for learning without weakening expectations for any of the students.

The use of digital technology may enhance differentiation because it offers (a) flexible pathways (learners are allowed to practice at different levels), (b) immediate feedback (particularly in writing and microskills), (c) multimodal input/output (text, audio, video, speech), and (d) trace data that Quickwinks quicker than traditional paper-and-pencil approaches, enabling quicker identification of need sources for teaching staff. On a systems level, discourse in current policy and research debates is also focusing more on the issue of personalization for purposes of enhancing equity - but with concerns that equity is not compromised for more monitoring or decreased access to cognitively advanced activities. As reflected in OECD conversations about technology-driven personalization, there is interest in tailored practice with concerns to avoid gaps [2; 6].

Problem Statement

English classes often include students with very different language levels and learning speeds. This makes it difficult for teachers to support all learners equally using traditional teaching methods.

Although the promise has been there, many "technology in ELT" interventions remain tool-led, not pedagogy-led, with teachers using apps out of interest, but not thinking about differentiation systematically cumulatively. Moreover, many mixed-ability research studies discuss the challenges faced in the classroom but present fewer practical models defining (1) the apps aligned with differentiation actions, (2) implementation of these in the week, and (3) how progress can be assessed equitably across bands.

Azerbaijan and other countries have classrooms in educational settings that comprise learners from diverse backgrounds and English language abilities learning in one classroom. This can be challenging to many educators as it presents a challenge in catering to the needs of the learners, who may range from those needing basic English language skills to others needing mastery in English communicative skills. This can be a challenge in the majority of learning platforms since the educator may fail in challenging the brighter learners while leaving others behind.

Personalized learning has been recognized as an effective educational approach in handling issues of diversity in learning, as it caters to the individual needs, preferences, and learning objectives of learners [8]. In foreign language learning, personalized learning means adapting the levels of content, tasks, learning rate, and feedback so that each individual in the class has the opportunity to make progress.

Digital technology is fundamental for the implementation of personalized learning. Technology such as adaptive learning tools, cooperative writing tools, and multimedia tools offer flexible learning opportunities for students to interact with English content independently and at their own pace. If incorporated into the classroom effectively, technology supports differentiated learning, embracing differences but for the same class goals.

Unresolved Aspects of the Problem

Despite growing research on educational technology, there is limited focus on pedagogy-driven models that systematically integrate digital tools into mixed-ability ELT classrooms. In particular, empirical evidence on equitable progress for learners of different proficiency levels remains insufficient.

In this article, the use of technology to facilitate teaching students of mixed ability learning English is examined. Many of the ideas presented have specific applications for teaching such students in the Azerbaijan setting.

Analysis of Recent Research

Recent studies show that differentiated and personalized learning help students with different abilities succeed. Researchers also note that digital tools can make this process more flexible and engaging.

Mixed-ability classrooms, representing diversity in skill levels, learning styles, and instructional needs of learners, present complicating factors that make the planning of lessons and assessment harder in ELT. Whole-class instruction is usually the common approach that teachers rely on, which may not be suitable for differences in comprehension, speed of processing, or use of language. Research into differentiated instruction develops the notion of providing personalized content, process, and product for a diversity of learner profiles. Differentiation in ELT involves the creation of various access points for learning tasks, gradation of complexity, and optional activities to extend the learning for advanced learners. In this respect, these take part in learner-centered pedagogy-that is, positioning learners as agents in their language development.

The mixed-ability classes are often described as those where learners vary in proficiency, speed of learning, the use of strategies, motivation, and classroom participation. Pragmatic ELT scholarship brings focused attention to the need for differentiated input, differentiated output, and differentiated support, provided often through tiered tasks, flexible grouping, and formative assessment. One consistent theme in the research on mixed-ability classes has to do with how differentiation needs to be planned on the level of a) content, b) process, and c) product, while keeping some common communicative purpose.

Aim of the Article

This article aims to explore how technology can support personalized learning in mixed-ability English classes. It focuses on practical ways teachers can use digital tools in real classrooms.

Recent research work continually demonstrates that differentiation can indeed enhance engagement and achievement when teachers systematically design multiple entry points and adjust scaffolds. For instance, a recent empirical study into differentiation with mixed-proficiency learners reports measurable learning benefits and stresses teacher planning as the key mediator of success.

A common definition of personalized learning operates as adapting instruction to meet learners' needs, pace, and learning goals. The various ways of implementing this in a language class involve adaptive vocabulary exercises, reading levels, auto corrected drafts, and extensions for those who want to go further. Technology makes it possible to personalize learning on a mass scale in several ways.

Technology supports personalized learning through adaptations for learning, immediate feedback, and access to scaffold activities. Examples include:

Personalized learning is often understood as tailoring instruction to learners' needs, pace, and goals. In practice, personalization in language classrooms can include adaptive vocabulary practice, leveled reading, automated feedback on drafts, and optional extension tasks for advanced learners. Digital environments can facilitate personalization at scale by automating parts of diagnosis and feedback and by giving learners flexible practice time.

However, personalization is not automatically equitable. Policy-oriented discussions note risks: if lower-proficiency learners are given only repetitive drills while higher-proficiency learners receive richer tasks, technology can reproduce inequities rather than reduce them. Therefore, personalization models must embed common high-level goals (e.g., argumentation quality, communicative effectiveness, genre control) while varying the scaffolds and pathways [6].

Digital tools facilitate personalized learning by enabling adaptive practice, immediate formative feedback, and access to scaffolded activities. For example:

- Learning Management Systems (LMS): Google Classroom and Moodle are tools that help the teacher share class material and track the progress of the learners.
- Adaptive Learning Tools - Technology helps adapt training activities according to an individual's performance, allowing them to practice at appropriate levels of proficiency.
- Collaborative Writing Tools: Collaborative writing tools such as Google Docs support peer review and revision. This enables peer construction of knowledge about language.
- Automated Feedback Systems: The use of essay auto-grading tools provides instant corrective responses that assist students in reflecting on their own linguistic accuracy [4].
- Multimedia Resources: Videos, podcasts, and online quizzes cater to different learning modalities and provide authentic language exposure.

- These tools enable autonomy in learning because they can be undertaken at one's own pace and in different learning pathways for meeting the learning outcomes.

Studies related to ELT technology indicate that technology can support differentiated learning if it meets learning objectives. Adaptive vocabulary tools allow those learning vocabulary to target frequently used vocabulary at the right levels, whereas multimedia listening exercises can be created for learners depending on their understanding levels. Collaborative learning tools enable learners to learn from each other through peer support where superior learners can tutor others. Research suggests that technology can close gaps in proficiency even in some mixed-ability classes through tasks completed for practice and feedback [7]. Nevertheless, it's clear that working with technology alone will not provide the means for task design and valid interpretation of feedback.

Main Content

The article examines digital tools such as learning platforms, adaptive tasks, collaborative writing, and automated feedback. These tools are discussed in terms of how they support different learners while keeping the same learning goals.

In this study, a qualitative analysis and classroom synthesis are carried out. The study is based on previous research to demonstrate how technology is beneficial to mixed-ability students in ELT. The search for research articles related to technology-based personalization in ELT in prominent academic databases such as ERIC, Web of Science, or Google Scholar facilitated gaining knowledge on the topic. The literature review targeted the literature that in some way related to the use of digital technology in language teaching, addressed issues related to variations in learner ability or language proficiency levels, and also touched upon issues related to learning engagement, autonomy, or language development. These issues are complemented by classroom examples related to the application of specific digital technologies in meeting the aspects covered in the literature review.

According to the literature, digital tools can support mixed-ability learners with several functions, including:

LMS tools give teachers tools for organizing learning materials, assigning tasks, and tracking learner actions. Using LMS tools, teachers are able to allocate leveled reading passages to students depending on their learning profiles. From the LMS dashboards, teachers are in a position to track the completion levels of learners for assigned activities.

"Adaptive platforms change practice exercise types based upon student responses. The system allows students to pursue their studies at their own levels of competency. Less able students are given foundational-level practice, and stronger students are challenged with higher-level tasks for deeper language use."

Google Docs is a collaboration tool where students are able to write, share, and share feedback on written work in real time. Learning together is supported by peer collaboration where students with different levels are able to learn together; students with knowledge assist in modeling while students with less knowledge get supported by peers.

Adaptive platforms adjust practice tasks based on learner responses. These tools support learners working at their own proficiency levels. Lower-ability learners receive more foundational practice, while higher-ability learners encounter challenging tasks that promote deeper language use.

Grammar-correcting machines and feedback systems provide immediate corrective input that assists learners with revision of language use. Although machine feedback will never replace teacher assessment, it speeds up the process of return of feedback.

Videos, podcasts, and quizzes vary the channels of input, offering learning preferences for different people. Multimedia aids listening understanding and vocabulary mastery for differentiated levels.

The use of technology to integrate personalized learning has numerous learning advantages in mixed-ability classrooms:

- Increased Engagement: Students become more actively engaged when tasks are suited to their level and interest.
- Learner Autonomy: Technology provides self-paced practice, allowing students to take charge of their learning [5].
- Rich Feedback & Comments: Computerized and classroom teacher

comments aid in processing drafts, improving skills.

- Flexible Differentiation: The teacher can differentiate instruction online to provide access to content that meets their skill level.
- Collaborative Learning: Electronic learning systems promote peer interaction and the co-construction of knowledge [10].

This meets the aims of the theories of communicative language learning, constructivism, and self-regulated learning, in that it emphasizes active participation of the learner in the learning process of language.

Though technology has the potential for personalized learning, its effective implementation requires strategic planning on the part of the teachers:

- Technical Access: Students must be able to access computers and the internet.
- Teacher Training: Teachers also require training to be able to integrate the tools in an effective manner and interpret the data provided
- Task Design: The technological tasks undertaken by students cannot replace learning.
- Equity: Teachers must see that personalization does not have a negative effect of segregation on some learners, rather all learners must strive towards collective communicative goals.

Conclusions and Recommendations

This study draws attention to the use of digital applications as a resource in fulfilling the learning needs of mixed-ability students learning English. Technology-based tools such as LMS, adaptive practices, collaborative writing tools, automated feedback tools, and multimedia resources have the ability to help teachers implement differentiated instruction for English language learners.

If technology is employed for specifically identified educational purposes, it can contribute significantly towards engagement, autonomy, and the cultivation of inclusive learning environments that facilitate the progress of all learners.

Implications for practice include selecting tools that align with learning objectives, designing tasks that provide varied pathways without lowering expectations, and developing teacher competence in interpreting digital feedback. It would now be appropriate to conduct empirical research that measures gains in proficiency and learner perceptions across diverse contexts, particularly in the secondary and high school settings and multilingual environments.

References

1. Bhandari, B.L., Bhandari, L.P., & Baguinat, N.S. English language teachers' practices of differentiated instruction in mixed-ability classrooms. JOLLT Journal of Languages and Language Teaching, 13(2), 2025. Pp. 199–218. https://doi.org/10.33394/jollt.v13i2.13573 ojspanel.undikma.ac.id

2. Dudeney, G., & Hockly, N. How to teach English with technology. Pearson. 2012.

3. Harmer, J. The practice of English language teaching (5th ed.). Pearson. 2015.

4. Huang, J., & Mizumoto, A. Examining the relationship between the L2 motivational self-system and technology acceptance model post ChatGPT introduction and utilization. Computers and Education: Artificial Intelligence, 7, 100302. 2024. https://doi.org/10.1016/j.caeai.2024.100302

5. Li, B., Bonk, C.J., Wang, C., & Kou, X. Reconceptualizing self-directed learning in the era of generative AI: An exploratory analysis of language learning. IEEE Transactions on Learning Technologies, 17, 2024. Pp. 1515–1529. https://doi.org/10.1109/TLT.2024.3386098

6. OECD. Country digital education ecosystems and governance: A companion to digital education outlook 2023. OECD Publishing. 2023. https://doi.org/10.1787/906134d4-en

7. Scrivener, J. Learning teaching: The essential guide to English language teaching (3rd ed.). Macmillan Education. 2011.

8. Tomlinson, C.A. The differentiated classroom: Responding to the needs of all learners (2nd ed.). ASCD. 2014.

9. Ur, P. A course in English language teaching (2nd ed.). Cambridge University Press. 2012.

10. Vo, A., & Nguyen, H. Generative artificial intelligence and ChatGPT in language learning: EFL students' perceptions of technology acceptance. Journal of University Teaching and Learning Practice, 21(6), 2024. Pp. 63–87.

11. Zheng, S. The effects of chatbot use on foreign language reading anxiety and reading performance among Chinese secondary school students. Computers and Education: Artificial Intelligence, 7, 100271. 2024. https://doi.org/10.1016/j.caeai.2024.100271

PHYSICS AND MATHEMATICS

RE-EVALUATION OF JAPANESE GEOLOGICAL REFERENCE MATERIALS (JSD/JDO SERIES) BY EDXRF

Firanj R.,
Daci B.,
Ylli F.
University of Tirana, Institute of Applied Nuclear Physics
DOI: 10.5281/zenodo.18655637

ABSTRACT

The limited availability of matrix-matched Certified Reference Materials (CRMs) for geological applications necessitates the re-evaluation of legacy standards to ensure their continued analytical fitness. This work validated the performance of Japanese Geological Survey (GSJ) reference materials (JSD-2, JSD-3, and JDO-1) using Energy Dispersive X-ray Fluorescence (EDXRF) combined with Fundamental Parameters (FP) quantification. Calibration curves were established using Weighted Least Squares (WLS) regression to address instrumental sensitivity deviations. While the regression exhibited high linearity ($R^2 > 0.99$) for major oxides, the calibration slopes for light elements deviated significantly from the theoretical unity (Mg ≈ 0.098, Si ≈ 0.64), reflecting uncorrected attenuation losses at low photon energies. Validation using Z-scores demonstrated that the method provided robust accuracy for transition metals and trace elements (Cu, Zn, Pb, Sr) within silicate matrices, yielding satisfactory scores ($|Z| \leq 2.0$). However, the analysis revealed severe limitations for light elements in non-silicate matrices. This failure indicates a breakdown of the silicate-based calibration model when applied to carbonate lithologies due to differences in mass attenuation coefficients and dark matrix effects. The results confirm that while these legacy CRMs remain reliable for trace element validation in aluminosilicates, accurate quantification of light elements requires strictly matrix-matched calibration strategies.

Keywords: Energy Dispersive X-ray Fluorescence, Fundamental Parameters, Geological Reference Materials, Matrix Effects, GSJ Standards.

Introduction

X-ray fluorescence (XRF) spectrometry has established itself as a great analytical technique for the characterization of geological materials, including soils, sediments, and rocks. The method is valued in geochemical laboratories for its ability to perform non-destructive, multi-elemental analysis ranging from beryllium to uranium with high precision and speed (Jenkins, 1999; Van Grieken & Markowicz, 2002). The technique is particularly advantageous for the determination of major and trace elements in solid samples, which are typically prepared as fused glass disks or pressed powder pellets to minimize particle size and mineralogical effects (Yamasaki et al., 2011). Because XRF allows for the direct interrogation of solid matrices, it eliminates the need for complex acid digestion procedures often required by other spectroscopic methods, thereby reducing the potential for analyte loss or contamination (Potts, 2008).

To convert measured X-ray intensities into elemental concentrations, analysts frequently employ the Fundamental Parameters (FP) method (Rousseau, 2001). Based on the theoretical equations derived by Sherman (1955), the FP approach models the physical interactions of X-rays with matter, correcting for matrix absorption and secondary fluorescence enhancement effects based on physical constants rather than solely on empirical regression. While theoretically capable of "standardless" quantification, the accuracy of FP methods is constrained by uncertainties in fundamental physical data—such as mass attenuation coefficients and fluorescence yields—and the accuracy of the excitation source spectral distribution models (Jenkins et al., 1995). Furthermore, theoretical models cannot fully account for all instrumental variations; therefore, for high-accuracy geological analysis, FP methods must be coupled with a robust calibration strategy using reference materials (Rousseau, 2001).

Consequently, XRF remains a comparative technique where the ultimate accuracy depends on the quality of the Certified Reference Materials (CRMs) used for calibration and method validation (Sieber, 2002). CRMs provide the essential link for metrological traceability and are the primary tools for evaluating the bias of an analytical method (ISO Guide 33, 2015). However, the selection of commercially available CRMs that perfectly match the matrix composition of specific geological samples is often limited, and the development of new certified materials is a time-consuming and costly process (Potts, 2008). This scarcity necessitates the continued use of legacy reference materials to ensure that calibration curves cover the necessary dynamic range of elemental concentrations.

This study focuses on the validation of older Japanese soil CRMs, specifically those produced by the Geological Survey of Japan (GSJ), for use in modern XRF protocols. Although these materials have historically served as benchmarks, their continued fitness for purpose must be verified against modern analytical criteria, particularly regarding homogeneity and stability over long storage periods (Sieber, 2002). By re-evaluating these older standards, this work aims to confirm their suitability for calibrating and validating EDXRF methods, thereby ensuring they remain reliable tools for the analytical chemistry community in the assessment of environmental and geological samples.

Materials and Methods

To evaluate the performance of the proposed XRF methodology, a specific set of "old" Japanese geological reference materials produced by the Geological Survey of Japan (GSJ) were selected for validation. These materials, historically utilized for geochemical standardization, include the soil series (e.g., JSO-1, JSO-2) and associated geological materials (e.g., JA-1 Andesite, JG-1a Granodiorite) to represent a range of aluminosilicate matrices (Govindaraju, 1994). These materials were selected to assess their long-term stability and continued suitability for modern instrumental calibration.

For the calibration of the Fundamental Parameters (FP) method, a separate set of international Certified Reference Materials (CRMs) was employed to establish the instrument sensitivity profile. These included standards from the PT testing scheme organized by the IAEA and other standards, covering a wide concentration range for major oxides (SiO_2, Al_2O_3, Fe_2O_3) and trace elements. The Japanese CRMs used for validation in this study are JSD-2, JSD-3, and JDO-1 (Imaji, 1996).

Table 1.

The list of all Certified Reference Materials with respective elements used for calibration in this study.

Standard ID	Matrix Description	Elements Used for Calibration
GEOPT23 OU9	Ophiolite (Geological)	K, Ca, Ti, Mn, Fe, Ga, Ge, Rb, Y, Nb, Sb, Tl
GEOPT26 OPC 1	Portland Cement	K, Ca, Ti, V, Mn, Fe, Co, Ni, Cu, Zn, Ga, As, Sr, Y, Zr, Nb, W, Ba, Hf, Pb
IAEA SL-1	Lake Sediment	K, Ti, V, Cr, Mn, Fe, Ni, Cu, Zn, Ga, As, Se, Rb, Sr, Eu, Hf, Ba, Pb
IAEA-375	Soil	Ni, As, Rb, Ba
ISE 861	Calcareous Clay	Mg, Al, Si, P, S, K, Ca, Ti, Cr, Mn, Fe, Co, Ni, Cu, Ga, As, Br, Rb, Sr, Nb, Mo, Ba, Pb
ISE 970	River Clay	K, Ca, Ti, V, Cr, Fe, Co, Ni, Cu, Zn, Ga, As, Br, Sr, Zr, Nb, Mo, Tl, Pb
JDO-1	Dolomite	Mg, Al, Si, P, S, K, Ca, Fe, Cu, Zn, Sr
JGB-1	Gabbro	K, Ca, V, Cr, Ga, Nb, Mo, Ba, W
JLS-1	Limestone	Mg, Al, Si, P, S, K, Ca, Ti, Ba
JSD-2	Stream Sediment	Mg, Ca, Ti, V, Cr, Co, Zr, Rb, Sr
JSD-3	Stream Sediment	Mg, Al, Si, P, S, K, Ca, Ti, V, Mn, Fe, Co, Ni, Cu, Zn, As, Rb, Sr, Zr, W, Eu, Pb
JSL-2	Slate	Mg, Al, Si, P, S, Cl, K, Ca, Ti, V, Cr, Mn, Fe, Co, Ni, Cu, Zn, Ga, As, Rb, Sr, Y, Zr, Ba, W, Pb
OU-5	Ophiolite (Geological)	K, Mn, Fe, Ni, Cu, Zn, Ga, Ge, As, Rb, Sr, Y, Zr, Hf, Ba, Tl, Pb
OU-8	Ophiolite (Geological)	K, Mn, Fe, Co, Ni, Cu, Ga, Ge, As, Rb, Sr, Y, Zr, Hf, La, Ba, Tl, Pb
PTNATIAEA05	Marine Sediment	V, Cr, Mn, Fe, Co, Ni, Cu, Zn, As, Se, Br, Rb, Mo, I
PTNATIAEA08	Natural Soil	Al, Cr, Zn, Se, Br, Mo, I
PTNATIAEA09	River Clay	Mg, Al, Si, P, S, Zn, Br
PTNATIAEA10	Sandy Soil	Mo
PTNATIAEA13	Clay	Mg, Al, Si, P, S, Hg
PTNATIAEA21	Soil	Mg, Cl
PTNATIAEA2001	Lake Sediment	Se
Soil-5	Soil	Eu, Hf
Soil-7	Soil	Eu

Sample Preparation

To minimize particle size effects and ensure surface homogeneity—critical factors in obtaining accurate XRF intensities for light elements—samples were prepared as pressed powder pellets (Jenkins et al., 1995). Prior to preparation, all CRM powders were dried at 105°C until the change in mass was less than 1% over two consecutive days. This process helps remove adsorbed moisture, which is a known source of error in XRF analysis of hygroscopic soil matrices (Potts, 2008). The dried samples were comminuted to a fine powder using a ball mill, grinding for 20 minutes per session to ensure sample homogeneity. For XRF analysis, pressed pellets were prepared by mixing 5.0 g of pulverized sediment with 0.5 g of boric acid (binder), resulting in a dilution factor of 1.1 (Gauglitz & Vo-Dinh, 2003). The mixture was pressed at 20 Ton/cm² to form a solid pellet and stored in desiccators to prevent moisture re-absorption prior to analysis. The all procedure of sample treatment were performed in the Radiochemistry Laboratory, Institute of Applied Nuclear Physics.

Instrumentation and Analysis

Elemental concentrations were determined using a SKYRAY 6000C EDXRF spectrometer. To ensure ac-

curacy across the full elemental range, spectra were acquired under two distinct conditions: Low-Z elements (Mg, Al, Si): 15 kV tube voltage, 100 µA current, no filter, 60s acquisition time. Mid- and High-Z elements (K, Ca, Ti, and all PTEs): 40 kV tube voltage, 100 µA current, Ni-Al filter, 60s acquisition time (Firanj et al., 2024).

All measurements were conducted in an air path. The PYMCA software was used to implement the Fundamental Parameters workflow, calculating elemental concentrations by iteratively correcting for matrix absorption and secondary fluorescence enhancement effects (Gauglitz & Vo-Dinh, 2003).

The analytical performance of the method was validated following ISO/IEC 17025 guidelines and established geochemical protocols (Sieber, 2002). Trueness was evaluated by comparing the measured concentrations (C_{meas}) of the Japanese soil CRMs against their certified values (C_{cert}). Bias was assessed using z-scores, where a score of $|Z| \leq 2$, was considered satisfactory (Fiamegos & de la Calle, 2016).

Results and Discussion

Calibration curves were established using Weighted Least Squares (WLS) regression to account for heteroscedasticity inherent in X-ray intensity data across wide dynamic ranges. The regression statistics, summarized in **Table 2**, indicate high linearity for the majority of analytes. Coefficients of determination (R^2) exceeded 0.99 for critical rock-forming oxides (Mg, Si, Ca, Fe) and trace elements (Sr). Transition metals such as $Cu, Zn, and\ Pb$ exhibited R^2 values between 0.96 and 0.97, reflecting typical variance at trace concentration levels.

Table 2.
Calibration regression statistics utilizing Weighted Least Squares (WLS), illustrating instrumental sensitivity deviations for low-Z elements.

Element	Slope	Intercept	R-Squared
Mg	0.098138	0.003599	0.999694
Al	0.313195	-0.02368	0.989401
Si	0.63695	-0.00106	0.995311
Ca	0.979431	-0.00033	0.994702
Fe	0.965002	0.000266	0.990412
Cu	0.615631	-6.5E-06	0.96869
Zn	1.047265	-5.9E-06	0.970478
Pb	1.141555	-1.9E-07	0.972845
Sr	0.995321	-2.7E-06	0.992716

The regression slopes (m), however, revealed a pronounced dependence on atomic number (Z). While higher-Z elements like Calcium ($m = 0.979$) and Iron ($m = 0.965$) exhibited slopes approaching the theoretical unity, light elements deviated significantly. Specifically, the slopes for Magnesium ($m = 0.098$), Aluminum ($m = 0.313$), and Silicon ($m = 0.637$) were substantially lower than 1.0. These empirical values indicate that while the Fundamental Parameters (FP) model accounts for matrix interactions, substantial scaling factors are required to reconcile the theoretical intensities with the measured instrumental response at low photon energies.

The accuracy of the method was evaluated by analyzing the Japanese geological reference materials (JSD-2, JSD-3, JDO-1). Fitness for purpose was assessed using Z-scores (Z) derived from the Horwitz function. Results are classified as Satisfactory ($|Z| \leq 2.0$), Warning ($2.0 < |Z| \leq 3.0$), or Unsatisfactory ($|Z| > 3.0$), as detailed in Tables 3-5.

Table 3.
Validation audit of Japanese Certified Reference Materials JDO-1 (concentration values are in mass fraction) showing Z-scores and matrix-dependent recovery rates.

Element	Certified Value	Measured Value	Recovery %	Z-Score
Mg	0.111687	0.008473	7.58601	-33.2225
Al	0.000069	-0.00231	-3353.46	-23.8289
Si	0.000982	0.001422	144.8323	4.402527
Ca	0.241852	0.230733	95.40271	-1.85651
Fe	0.000147	0.000478	325.4904	3.314709
Cu	1.3E-06	8.59E-05	6609.564	0.846243
Zn	3.42E-05	3.72E-05	108.9148	0.030489
Sr	0.000118	0.000115	97.83991	-0.02549

Table 4.

Validation audit of Japanese Certified Reference Materials JSD-2 (concentration values are in mass fraction) showing Z-scores and matrix-dependent recovery rates.

Element	Certified Value	Measured Value	Recovery %	Z-Score
Mg	0.016946	0.016824	99.27743	-0.19558
Al	0.065996	0.031614	47.90362	-17.3027
Si	0.281741	0.198902	70.59731	-12.1495
Ca	0.025943	0.021526	82.97375	-4.91359
Fe	0.080506	0.060677	75.36898	-8.42907
Cu	1.11E-06	0.000667	59829.55	6.653872
Zn	2.07E-06	0.001729	83524.96	17.26897
Pb	1.51E-07	0.000145	95843.39	1.445725
Pb	1.51E-07	0.000119	78687.56	1.186672
Sr	2.02E-07	0.000176	87017.58	1.755735
Rb	2.7E-08	2.15E-05	79549.03	0.214512

Table 5

Validation audit of Japanese Certified Reference Materials JSD-3 (concentration values are in mass fraction) showing Z-scores and matrix-dependent recovery rates.

Element	Certified Value	Measured Value	Recovery %	Z-Score
Mg	0.007116	0.034705	487.7041	92.09413
Al	0.053665	0.051137	95.29009	-1.51636
Si	0.352281	0.328229	93.17239	-2.91773
Ca	0.00378	0.003599	95.21178	-1.03409
Fe	0.03	0.02886	96.19861	-1.12129
Cu	0.000426	0.000384	90.25388	-0.41518
Zn	0.000139	0.000141	101.2424	0.01727
Pb	0.000082	7.42E-05	90.50929	-0.07782
Sr	0.00006	5.83E-05	97.12008	-0.01728
Rb	0.000285	0.000286	100.2306	0.006573

The method demonstrated robust accuracy for transition metals across all tested matrix types. Iron (Fe) yielded passing Z-scores for both the silicate-based JSD-3 ($Z = -1.12$) and the dolomitic JDO-1 ($Z = 3.31$, noting a marginal positive bias). Trace elements including Copper, Zinc, Lead, and Strontium consistently returned Satisfactory Z-scores ($|Z| < 2.0$) in the JSD-3 standard, verifying the recoverability of these analytes in legacy sediment samples.

Performance for light elements (Mg, Al, Si) was strongly dependent on the geological matrix; The JSD-3 standard showed acceptable accuracy for Aluminum ($Z = -1.52$) but fell into the Warning category for Silicon ($Z = -2.92$). The JSD-2 standard exhibited significant negative biases for Aluminum ($Z = -17.3$) and Silicon ($Z = -12.1$), consistent with these analytes being excluded from the calibration set for this specific sample due to known mineralogical heterogeneity.

The analysis of JDO-1 (Dolomite) resulted in gross systematic underestimation for light elements. Magnesium returned to a Z-score of -33.22, and Aluminum returned -23.83. While Calcium performed acceptably Z=-1.86, the extreme failure in Mg and Al quantification indicates a breakdown of the calibration model when applied to non-silicate carbonate matrices.

Discussion

The observed calibration slopes for low-Z elements (Table 1) diverge from the idealized expectation of unity often associated with "standardless" FP quantification. In principle, the Sherman equation (Sherman, 1955) models the theoretical intensity R_i based on fundamental physical constants. However, as noted by Rousseau (2006), the practical application of FP requires an empirical slope correction to adapt theoretical physics to specific instrumental geometries.

The slope of 0.098 for Mg and 0.637 for Si suggests significant uncorrected attenuation losses in the detection path. Jenkins (1999) attributes such losses at energies below 2 keV to the quantum efficiency of the detector window (e.g., Beryllium thickness) and incomplete charge collection in the detector crystal surface dead layer. Because the theoretical model assumes an ideal detection efficiency unless explicitly characterized, the regression slope acts as a necessary "sensitivity factor," empirically correcting for these instrumental limitations to achieve accurate quantification (Van Grieken & Markowicz, 2002).

The severe negative bias observed for Magnesium in JDO-1 ($Z = -33.22$) underscores the limitations of

applying a silicate-based calibration to carbonate lithologies. Global calibration was established primarily using aluminosilicate standards, where Oxygen is the primary light element. JDO-1, being a dolomite $CaMg(CO_3)_2$, contains a high stoichiometric proportion of Carbon.

In XRF analysis, elements lighter than Sodium (such as Carbon and Oxygen) act as a "dark matrix", they are undetected by the spectrometer but significantly influence the sample's mass attenuation coefficient (Jenkins, 1999). The specific mass attenuation coefficient of a carbonate matrix differs from that of a silicate matrix, particularly for soft X-rays like Mg K_a (Sherman, 1955). The FP model, lacking explicit input for the Carbon content, likely overestimated the matrix absorption, or conversely, the "unmeasured" dark matrix balance calculation was skewed by the distinct O/C ratio of the carbonate. This confirms that for light elements in geologically diverse samples, a universal calibration is insufficient; accurate analysis requires matrix-matched calibration strategies or explicit "Dark Matrix" definition to resolve the attenuation differences (Gauglitz & Vo-Dinh, 2003).

Despite the matrix-induced biases observed for light elements, the performance of transition metals validates the continued utility of the older GSJ standards. The satisfactory recovery of Cu, Zn, and Pb in JSD-3 suggests that these materials have not suffered from element migration, segregation, or oxidation despite decades of storage, supporting Bertin's (1975) observations on the long-term stability of properly stored geological reference materials. However, their use as validation tools must be strictly context-dependent (Sieber, 2002): while robust for trace metals, they function as "matrix-specific" checks for major oxides, valid only when the unknown sample matrix aligns closely with the standard's aluminosilicate composition.

Conclusions

This study evaluated the fitness for purpose of legacy Japanese soil Certified Reference Materials (CRMs) for modern XRF applications. Based on the validation statistics and the theoretical framework of Fundamental Parameters, the following conclusions are drawn; JSD-2 and JSD-3 are validated as fit for purpose for the analysis of transition metals and trace elements (e.g.,Cu, Zn, Pb, Sr), demonstrating satisfactory accuracy ($|Z| \leq 2.0$). This confirms that the "sedimentary rock series" produced by the GSJ remains a reliable benchmark for aluminosilicate matrices, consistent with their original geochemical characterization (Govindaraju, 1994). However, they are not universally valid for all major oxides ($Z = -17.3\ in\ JSD - 2$) indicate that matrix-specific calibration adjustment are required for light elements.

The Dolomite standard JDO-1 made of carbonate matrix, is fit for purpose only for trace and transition metals. It is not recommended for the validation of light major elements (Mg, Al) within a silicate-based calibration curve. The gross systematic bias observed for Magnesium ($Z \approx -33$) and Aluminum ($Z = -23$) confirms that the method is invalid for light element quantification in carbonate matrices without explicit matrix-matching. JDO-1 remains fit for purpose only for the validation of higher -Z transition metals (Fe, Zn, Sr). Carbonate matrices require a specific, matrix-matched calibration separate from silicates to account for attenuation differences, reinforcing the guidelines on CRM selection and matrix matching provided by Sieber (2002).

The deviation of calibration slopes from unity for light elements (e.g., $Si \approx 0.64$) highlights the necessity of using Weighted Least Squares (WLS) regression. This approach effectively scales the theoretical Fundamental Parameters intensities to the actual instrumental sensitivity. As described by Rousseau (2006), this empirical scaling is essential to compensate for instrumental factors such as detector efficiency and window absorption that are not fully captured by the theoretical physics model alone.

References

1. Badla, C., & Wewers, F. (2020). Optimization of X-ray Fluorescence Calibration through the Introduction of Synthetic Standards for the Determination of Mineral Sands Oxides. *South African Journal of Chemistry*, 73, 92–102.

2. Bertin, E. P. (1975). *Principles and Practice of X-Ray Spectrometric Analysis* (2nd ed.). Plenum Press.

3. Fiamegos, Y., & de la Calle, M. B. (2016). Validation strategy for an ED-XRF method to determine trace elements in a wide range of organic and inorganic matrices based on fulfilment of performance criteria. *Spectrochimica Acta Part B: Atomic Spectroscopy*, 118, 52–59.

4. Firanj, R., Osmeni, A., Ylli, A., Daci, B., Ylli, F., & Maci, A. (2025). Assessment of Metal Contamination in the Ishmi River Sediments Using XRF Spectrometry and Pollution Indices. *12th International Conference of the Balkan Physical Union (BPU12)*, Bucharest, Romania.

5. Gauglitz, G., & Vo-Dinh, T. (Eds.). (2003). *Handbook of Spectroscopy* (Vol. 1). Wiley-VCH.

6. Govindaraju, K. (1994). 1994 Compilation of working values and sample description for 383 geostandards. *Geostandards Newsletter*, 18(Special Issue), 1–158.

7. Imai, N., Terashima, S., Itoh, S., & Ando, A. (1996). 1996 compilation of analytical data on nine GSJ geochemical reference samples, "Sedimentary rock series". *Geostandards Newsletter*, 20(2), 165-216.

8. Jenkins, R. (1999). *X-Ray Fluorescence Spectrometry* (2nd ed.). Wiley-Interscience.

9. Jenkins, R., Gould, R. W., & Gedcke, D. (1995). *Quantitative X-ray Spectrometry* (2nd ed.). Marcel Dekker.

10. Potts, P. J. (2008). *A Handbook of Silicate Rock Analysis*. Springer Science & Business Media.

11. Rousseau, R. M. (2001). Corrections for matrix effects in X-ray fluorescence analysis—A tutorial. *Spectrochimica Acta Part B: Atomic Spectroscopy*, 56(6), 915–949.

12. Rousseau, R. M. (2006). Practical XRF Calibration Procedures for Major and Trace Elements. *Spectrochimica Acta Part B: Atomic Spectroscopy*, 61(7), 759–777.

13. Sherman, J. (1955). The theoretical derivation of fluorescent X-ray intensities from mixtures. *Spectrochimica Acta*, 7, 283–306.

14. Sieber, J. R. (2002). How to use and how not to use certified reference materials in industrial chemical metrology laboratories. *Accreditation and Quality Assurance*, 7(1), 26–30.

15. Van Grieken, R., & Markowicz, A. (Eds.). (2002). *Handbook of X-Ray Spectrometry* (2nd ed.). Marcel Dekker.

16. Yamasaki, S. I., Yamagishi, H., & Tsuchiya, N. (2011). Major element analysis of geological samples with wavelength Dispersive X-ray Fluorescence (WDXRF) spectrometry using glass disks and pressed powder pellets. *Journal of the Mineralogical and Petrological Sciences*, 106, 221–227.

SOCIAL SCIENCES

WATER DIPLOMACY IN CENTRAL ASIA: INSTITUTIONAL MECHANISMS OF TRANSBOUNDARY WATER RESOURCES MANAGEMENT

Baigabylov N.
Eurasian National University, Professor
Astana, Kazakhstan,
Torez Sh.
Eurasian National University, Astana, Kazakhstan
Kudabekov M.
Eurasian National University, Astana, Kazakhstan
DOI: 10.5281/zenodo.18655649

ABSTRACT

Central Asia is characterized by a high degree of transboundary interdependence in the sphere of water resources, where major river systems cross national borders and are shared by multiple states. This structural configuration creates persistent challenges for water governance and necessitates institutionalized mechanisms of interstate coordination. This paper examines water diplomacy in Central Asia through the lens of institutional mechanisms of transboundary water resources management. The study combines empirical analysis of transboundary water dependence and water availability with an institutional examination of regional cooperation frameworks. The findings demonstrate pronounced asymmetry in transboundary water dependence and heterogeneous baseline water conditions across the region, which shape divergent national interests and constrain the operability of regional water diplomacy institutions. The paper contributes to the literature on water diplomacy by linking empirical indicators of water interdependence with institutional analysis of regional governance mechanisms.

Keywords: water diplomacy, transboundary water resources, Central Asia, institutional mechanisms, regional cooperation.

Introduction

Central Asia represents a region with a pronounced transboundary configuration of water resources, where major river systems are formed beyond the borders of individual states and shared among multiple countries. The system of water allocation inherited from the Soviet period relied on centralized planning and coordination mechanisms, which were subsequently transformed into interstate formats following the dissolution of the USSR. As a result, contemporary water governance in the region operates under conditions of persistent interdependence and institutional fragmentation.

In recent decades, the transboundary nature of water resources has gained increased importance due to rising water demand, socio-economic development, climate variability, and growing pressure on water management systems. In this context, water functions not only as a natural resource but also as a factor shaping economic stability, food security, and interstate relations. Consequently, transboundary water governance in Central Asia extends beyond technical regulation and becomes embedded in broader political and institutional interactions.

In the absence of a supranational authority responsible for water management, water diplomacy plays a central role in coordinating interstate relations over shared water resources. In this study, water diplomacy is understood as a set of institutionalized practices through which states negotiate, coordinate, and manage the use of transboundary water resources. These practices are embedded in formal agreements, regional organizations, and regular consultation mechanisms that collectively form the institutional architecture of regional water governance.

Despite the existence of regional water cooperation institutions, questions remain regarding their functional effectiveness under conditions of asymmetric water dependence and divergent national interests. Differences between upstream and downstream states, as well as unequal levels of water availability, create structurally uneven starting positions for cooperation. This paper addresses this gap by analyzing water diplomacy in Central Asia not as a declarative political framework, but as a system of institutional mechanisms operating within an asymmetric configuration of transboundary water interdependence. The study contributes to the literature by linking empirical indicators of transboundary water dependence with institutional analysis of regional water governance mechanisms.

Results

Transboundary water interdependence constitutes a fundamental structural characteristic of Central Asia. Comparative analysis of transboundary water dependence across the region reveals a pronounced asymmetry in the degree to which states rely on water resources formed beyond their national territories.

The results indicate that Central Asian countries occupy structurally distinct positions within the system of transboundary water governance. Some states exhibit high levels of dependence on external water inflows, while others maintain relatively autonomous water resource bases. These differences reflect the upstream–downstream configuration of the region and generate unequal starting conditions for participation in regional water cooperation mechanisms.

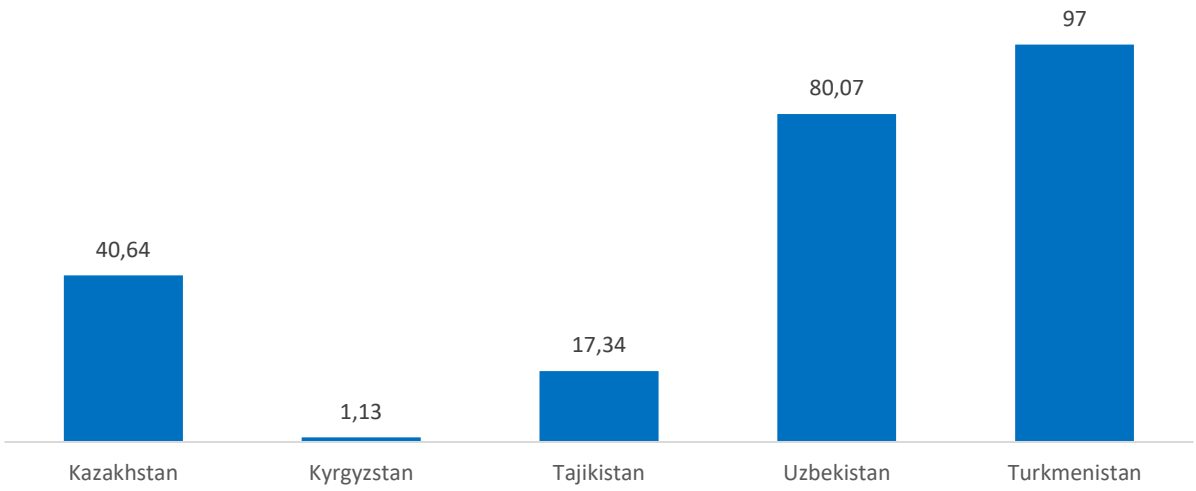

Figure 1. Dependency ratio in Central Asian countries (%), latest available data.
Source: FAO AQUASTAT.

As illustrated in Figure 1, downstream countries demonstrate the highest levels of transboundary water dependence, whereas upstream states show minimal reliance on external water resources. Kazakhstan occupies an intermediate position, indicating partial vulnerability to transboundary water regimes alongside a structural need for participation in coordinated governance arrangements.

Importantly, these differences are structural rather than temporary, reflecting the long-term hydrological configuration of the region. In this sense, empirical indicators of transboundary dependence provide a foundation for understanding the institutional dynamics of water diplomacy in Central Asia.

In addition to transboundary dependence, Central Asian countries also differ substantially in terms of overall water availability. While dependency ratios capture reliance on external inflows, they do not account for baseline levels of water endowment. To complement the analysis, renewable water resources per capita are considered as an indicator of general water availability. This variation provides important contextual insight into the heterogeneous hydrological conditions under which regional water governance and water diplomacy mechanisms operate.

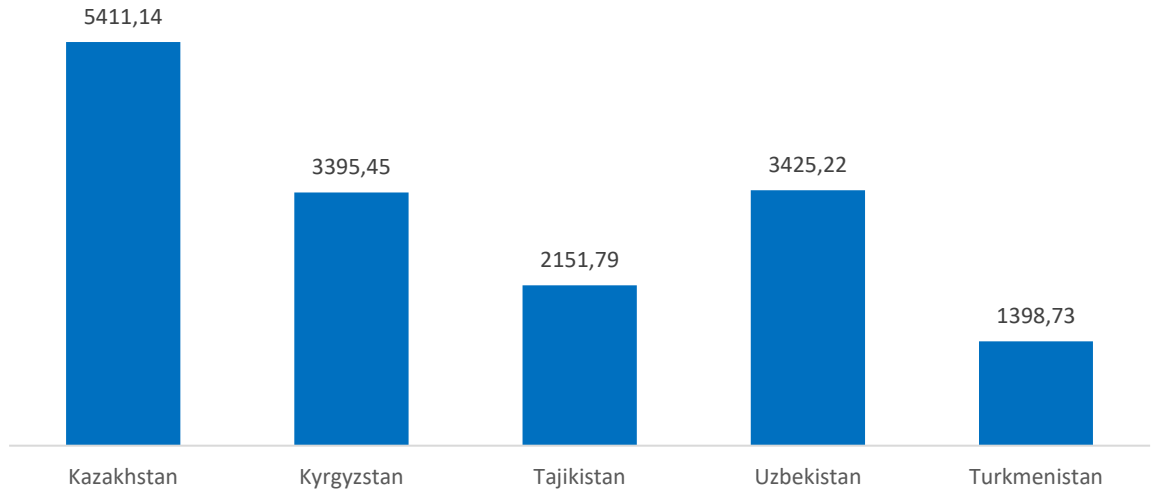

Figure 2. Total renewable water resources per capita in Central Asian countries (m³ per inhabitant per year), latest available data.
Source: FAO AQUASTAT.

Discussion

The empirical findings indicate that water diplomacy in Central Asia operates within a structurally asymmetric environment shaped by uneven transboundary water dependence and heterogeneous water endowment. These conditions influence state incentives for cooperation and constrain the operability of institutional mechanisms.

For countries with high transboundary dependence, predictability and stability of water allocation re-

gimes are of critical importance. In contrast, more autonomous states may approach water diplomacy with different strategic priorities. Regional institutions therefore perform a balancing function, mediating divergent interests without fully resolving underlying asymmetries.

Differences in overall water availability further reinforce variation in national water use strategies. Institutional mechanisms do not redistribute water resources but facilitate coordination and negotiation under unequal hydrological conditions. As a result, water diplomacy functions primarily as a mechanism for managing interdependence rather than eliminating structural disparities.

Regional organizations such as the Interstate Commission for Water Coordination and the International Fund for Saving the Aral Sea provide formalized channels for dialogue and reduce the risk of unilateral actions. At the same time, their effectiveness depends on operability—the capacity to implement agreements, exchange information, and adapt to changing conditions. Limitations in operability reflect a persistent gap between formal institutionalization and practical execution.

Overall, water diplomacy in Central Asia exhibits a stabilizing but constrained character. It supports a minimum level of coordination while limiting prospects for deeper institutional integration under conditions of persistent structural asymmetry.

Conclusion

This paper has analyzed water diplomacy in Central Asia through an institutional lens, integrating empirical indicators of transboundary water dependence and water availability with an examination of regional cooperation mechanisms. The analysis demonstrates that water diplomacy in the region operates within a stable but asymmetric structural configuration that shapes institutional capacity and state behavior.

The findings show that regional water institutions contribute to the manageability of interstate water relations by providing formalized mechanisms for coordination and dialogue. At the same time, their effectiveness is constrained by underlying asymmetries and varying levels of operability. Water diplomacy thus functions as an instrument for managing interdependence rather than resolving it.

The contribution of this study lies in linking empirical measures of transboundary water dependence with institutional analysis of regional water governance. This approach provides a foundation for further research on the adaptive capacity and operability of water diplomacy under evolving hydrological and socio-economic pressures.

References

1. FAO AQUASTAT Country Profiles: Central Asian Countries. Food and Agriculture Organization of the United Nations. Available at: https://www.fao.org/aquastat/

2. FAO AQUASTAT Country Profile: Kazakhstan. Food and Agriculture Organization of the United Nations. Available at: https://www.fao.org/aquastat/

3. FAO AQUASTAT Country Profile: Uzbekistan. Food and Agriculture Organization of the United Nations. Available at: https://www.fao.org/aquastat/

4. FAO AQUASTAT Country Profile: Kyrgyzstan. Food and Agriculture Organization of the United Nations. Available at: https://www.fao.org/aquastat/

5. FAO AQUASTAT Country Profile: Tajikistan. Food and Agriculture Organization of the United Nations. Available at: https://www.fao.org/aquastat/

6. FAO AQUASTAT Country Profile: Turkmenistan. Food and Agriculture Organization of the United Nations. Available at: https://www.fao.org/aquastat/

7. UN-Water (2023). Progress on Transboundary Water Cooperation: Global Status of SDG Indicator 6.5.2. United Nations. Available at: https://www.sdg6data.org/

8. UNECE & UNESCO (2021). Progress on Transboundary Water Cooperation under the UNECE Water Convention. United Nations Economic Commission for Europe.

9. Interstate Commission for Water Coordination (ICWC) (2022). Mandate and Activities of the ICWC in Central Asia. Available at: http://www.cawater-info.net/

10. International Fund for Saving the Aral Sea (IFAS) (2021). Institutional Framework and Regional Cooperation Mechanisms in the Aral Sea Basin.

TECHNICAL SCIENCES

LOG-DRIVEN COUNTERFACTUAL EXPLANATIONS FOR CYBER INCIDENTS IN SIEM PIPELINES

Gurbanaliyev I.
Vizja University, Department of Computer Science, Master's student
Warsaw, Poland
DOI: 10.5281/zenodo.18655669

ABSTRACT

Security Information and Event Management (SIEM) pipelines excel at collecting and correlating telemetry, yet incident outcomes often remain hard to interpret operationally: analysts can see *what happened*, but not clearly *what would need to be different* for the incident to be prevented, downgraded, or resolved faster. This paper proposes a log-driven counterfactual explanation approach tailored to cyber incidents detected in SIEM environments. We define counterfactuals as minimally invasive, operationally feasible changes to log-evidenced conditions (e.g., identity posture, authentication controls, network segmentation, endpoint hardening, alert routing) that would plausibly alter the incident outcome produced by a detection/correlation model.

Building on established counterfactual explanation principles—actionability, proximity, and diversity we adapt them to the constraints of security logs: temporal ordering, entity relationships (user-host-resource), and policy immutables. We present an end-to-end architecture for generating counterfactuals inside SIEM pipelines, including log normalization, incident graph construction, model-agnostic counterfactual search with security constraints, and human-readable "playbook-style" outputs. We also propose evaluation criteria for SOC usage (validity, feasibility, cost, stability, and analyst utility) and outline realistic scenarios such as credential compromise, lateral movement, and cloud misconfiguration. The approach aims to improve triage speed, support defensible post-incident learning, and enable "what-if" hardening decisions without exposing model internals.

Keywords: SIEM, cybersecurity, incident response, explainable AI, counterfactual explanations, log analytics, SOC operations, causal reasoning, security graphs.

1. Introduction

The increasing complexity of enterprise information systems and the growing sophistication of cyber threats have made centralized security monitoring indispensable. SIEM platforms serve as the backbone of this monitoring by collecting heterogeneous logs from endpoints, networks, identity systems, and cloud services. Through correlation rules and machine-learning–based analytics, SIEM systems identify suspicious behavior and generate security incidents for analyst review. Despite advances in detection accuracy, a persistent challenge remains: understanding *why* a specific set of log events resulted in a particular incident classification and *how* the incident outcome could have been different. Analysts are frequently presented with high-severity alerts without clear guidance on which security controls failed or what minimal changes could have prevented escalation. Traditional explainability methods in cybersecurity often rely on feature importance or rule tracing, which describe contributing signals but rarely translate into actionable remediation insight [1, p.841,2, p. 607].

Counterfactual explanations offer a promising alternative by focusing on actionable "what-if" scenarios. Rather than explaining model internals, counterfactuals describe how changing certain controllable conditions would lead to a different decision outcome. In the context of SIEM, this perspective aligns naturally with operational security thinking, where analysts and defenders routinely ask: *Which control, if it had been in place, would have stopped this attack?* This study proposes a log-driven counterfactual explanation framework tailored to SIEM pipelines. By grounding counterfactuals directly in log evidence and operationally feasible security controls, the approach aims to bridge the gap between detection and actionable defense improvement [4, p.93].

2. Related Work. Explainable artificial intelligence (XAI) has gained increasing attention in cybersecurity, particularly for intrusion detection and security analytics. Prior research highlights that transparency alone is insufficient unless explanations support human decision-making and operational response. Recent surveys emphasize the importance of explanation methods that are interpretable by security analysts and aligned with real-world workflows. Counterfactual explanations have emerged as a practical XAI paradigm because they provide user-centered guidance without requiring full access to model internals. Existing work on counterfactual explanations primarily focuses on tabular or image-based machine-learning decisions, such as credit scoring or medical diagnosis. Some recent studies have explored counterfactual reasoning in intrusion detection systems, demonstrating that actionable counterfactuals can suggest effective mitigation strategies.

However, SIEM incidents differ from isolated classification tasks. They are the result of multi-source log correlation, temporal dependencies, and complex entity relationships. Existing counterfactual approaches rarely address these characteristics explicitly. This paper extends counterfactual explanation principles to a log-native, incident-centric setting suitable for SIEM-based cybersecurity operations.

3. Problem Definition. In modern Security Information and Event Management (SIEM) environments, a security incident is not the result of a single alert but

rather the aggregation of multiple security-relevant events observed within a defined temporal window. These events originate from heterogeneous sources such as endpoints, network devices, identity systems, cloud services, and application logs. After normalization and enrichment, each event typically contains information related to time, source, action, outcome, and associated entities, including users, hosts, applications, or cloud resources. Detection mechanisms whether rule-based, statistical, or machine-learning–driven correlate these events and elevate them into an incident with an assigned classification, severity level, and confidence score.

From an operational perspective, a SIEM incident represents a structured interpretation of observed behavior rather than a simple reflection of raw telemetry. The incident encapsulates not only the triggering signals but also contextual information such as privilege level, authentication method, device state, network location, and asset criticality. Importantly, the incident outcome emerges from the interaction of these factors over time, where early-stage events often enable subsequent actions, leading to escalation. This temporal and relational structure means that incident outcomes are inherently path-dependent, making post-hoc reasoning based solely on isolated signals insufficient for understanding how and why escalation occurred. The core problem addressed in this study arises from the gap between incident detection and actionable understanding. While SIEM platforms are effective at identifying suspicious behavior and prioritizing alerts, they rarely provide clear guidance on which specific security conditions enabled the incident or how the outcome could have been different. Analysts are typically left to infer, through manual investigation, which control failures or configuration weaknesses contributed most to escalation. This process is time-consuming, subjective, and difficult to standardize across incidents and environments.

The objective of this work is to address this gap by formulating the generation of counterfactual explanations for SIEM incidents. In this context, a counterfactual explanation describes a minimal and feasible change to defender-controllable security conditions—observable or inferable from log data—that would plausibly have altered the incident outcome. Rather than modifying historical events, the focus is on identifying security interventions that could have prevented incident creation, reduced severity, limited scope, or enabled earlier containment under similar future conditions.

A critical requirement of this objective is operational realism. Counterfactual explanations must be grounded in security controls that organizations can realistically deploy, such as authentication policies, endpoint protection configurations, network segmentation rules, cloud access restrictions, or alerting and automation logic. Conditions that are immutable or not meaningfully controllable by defenders are excluded from consideration. Furthermore, proposed changes must be minimal in the sense that they aim to achieve the desired outcome with the least disruption, cost, or complexity, reflecting the practical constraints of security operations centers [5, p.89,6, p.227].

Another essential aspect of the problem formulation is the reliance on log-evidenced conditions. Counterfactual explanations are derived from patterns and relationships observed in the incident's log data, ensuring that recommendations are incident-specific rather than generic best practices. This grounding in observable evidence enhances trust in the explanation and supports defensible decision-making during incident response and post-incident review. In summary, the problem addressed in this study is the lack of systematic, actionable explanations within SIEM pipelines that connect incident outcomes to concrete, controllable security conditions. By framing this challenge as a counterfactual explanation task rooted in log data, the study seeks to transform SIEM incidents from opaque detection outputs into structured opportunities for targeted security improvement and preventive action.

4. Log-Driven Counterfactual Explanation Framework

The proposed framework is designed to generate counterfactual explanations directly from log evidence produced and processed within SIEM pipelines. Its central assumption is that incidents emerge from structured, time-ordered interactions among entities (users, hosts, applications, cloud resources) and that meaningful explanations must therefore respect both the temporal structure of events and the operational constraints of cybersecurity controls. In practice, the framework operates on normalized and enriched logs, where heterogeneous telemetry is mapped into a consistent schema and augmented with security context such as asset criticality, identity privilege level, device compliance, authentication method, and network zone. This contextualization is essential because counterfactual statements that ignore operational context tend to become generic recommendations rather than incident-specific explanations.

Within the incident time window, the framework constructs a coherent representation of the incident as an evidence-backed behavioral pattern, capturing not only which events occurred, but also how they relate across entities and time. Instead of treating an incident as a flat set of features, the approach emphasizes relational structure: repeated authentications between specific endpoints, unusual sequences of administrative actions, privileged access followed by configuration change, or data-access bursts following suspicious sign-in behavior. This representation enables counterfactual reasoning that aligns with how analysts naturally interpret incidents through attack paths and enabling conditions—rather than through isolated indicators.

Counterfactual generation is formulated as a constrained search over defender-controllable conditions that are plausible, implementable, and consistent with security policy. The framework deliberately distinguishes between immutable facts (e.g., historical timestamps or the existence of an entity) and actionable conditions (e.g., MFA enforcement, token issuance policies, endpoint hardening configurations, network segmentation rules, cloud access guardrails, and alert routing or automation logic). Candidate counterfactuals are produced by proposing minimal changes to these actionable conditions such that the incident outcome

would plausibly change—whether by preventing escalation, reducing severity, limiting scope, or accelerating containment. Minimality is interpreted operationally: interventions are preferred when they require fewer changes, apply to a narrower scope, introduce lower disruption, and are feasible within realistic deployment timelines. Feasibility is treated as a first-class constraint rather than a secondary consideration, ensuring that explanations are not merely theoretically valid but practically usable [8, p.4564].

To make the output suitable for SOC workflows, the framework renders each counterfactual as an action-oriented explanation supported by explicit log evidence. The explanation is expressed in a form that resembles mitigation reasoning used by analysts: what control should be changed, why that change is justified given the observed signals, and what outcome difference is expected. Where possible, the framework produces multiple counterfactual options that reflect alternative defense strategies, such as identity-centric controls, endpoint-centric controls, network-centric restrictions, or cloud-policy guardrails. This plurality is important because there is rarely only one correct defensive action, and organizations differ in which controls they can deploy quickly. At the same time, governance and safety constraints are incorporated to reduce the risk of disclosing sensitive detection logic or creating explanations that could be misused as evasion guidance. The overall goal is to integrate counterfactual explanations as a practical layer in SIEM pipelines that transforms incident outputs into structured, evidence-based guidance for prevention and improvement [9, p.243].

5. Application Scenarios

The usefulness of log-driven counterfactual explanations becomes most visible when applied to incident categories that frequently appear in real SOC operations and where the relationship between enabling conditions and outcomes is strongly reflected in logs. One common scenario is identity compromise, where incidents are triggered by anomalous sign-in behavior followed by sensitive actions such as token issuance, mailbox access, privilege changes, or the creation of persistence mechanisms. In such cases, the framework can produce counterfactuals centered on defender-controllable identity conditions that are directly grounded in observed evidence, such as requiring stronger MFA for risky sign-ins, restricting token issuance under uncertain device posture, disabling legacy authentication paths, or enforcing conditional access rules tied to location, device compliance, or user risk. The counterfactual explanation in this scenario is not “the user should be careful,” but a concrete policy-level change that plausibly breaks the observed sequence and reduces incident severity.

A second scenario involves lateral movement and internal propagation, often detected when a host or account begins authenticating to many peer systems, when administrative protocols are used unusually, or when remote service creation and credential reuse are observed. Here, the framework produces counterfactuals that focus on limiting propagation paths through segmentation, privilege reduction, and endpoint hardening. Because lateral movement is inherently relational, log-based representations that link source host, target hosts, authentication events, and privilege context are particularly suitable for counterfactual reasoning. Recommendations can therefore be framed as minimal changes that would have interrupted the observed path, such as restricting east-west access for specific protocols, removing unnecessary local administrator rights, strengthening credential protections, or expanding endpoint sensor coverage in the part of the environment where evidence shows the attack initiated [10, p.69].

A third scenario concerns cloud misconfiguration and data exposure, where incidents arise from policy changes that enable public access, over-permissive IAM roles, or unexpected bulk access patterns to storage and databases. Cloud audit logs often provide clear evidence of configuration changes and access events, allowing counterfactual explanations to map directly to guardrails that prevent similar outcomes. In this setting, counterfactuals may emphasize organization-level policy controls that block public exposure, enforce least privilege, require private endpoints, or constrain sensitive actions such as key creation and privilege escalation. The strength of the framework in such cases lies in converting a complex incident outcome into a small set of feasible preventative actions tied to the exact control plane events visible in logs.

Across these scenarios, the core advantage is that counterfactual explanations remain incident-specific, evidence-based, and operationally realistic. They provide analysts and defenders with structured “what-if” guidance that can support faster triage decisions, clearer mitigation justification, and more systematic post-incident improvement planning. By translating incident outcomes into minimal control-based alternatives, the framework aims to make SIEM incidents not only detectable but also decisively actionable in a consistent and scalable way.

6. Evaluation Criteria The effectiveness of log-driven counterfactual explanations in SIEM environments should be assessed using criteria that reflect the practical needs of security operations rather than purely theoretical model properties. First, a counterfactual explanation must demonstrate **outcome validity**, meaning that the proposed intervention would plausibly alter the incident outcome, such as preventing incident creation, reducing severity, limiting scope, or enabling earlier containment. Second, **operational feasibility** is essential; recommended changes must be implementable using existing security controls and align with organizational policies and technical constraints. Third, **minimality** should be considered from a defensive perspective, favoring interventions that require fewer changes, affect a limited scope, and introduce minimal disruption to users and systems.

In addition, **stability under log uncertainty** is an important criterion, as SIEM data is often incomplete or noisy. Counterfactuals should remain meaningful even when some events or attributes are missing or imprecise. Finally, **analyst utility** serves as a holistic evaluation measure, capturing whether the explanation reduces investigation time, improves confidence in mitigation decisions, and supports consistent post-incident

learning. Together, these criteria ensure that counterfactual explanations are not only technically sound but also genuinely useful in real SOC workflows.

7. Security and Governance Considerations. The introduction of counterfactual explanations into SIEM pipelines raises important security and governance considerations. Explanations must be carefully designed to avoid disclosing sensitive detection logic or operational thresholds that could be exploited by adversaries. For this reason, access to counterfactual explanations should be restricted to authorized security personnel, and the level of detail presented should be aligned with the user's role.

Another key consideration is the reliability of explanations in the presence of imperfect log data. When critical signals are missing or uncertain, counterfactual outputs should reflect this limitation by indicating reduced confidence or by recommending improvements in telemetry coverage rather than definitive control changes. From a governance perspective, storing counterfactual explanations as part of incident records can support auditability and continuous improvement, allowing organizations to track which recommended interventions were implemented and how they influenced future incident outcomes. Overall, appropriate governance ensures that counterfactual explanations enhance defensive capability without increasing operational or security risk.

8. Discussion. Log-driven counterfactual explanations offer a conceptually and practically well-aligned approach to the challenges faced by modern cybersecurity operations. By translating SIEM detection outcomes into concrete, control-oriented alternatives, they bridge the long-standing gap between alert generation and actionable defensive decision-making. Unlike traditional feature-based or signal-attribution explanations, which primarily describe why an incident was flagged, counterfactual explanations emphasize how the outcome could have been different under realistic security configurations. This shift in perspective closely matches the reasoning processes of security analysts, who are primarily concerned with prevention, containment, and improvement rather than model introspection.

A key advantage of the proposed approach is its compatibility with the heterogeneous and evolving nature of SIEM environments. Because counterfactual explanations are formulated in a model-agnostic manner, they can be applied across diverse detection mechanisms, including rule-based correlations, statistical anomaly detectors, and machine-learning models. This flexibility is particularly important in real-world SOCs, where detection stacks are rarely uniform and often change over time. By operating at the level of log-evidenced conditions and security controls, the framework remains robust to such changes and can serve as a unifying explanatory layer.

Furthermore, log-driven counterfactual explanations naturally support structured post-incident learning. By explicitly linking incident outcomes to specific, controllable security conditions, they enable organizations to systematically identify recurring weaknesses and prioritize defensive investments based on demonstrated impact. Over time, this can contribute to more informed security architecture decisions and a gradual reduction in high-severity incidents. In this sense, counterfactual explanations function not only as an investigative aid but also as a strategic tool for continuous security improvement.

9. Limitations and Future Work. Despite its advantages, the proposed framework has several limitations that should be acknowledged. First, counterfactual explanations rely on assumptions about causal relationships inferred from log data. While logs provide rich observational evidence, they do not always capture the full context necessary to establish causality with certainty. As a result, counterfactuals should be interpreted as plausible alternatives rather than definitive causal claims. Future work could integrate stronger causal inference techniques or domain-specific causal models to improve the robustness of explanations. Second, the feasibility of recommended interventions may vary across organizations due to differences in infrastructure, policy constraints, and operational maturity. A counterfactual that is realistic in one environment may be impractical in another. Addressing this limitation requires further customization mechanisms that incorporate organization-specific constraints, cost models, and risk tolerance into the counterfactual generation process.

Third, the quality of counterfactual explanations is inherently dependent on the completeness and accuracy of log data. In environments with limited telemetry coverage or inconsistent normalization, explanations may be less reliable or overly conservative. Future research should explore methods for quantifying explanation uncertainty and for explicitly incorporating telemetry gaps into the explanation output. Finally, empirical validation of log-driven counterfactual explanations at scale remains an open research direction. While the framework is conceptually grounded in real SOC workflows, large-scale evaluations using real incident datasets and analyst feedback would provide stronger evidence of effectiveness. Future studies could focus on controlled deployments within SOCs, measuring improvements in triage time, mitigation quality, and long-term security posture resulting from the adoption of counterfactual explanations [11, p125724,13, p.453].

Conclusion

This paper presented a log-driven counterfactual explanation framework designed to address a critical gap in contemporary SIEM-based cybersecurity operations: the lack of actionable, evidence-grounded explanations that connect incident outcomes to concrete defensive choices. By treating SIEM incidents as structured, time-dependent aggregations of log evidence rather than isolated alerts, the proposed approach reframes explainability around operational relevance and defender agency. Grounding counterfactual explanations directly in log data allows recommended interventions to remain closely tied to observable security conditions, increasing their credibility and usefulness for security analysts. Instead of abstract indicators or opaque model outputs, the framework emphasizes minimal and feasible changes to controllable security settings, such as identity policies, endpoint protections,

network restrictions, and cloud access controls. This focus supports faster and more confident decision-making during incident response while also providing clear guidance for post-incident hardening and prevention.

Moreover, the log-driven nature of the framework enables it to operate in a model-agnostic manner, making it compatible with diverse SIEM detection strategies, including rule-based, statistical, and machine-learning–driven systems. By offering multiple plausible counterfactual pathways, the approach acknowledges the reality that there is rarely a single optimal defensive action and instead supports flexible, context-aware mitigation planning aligned with organizational constraints.

Overall, log-driven counterfactual explanations represent a practical and scalable step toward explainable, action-oriented cybersecurity analytics. By transforming SIEM incidents from opaque detection outputs into structured opportunities for targeted security improvement, the proposed framework contributes to more transparent, resilient, and continuously improving security operations in complex enterprise environments.

References

1. Wachter, S., Mittelstadt, B., & Russell, C. (2018). Counterfactual explanations without opening the black box: Automated decisions and the GDPR. *Harvard Journal of Law & Technology*, 31(2), 841–887. https://jolt.law.harvard.edu/assets/articlePDFs/v31/Counterfactual-Explanations-without-Opening-the-Black-Box-Sandra-Wachter-et-al.pdf

2. Mothilal, R. K., Sharma, A., & Tan, C. (2020). Explaining machine learning classifiers through diverse counterfactual explanations. *Proceedings of the ACM Conference on Fairness, Accountability, and Transparency*, 607–617. https://doi.org/10.1145/3351095.3372850

3. Sharma, A., & Aggarwal, A. (2020). Counterfactual explanations in machine learning: A survey. *arXiv preprint*. https://arxiv.org/abs/2005.03930

4. Guidotti, R., Monreale, A., Ruggieri, S., et al. (2019). A survey of methods for explaining black box models. *ACM Computing Surveys*, 51(5), Article 93. https://doi.org/10.1145/3236009

5. Choudhury, S., & Bhowal, A. (2022). Explainable AI in intrusion detection systems: State of the art and research challenges. *Journal of Information Security and Applications*, 66, 103158. https://doi.org/10.1016/j.jisa.2022.103158

6. Khan, N., Yaqoob, I., Hashem, I. A. T., et al. (2022). Big data analytics for intrusion detection: A review of data sources, techniques, and challenges. *Future Generation Computer Systems*, 131, 227–246. https://doi.org/10.1016/j.future.2022.01.008

7. Sarker, I. H. (2021). Machine learning: Algorithms, real-world applications and research directions. *SN Computer Science*, 2(3), Article 160. https://doi.org/10.1007/s42979-021-00592-x

8. Zhang, Y., Chen, J., & Li, X. (2023). Actionable explainable AI for network intrusion detection systems. *IEEE Access*, 11, 45621–45634. https://doi.org/10.1109/ACCESS.2023.3272146

9. Abdar, M., Pourpanah, F., Hussain, S., et al. (2021). A review of uncertainty quantification in deep learning: Techniques, applications and challenges. *Information Fusion*, 76, 243–297. https://doi.org/10.1016/j.inffus.2021.05.008

10. Ullah, I., Mahmoud, Q. H., & Ahmed, M. (2024). Explainable security analytics: Bridging detection and decision-making in SOC environments. *Security and Communication Networks*, Article ID 8893142. https://doi.org/10.1155/2024/8893142

11. Karim, M. R., Cochez, M., Beyan, O., & Decker, S. (2021). Explainable AI for trust and transparency in decision support systems. *IEEE Access*, 9, 125724–125741. https://doi.org/10.1109/ACCESS.2021.3111105

12. Shone, N., Ngoc, T. N., Phai, V. D., & Shi, Q. (2020). A deep learning approach to network intrusion detection. *IEEE Transactions on Emerging Topics in Computational Intelligence*, 4(1), 41–50. https://doi.org/10.1109/TETCI.2019.2895344

13. Ahmad, Z., Shahid Khan, A., Shiang, C. W., Abdullah, J., & Ahmad, F. (2021). Network intrusion detection system: A systematic study of machine learning and deep learning approaches. *Transactions on Emerging Telecommunications Technologies*, 32(1), e4150. https://doi.org/10.1002/ett.4150

SUBMERGED ARC WELDING OF BUTT JOINTS OF GRADE A SHIPBUILDING STEEL SHEETS ON ONE SIDE IMMEDIATELY AFTER PLASMA CUTTING

Peleshenko S.,
Korzhyk V.,
Lahodzinskyi I.,
Vdovychenko I.,
Tereshchenko O.,
Vdovychenko D.
E.O. Paton Electric Welding Institute, National Academy of Sciences of Ukraine
Kyiv, Ukraine
Haichao Wang,
Yuejun Sun
Shandong (Yantai) Sino-Japan Industrial Technology Research Institute (Yantai) Industrial Technology Research Institute / West Tower of the Chuangye Building, No. 69, Keji Avenue, High-tech Zone, Yantai, Shandong, China
Khaskin V.,
Guirong
E.O. Paton Electric Welding Institute, National Academy of Sciences of Ukraine
Kyiv, Ukraine
DOI: 10.5281/zenodo.18655683

ABSTRACT

This study is dedicated to developing approaches for applying submerged arc welding to extended sheet shipbuilding structures (such as panels and beams) made of low-carbon steel immediately after plasma cutting, without additional edge preparation. The selected submerged arc welding parameters allow for achieving satisfactory weld quality when welding edges produced by plasma cutting without further processing. A positive effect was observed in all specimens. It has been established that without securing the welding head to the deforming surface of the welded components, the electrode overhang decreases, and welding mode parameters change up to arc interruption. Specialized equipment is required to correct such deflection, and the presence of weld reinforcement complicates the straightening operation. Furthermore, conventional single-sided, single-pass submerged arc welding on ceramic forming backing strips, despite the beneficial influence of the substantial heat capacity of the welding flux, leads to the formation of hardened microstructures in the weld metal and reduces its ductility due to significant cooling rates and the rapid progression of phase transformations.

Keywords: single-sided single-pass submerged arc welding, shipbuilding steel grade A, edge welding after plasma cutting, weld bead shaping, microstructure, pore minimization.

Submerged arc welding, as the primary method for fabricating panels and beams in shipbuilding, has been utilized since the early twentieth century [1]. Despite considerable research [2–4] aimed at improving the efficiency of submerged arc welding in shipbuilding practice, this technology has not experienced significant changes. The primary challenge in its application is the welding distortions occurring during the fabrication of large-scale components, which adversely affect both sectional and slipway assembly procedures, as well as the vessel's aesthetic quality. Submerged arc welding of hull structures in the vertical position is predominantly performed in a double-sided configuration (for butt joints of small thicknesses, type C7 is applied, while for thicknesses of 14 mm, type C21 is used in accordance with ISO 9692-1 and ISO 15792). The employment of such joints is justified solely from the perspective of tempering the initial pass with the subsequent one and partially reducing distortion levels, rather than fully eliminating them. Simultaneously, a double-sided weld requires operations such as structural restraint release, edge bending of the sheet, cleaning of the reverse side, and additional fastening, which are performed along the sheet perimeter rather than within the heat-affected zone. The ability of the weldable structures and fixtures to accumulate heat under constant welding parameters leads to increased penetration depth and uneven fusion along the weld length. The effect of energy balance shifting towards melting of the welding wire with increased welding current, necessitating bead overlap, causes an increase in weld width and reinforcement height, but decreases penetration depth [5] and increases the likelihood of lack of fusion.

Studies [6–8] on mathematical modeling of the submerged arc welding process are documented; however, the multivariate nature and complexity of factors affecting the characteristics of submerged arc welding—including the thermophysical properties of the flux, welding wire, and base metal; structural differences in the deposited metal between the first and second passes; the considerable length of welds; and environmental conditions such as drafts in workshops—diminish the effectiveness of such modeling. In submerged arc welding modeling, the possibility of utilizing blanks obtained directly by plasma cutting without any mechanical processing is generally not considered. From the standpoint of enhancing the productivity of ship structure fabrication and reducing their manufacturing cost, this aspect is of critical importance.

The process of single-pass, one-sided automatic submerged arc welding using forming devices (ceramic, copper, and flux backing, copper runners) is also

preferable and economically advantageous; however, increasing the power of the heat source elevates the volume of molten metal in the weld pool and, accordingly, increases the volume of solidifying metal, thereby augmenting the degree of deformation. This phenomenon is particularly pronounced in extended joints.

Patent [9] describes an arc welding method that significantly reduces internal stresses and deformations in extended single-pass, single-sided welded joints. The concept involves suppressing the sequential polymorphic phase transformations in the weld metal that contribute to the accumulation of internal stresses, followed by post-weld tempering of the entire joint to guarantee the formation of a homogeneous ferrite-pearlite microstructure within the heat-affected zone (HAZ).

Despite recent research efforts (e.g., studies [10, 11]), the predominant approach to welding steel components cut by plasma methods remains mechanical edge preparation. This approach necessitates the implementation of a corresponding technological operation. To reduce the cost and duration of preparing the edges of steel components for subsequent submerged arc welding, it is advisable to develop welding approaches that enable the formation of high-quality joints with minimal internal porosity and acceptable mechanical properties.

The objective of this study is to develop methodologies for applying the submerged arc welding technique to extended sheet shipbuilding structures (such as panels, beams, etc.) composed of low-carbon steel immediately following plasma cutting, without additional edge preparation.

Figure 1 depicts the external appearance of the assembled joint prepared for welding. Welded specimens (1) of grade A sheet steel measuring 100×430×5 mm were assembled according to node C4 without a gap (ISO 9692-1 and ISO 15792), on technological bars (100×40×5 mm), secured by two tack welds (10–15 mm), with placement of flat ceramic pads PZ 1500/72 (2) and ceramic electric heaters KEN B-60-21-5 sized 525×105 at the root of the assembly (3).

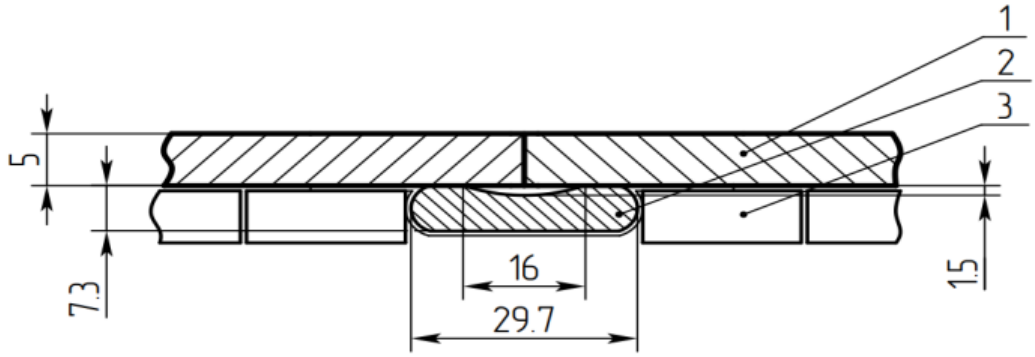

Fig. 1. Sample assembled for welding.

Welding of the samples was performed on the automatic ADF-1250 machine using Sv-08A wire, Ø4 mm, with AN-348A flux, and the VDU-1250 unit. Heat treatment was conducted using a 70 kW power unit, model RT70-6. The feedback sensor was a type XA thermocouple (chromel–alumel). Thermal insulation material Supersil, 10 mm thick. Welding and heat treatment modes are presented in Table 1.

Table 1.

Welding and heat treatment modes.

Sample number	Current I, A	Arc voltage U, V	Welding speed V, cm/min	Preheating temperature, °C	Cooling rate, °C/h
1	250	24	21	400	150
2	200	24	50	600	150
3	280	24	30	400	150
4	300	24	25	450	150
5	325	24	25	450	150
6	350	24	23	450	150

To ensure complete thermal insulation of the sample and eliminate the need to mount the tractor on the workpiece, a test rig was developed (Fig. 2) featuring two independent platforms: a welding table and a tracker for the welding tractor.

Fig. 2. Experimental test rig.

Welding was performed without the use of fastening or clamping devices securing the sample. The assembled welding sample was placed on the table over a layer of thermal insulation material. Each plate was covered with a strip of thermal insulation, leaving a gap of 35–40 mm between the strips to allow for welding. During heating, it was also covered with a strip of thermal insulation material.

Upon reaching the programmed heating temperature, the upper layer of insulation was removed, welding was performed, and without flux removal, the sample was covered with thermal insulation, followed by programmed cooling to 150°C. The geometric parameters of the welds were measured using a metal ruler and calipers. The longitudinal deflection of the welded specimen was measured with a feeler gauge placed between the plate and an applied metal ruler.

Static tensile tests were performed using a universal servo-hydraulic testing machine, MTS 318.25 (USA, Material Test System), on type XII specimens according to GOST 6996-66. Hardness was measured using an HR-150A hardness tester on the HRA scale on both the face and root surfaces of the welded joint with 1 mm measurement intervals from the weld center toward the base metal. Microhardness measurements across the weld cross-section were conducted on polished specimens using a Shimadzu HMV-2 series microhardness tester.

The preparation of templates cut from the welds for microstructural investigations was performed on a DeltaAbrasiMet bench abrasive machine and an EcoMet 250 Pro grinding and polishing system. Sample etching was carried out in a 5% alcoholic nitric acid solution. Structural analysis and internal defect detection were carried out using MIM-8 microscopes (magnifications 100 to 1350×) and NEOPHOT-32 microscopes (magnifications 25 to 1500×).

The application of Mode 1 (Table 1) resulted in burn-through defects (Table 2). The cause of this defect is the detachment of the ceramic backing from the sample surface, caused by excessive welding wire feed at low welding speed.

Table 2.

Appearance and dimensions of the face and root sides of the weld.

Sample		Reinforcement height, mm	Reinforcement width, mm	Longitudinal deflection, mm	Weld appearance
Number	Side				
1	Face	-4,0	17,4	10	
	Root	4,0	20,2		
2	Face	1,4	10,4	1	
	Root	0	0		
3	Face	1,3	18,3	2,5	

	Root	1,6	7,5		
4	Face	0,8	19,8	3,5	
	Root	1,4	10,6		
5	Face	1,3	23,0	3,5	
	Root	1,4	11,6		
6	Face	1,0	24,6	3	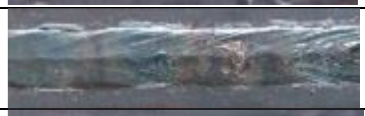
	Root	1,8	16,4		

The increase in welding speed and the decrease in welding current in mode 2 resulted in the absence of root reinforcement formation. In sample 3, partial filling of the backing form by the root reinforcement was achieved, whereas in samples 4, 5, and 6, the weld root metal followed the contours of the ceramic backings along the entire length. The geometric parameters of the welds in welded joints produced under modes 4 and 5 correspond to joint type C4 according to ISO 9692-1 and ISO 15792, with a maximum deflection of 3.5 mm. The greatest deflection value was observed in the first specimen—10 mm.

Thermograms of all specimens are presented in Fig. 3, which demonstrates that following uniform programmed heating and welding under a thermal insulation layer at the thermocouple locations, an additional temperature increase up to 600°C occurred, substantiating that the polymorphic transformation temperature was reached in the heat-affected zone. It is also notable that in Mode 2 (preheating to 600°C), no significant temperature increase occurs during welding, indicating the impracticality of such thermal saturation, as the temperature rise after welding caused by the arc action in other modes results in self-tempering of the entire deposited metal volume and the heat-affected zone of the welded joints from the polymorphic transformation temperature, without additional heating.

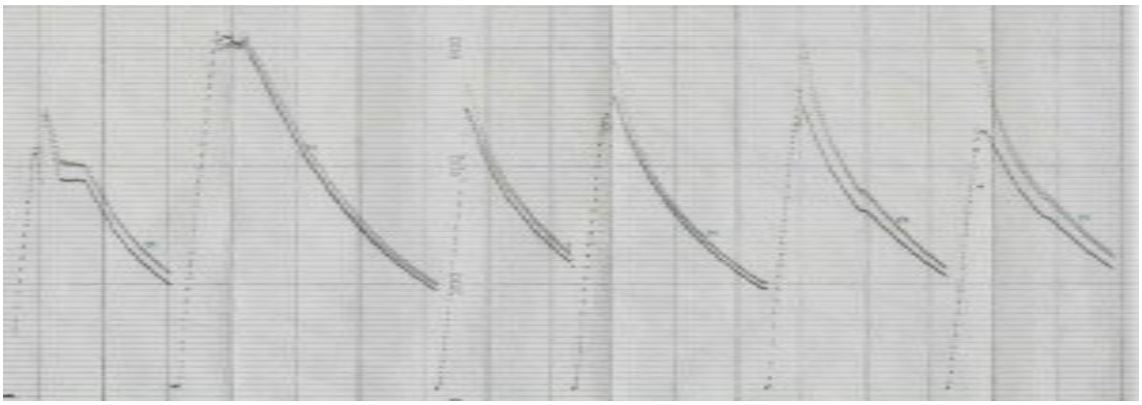

Fig. 3. Thermograms of samples (vertical axis – temperature; horizontal axis – time).

Mechanical properties and microstructure tests were performed on samples with fully formed welds: 4, 5, and 6. Results of static tensile tests are presented in Table 3.

Table 3.

Results of static tensile testing.

Sample numbers	Tensile strength $\sigma_в$, MPa	Yield strength $\sigma_т$, MPa	Proportional limit $\sigma_{0,2}$, MPa	Relative elongation δ, %	Young's modulus, MPa
4.1	660	500	128	43	31685
4.2	548	415	89	42	25480
4.3	552	470	46	41	13697
5.1	533	390	40	42	5782
5.2	530	390	44	42	15008
5.3	527	395	36	43	12924
6.1	522	380	49	42	6809
6.2	533	390	55	47	19741
6.3	523	380	38	41	15315
Not less than					
GOST 5521-93	400-490	315	-	22	-

All specimens fractured in the base metal, and their mechanical properties comply with the requirements of ISO 630-6 for Grade A hot-rolled steel sheets. Meanwhile, the values of σв, σт, and σ0.2 for specimen 4 are higher than those of specimens 5 and 6. The relative elongation values of the specimens are practically identical and exceed the base metal requirements by a factor of two.

The conducted experiments indicate that isothermal tempering positively influences not only the mechanical properties of the welded joint but also the base metal.

The microstructure of the investigated samples (Table 4, Fig. 4) is characterized by four zones: weld metal (I), recrystallization zone (II), overheating zone (III), and base metal (IV).

In the deposited metal, the weld microstructure exhibits a ferrite-pearlite structure with globular grains lacking preferred orientation. The grain size is four times larger than that of the base metal. At the fusion line, the grain size remains unchanged, but the grains are oriented from the fusion line towards the weld center.

The recrystallization zone in samples 4, 5, and 6 exhibits an identical structure. The grain size from the fusion line towards the base metal is identical to that from the fusion line towards the weld center. This zone is characterized by a random arrangement of grains. Areas of stringer structure corresponding to the rolled material are observed at the center. This zone exhibits a gradual transition to a finer structure of the third zone.

The base metal is characterized by a fine-grained laminar structure. Sample 6 demonstrated the greatest extent of the heat-affected zone (Table 5); the smallest HAZ length on the face side was observed in sample 4, while on the reverse side of the weld, it was sample 5.

Table 4.

Microstructure of the weld joint zones, ×400.

Region	Sample No.		
	4	5	6
Weld metal (I)	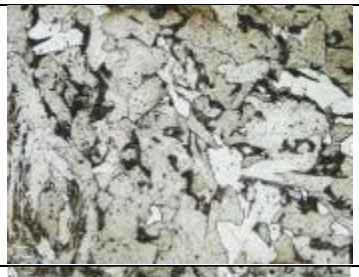		
Fusion line	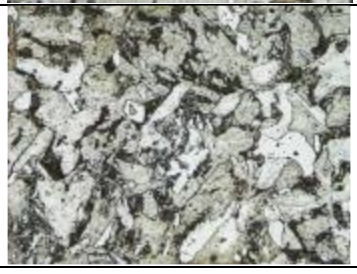	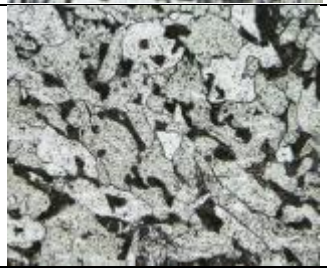	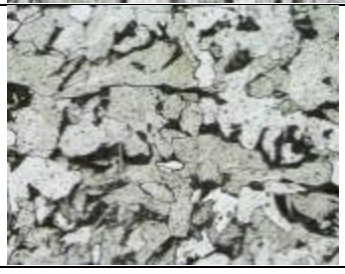

Re-crys-talli-zation zone (II)		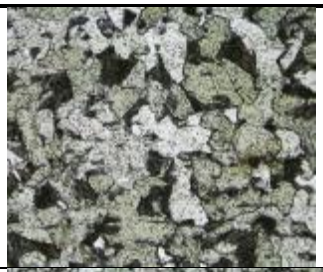	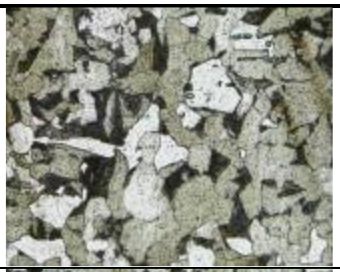
Over-heated zone (III)	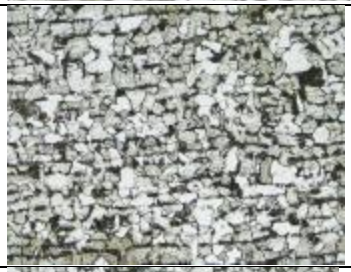	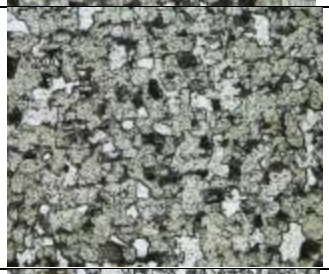	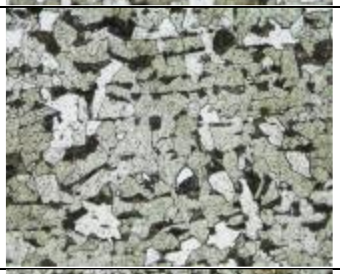
Base metal (IV)	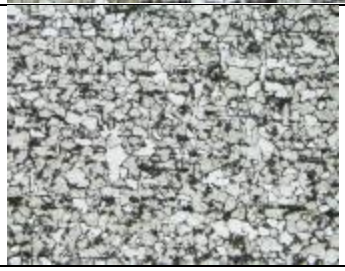	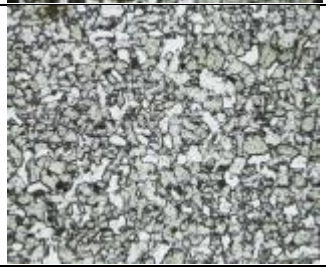	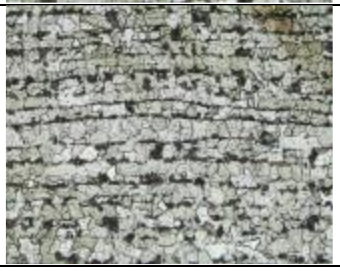

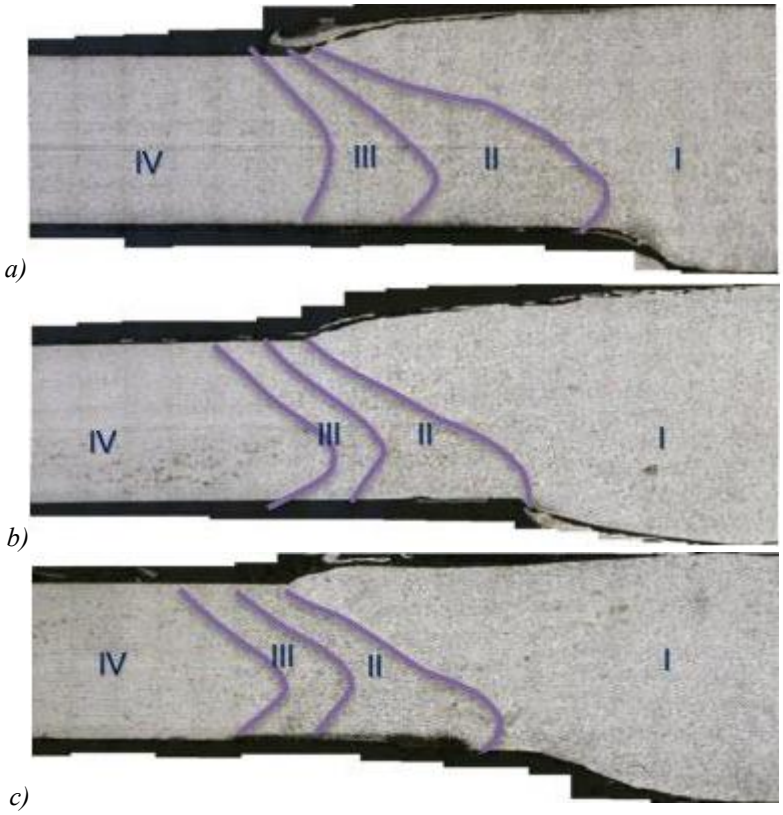

Fig. 4. Microstructure of welds: a) – sample No. 4; b) – sample No. 5; c) – sample No. 6.

Table 5.

Dimensions of heat-affected zones.

Sample number	HAZ dimension on the weld face side, mm	HAZ dimension on the weld root side, mm	Recrystallization zone area, mm^2	Transition zone area, mm^2	Total HAZ area, mm^2
4	3,7	9,4	26,4	20	46,4
5	3,9	8,2	26,5	15	41,5
6	5,2	10	32,2	22	54,2

The highest heat-affected zone areas were observed in sample 6, and the lowest in sample 5, due to an increase in welding current. Therefore, the welded joint produced under mode 5 is the most optimal.

The hardness profiles across the surfaces of the examined samples (Fig. 5) revealed a minimum hardness value of 47 HRA in the outer reinforcement regions of samples 4 and 5, corresponding to the hardness values specified for Grade A steel sheet in the as-delivered state (42 HRA).

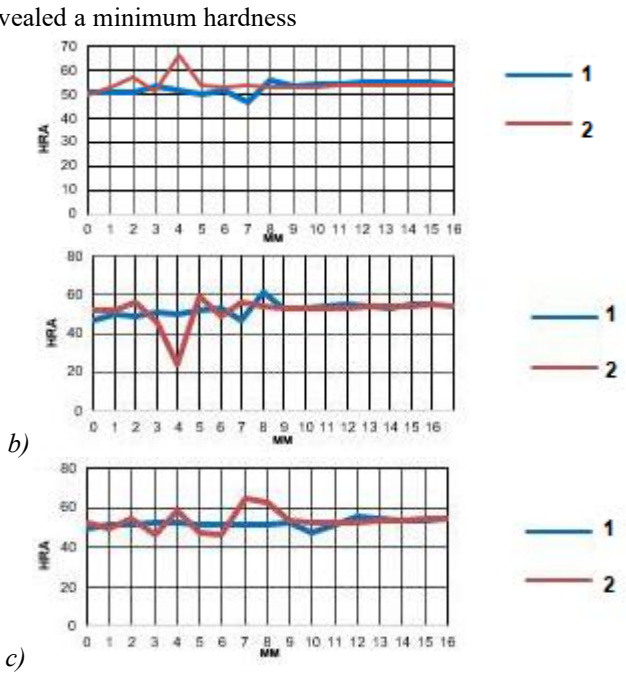

Fig. 5. Graphs of hardness distribution across the surfaces of the face and reverse sides of the weld (1 – hardness of the outer weld surface; 2 – hardness at the weld root): a) sample No. 4; b) sample No. 5; c) sample No. 6.

In the deposited metal and heat-affected zone (HAZ), on both the face and reverse sides of the weld, the average hardness values of the samples are identical. When comparing the hardness of the samples, the values are approximately equal. The hardness value exhibits a uniform distribution from the center of the weld to the base metal. Graphs of microhardness distribution across the cross-section are presented in Figure 6. Samples 4, 5, and 6 demonstrate uniform microhardness distribution in the heat-affected zone.

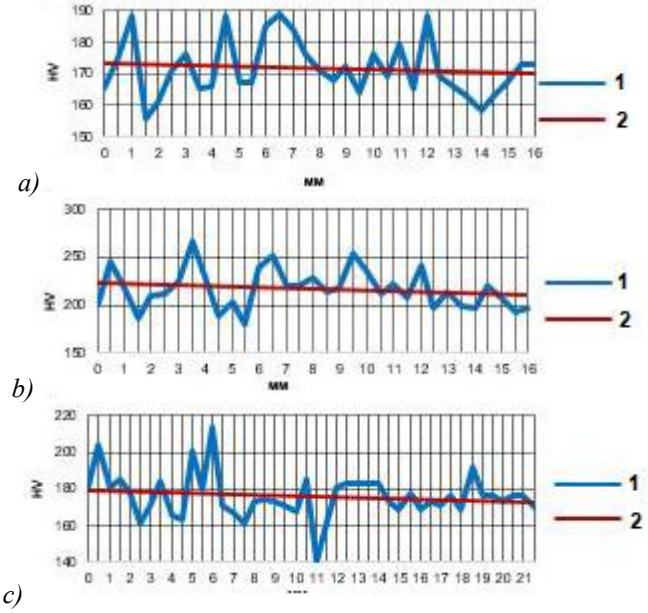

Fig. 6. Graphs of microhardness distribution across the weld cross-section (1 – measured hardness; 2 – linear hardness): a) Sample No. 4; b) Sample No. 5; c) Sample No. 6.

The boundary complexity was evaluated by fractal dimension, determined using Image-Pro Plus software. Figure 7 presents the measurement results and calculated quantitative indicators of the perimeter and area of microstructural features.

The histograms of the distribution indicate that the first sample exhibits the highest values of average area and fractal dimension, reflecting more developed grain boundary interfaces. This observation corresponds to superior strength characteristics of the welded joint, consistent with the distinctly dendritic structure of the sample.

In samples 4, 5, and 6, from the weld metal zone to the recrystallization zone, an increase in fractal dimension is observed, followed by a decrease toward the base metal zone; this is attributed to the well-developed boundaries in the recrystallization zone, corresponding to higher hardness values in this region.

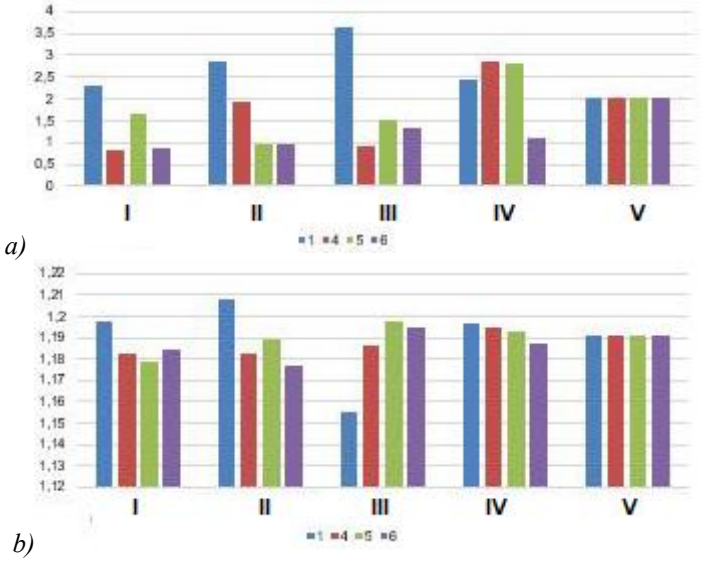

Fig. 7. Histograms of distribution (I – weld metal zone; II – fusion line; III – recrystallization zone; IV – heat-affected zone; V – base metal): a) mean object area; b) fractal dimension.

No internal defects were detected during microstructural analysis.

Conclusion.

The selected submerged arc welding parameters allow for achieving satisfactory weld quality when welding edges produced by plasma cutting without further processing. A positive effect was observed in all specimens. The dimensions of the welded and tested samples are limited in size, which enables evaluation of the weld quality formed when welding edges immediately after plasma cutting and only allows indirect assessment of the success of welding extended joints without deformation. The final point requires further investigation. Nevertheless, welding without preheating or controlled volumetric cooling, and without clamping the welded parts to the fixture, necessitates higher welding current values and induces longitudinal

deformations with deflections up to 50 mm over a weld length of 430 mm. When the welding head is not fixed to the deforming surface of the welded parts, electrode extension decreases and welding mode parameters change, potentially leading to arc interruption. Specialized equipment is required to correct such deflection, and the presence of weld reinforcement complicates the straightening operation. Furthermore, conventional single-sided, single-pass submerged arc welding on ceramic forming backing strips, despite the beneficial influence of the substantial heat capacity of the welding flux, leads to the formation of hardened microstructures in the weld metal and reduces its ductility due to significant cooling rates and the rapid progression of phase transformations.

References

1. Khokhlov B.Z. Svarka v sudostroenii L.: Sudoverfi – 160 s.

2. Lebedev V.A., Zhuk G.V., Dragan S.V., Simutenkov I.V., Goloborod'ko Zh.G. (2017). Razrabotka tekhnologii avtomaticheskoy naplavki pod flyusom s poperechnymi vysokochastotnymi kolebaniyami elektrodnoy provoloki // Tyazheloe mashinostroenie, 6: 15-18.

3. Razmyshlyaev A. D., Ageeva M. V. (2019). Povyshenie effektivnosti elektrodugovoy naplavki v prodol'nom magnitnom pole // Vestnik DGMA, 2 (46): 35–40. Kumar, A., Singkh, K. (2020). Razrabotka ekzotermicheskogo flyusa dlya uluchshennogo proplavleniya pri dugovoy svarke pod flyusom // Journal of Advanced Manufacturing Systems, 19 (1): 131-146. DOI: 10.1142/S0219686720500079

4. Bakhmatov P.V., Moskaeva A.V., Startsev E.A., Usanov G.I. (2019). Opyt primeneniya flyusa OK FLUX 10.71 i provoloki 12-22 dlya svarki dvukhstoronnikh stykovykh soedineniy nizkouglerodistoy stali // Uchenye zapiski Komsomol'skogo-na-Amure gosudarstvennogo tekhnicheskogo universiteta, III-1(39): 81-95.

5. Dzhindal S., Chibber R., Mekhta N. P. (2014). Modelirovanie khimicheskogo sostava flyusa dlya svarki pod flyusom vysokoprochnykh nizkolegirovannykh staley // Trudy Instituta inzhenerov-mekhanikov, Chast' B: Zhurnal mashinostroeniya, 228 (10): 1259-1272. DOI: 10.1177 / 0954405413517364

6. Karaoğlu, S., Seçgin, A. (2008). Sensitivity analysis of submerged arc welding process parameters // Journal of Materials Processing Technology, 202 (1-3): 500-507. DOI: 10.1016/j.jmatprotec.2007.10.035

7. Choudkhari A., Kumar M., Gupta M.K. i dr. (2020). Popravki k: Matematicheskomu modelirovaniyu i intellektual'noy optimizatsii parametrov protsessa svarki pod flyusom s ispol'zovaniem gibridnykh evolyutsionnykh algoritmov PSOGA // Neyronnye vychisleniya i prilozhenie, 32: 11961. DOI: https://doi.org/10.1007/s00521-019-04490-5

8. Pat. 2557041 RF, MPK V 23 K 9/035, V 23 K 9/32. Sposob svarki plavleniem satl'nykh konstruktsiy i ustroystvo dlya ego realizatsii / Bakhmatov P. V. Tishkova E. E. Murav'ev V. I. Melkostupov K. A. Frolov A. V.; zayavitel' i patentoobladatel' Komsomol'sk-na-Amure «KnAGTU». - № 2014104339/02; zayavl. 07.02.2014; opubl. 20.07.2015, Byul. № 20. - 6 s.: il.

9. Easterling K. E. (1992). Introduction to the Physical Metallurgy of Welding, 2th ed., Oxford, UK: Butterworth-Heinemann Ltd.

10. Murphy A. B, Colombo V., Mostaghimi J. Arc welding, plasma cutting and plasma spraying. Journal of Physics D: Applied Physics, 2013, Volume 46, Number 22, 46 220301. DOI: https://doi.org/10.1088/0022-3727/46/22/220301

11. Nishiguchi K. Plasma Arc Welding and Cutting. In: North, T.H. (eds) Advanced Joining Technologies. Springer, Dordrecht, 1990. DOI: https://doi.org/10.1007/978-94-009-0433-0_3

SPOOFING-AWARE TRAFFIC SIGN RECOGNITION USING SELF-SUPERVISED ANOMALY DETECTION AND PREDICTIVE UNCERTAINTY

Mustafayev O.
Vizja University, Department of Computer Science, Master's student
Warsaw, Poland
DOI: 10.5281/zenodo.18655710

ABSTRACT

Traffic Sign Recognition (TSR) models are increasingly deployed in driver-assistance and autonomous driving pipelines, yet they remain vulnerable to *spoofing* and real-world manipulations such as stickers, overlays, graffiti, adversarial posters, and reflective film additions. These attacks can trigger confident misclassification—an especially hazardous failure mode because downstream planning and control subsystems often trust high-confidence predictions. This paper proposes a spoofing-aware TSR framework that integrates (i) self-supervised anomaly detection to identify distribution shifts and suspicious sign appearances without requiring labeled spoof examples, and (ii) predictive uncertainty modeling to quantify epistemic and aleatoric uncertainty and suppress overconfident errors. The approach combines representation learning from large-scale unlabeled driving data with reconstruction/consistency-based anomaly scoring and uncertainty-aware decision logic. We outline architecture components, training objectives, deployment strategy, and an evaluation protocol spanning physical tampering, synthetic spoofs, and natural corruptions. The framework aims to improve operational safety by enabling "detect–defer–downweight" behaviors: detect suspicious signs, defer to cautionary policies, and reduce the impact of unreliable predictions.

Keywords: Traffic sign recognition, spoofing, anomaly detection, self-supervised learning, uncertainty estimation, out-of-distribution detection, autonomous driving safety, robustness.

1. Introduction

Traffic Sign Recognition (TSR) has become a foundational capability for advanced driver-assistance systems and autonomous driving platforms, where perception outputs directly influence speed regulation, right-of-way compliance, lane discipline, and hazard anticipation. Over the past decade, deep learning has substantially improved TSR accuracy under benchmark conditions; nevertheless, real-world deployments continue to expose a persistent gap between laboratory performance and operational reliability. This gap is particularly important because TSR decisions are safety-critical: even rare recognition failures can have disproportionate downstream consequences when integrated into automated planning and control loops. A key reason for this mismatch lies in the nature of roadside environments. Traffic signs are observed under rapidly changing illumination, weather, motion blur, partial occlusion, aging materials, and sensor artifacts. In addition to these natural sources of variability, an increasingly urgent challenge is spoofing and physical manipulation. Signs may be altered intentionally (e.g., targeted overlays, deceptive patches, adversarial posters) or incidentally (e.g., stickers, graffiti, tape, dirt patterns, reflective films). Such interventions can distort the sign's iconography, shape cues, contrast boundaries, or reflective properties while still appearing plausible to human drivers. For data-driven TSR models, these manipulations often behave as distribution shifts: inputs deviate from the training distribution in a way that standard supervised learning does not explicitly model [1,p.69].

Critically, spoofing-related errors are not only about misclassification; they are also about miscalibrated confidence. Many modern classifiers can produce incorrect predictions with high confidence under out-of-distribution (OOD) inputs. In a safety pipeline, this failure mode is more hazardous than uncertainty-aware errors, because downstream modules may treat high-confidence outputs as reliable and act immediately. Therefore, a robust TSR system should not merely maximize nominal accuracy; it should also provide mechanisms to detect suspicious inputs and quantify when predictions are unreliable. Traditional robustness strategies such as larger labeled datasets, aggressive augmentation, and architectural scaling improve performance under common corruptions but remain insufficient for spoofing scenarios that are diverse, evolving, and difficult to label comprehensively. In realistic settings, collecting and annotating a complete taxonomy of physical spoofs is costly and often lags behind emerging attack patterns [2, p.236].

This motivates methods that can generalize beyond known manipulations and remain effective even when spoof labels are limited or absent. Recent progress in self-supervised learning (SSL) offers a promising foundation for this goal. SSL enables models to learn strong visual representations from large volumes of unlabeled data by exploiting intrinsic supervisory signals (e.g., consistency across augmentations, reconstruction of missing content, or temporal coherence in videos). For TSR, such representations can capture stable structural regularities of "normal" sign appearance, which can be leveraged for anomaly detection—flagging inputs that deviate from learned normality. Complementarily, predictive uncertainty estimation provides a principled way to reduce overconfident failures by assigning higher uncertainty to inputs where the model lacks reliable knowledge, especially under OOD and spoofing conditions. Despite the relevance of these directions, spoofing-aware TSR is still underdeveloped as an integrated, deployment-oriented solution. Many studies address robustness, anomaly detection, or uncertainty modeling separately, leaving open the practical question of how to combine these components into a unified pipeline that supports safety-oriented decision logic in real traffic [3, p.342]

Purpose of the study. Motivated by this gap, this paper proposes a spoofing-aware TSR framework that combines self-supervised anomaly detection with predictive uncertainty estimation to mitigate the risk of confident misrecognition under physical manipulation and distribution shift. The central idea is to move from "always predict a label" to "predict only when reliable," enabling operational behaviors such as *detect–defer–downweight*: detect suspicious signs, defer decisions when necessary, and downweight unreliable predictions through uncertainty-aware gating. By aligning recognition with reliability assessment, the proposed approach targets safer TSR deployment in next-generation intelligent transportation systems.

2. Problem statement and threat model

Traffic sign recognition systems typically generate a sign label together with a confidence score that is assumed to reflect prediction correctness under normal conditions. In real-world environments, however, this assumption often breaks down due to spoofing, physical manipulation, or out-of-distribution inputs. Visual alterations or unexpected patterns may lead to incorrect predictions with misleadingly high confidence, creating a serious risk in safety-critical applications where downstream modules may rely directly on perception outputs. Consequently, the key challenge addressed in this study is not only recognition accuracy but the reliability of traffic sign recognition under abnormal and adversarial conditions. To address this challenge, traffic sign recognition must extend beyond single-label prediction and incorporate reliability-aware outputs. A spoofing-aware system should indicate when a prediction is unreliable, detect deviations from normal sign appearance, and explicitly represent uncertainty. This shifts traffic sign recognition from a purely classification-based task to a risk-aware perception process, where uncertainty and abnormality are central to decision-making. Traffic sign spoofing in real road environments appears in diverse and often unpredictable forms. Common manipulation patterns include surface-level alterations such as stickers, graffiti, dirt, fading, or partial occlusion, as well as overlay-based modifications designed to induce targeted misclassification. Contextual spoofing further complicates recognition when signs are placed in atypical or conflicting environments that challenge local, appearance-based models. These manipulation types represent realistic threats that cannot be exhaustively anticipated or labeled in advance. Addressing such threats requires a spoofing-aware design that preserves high performance under nominal conditions while avoiding overconfident errors under manipulation or distribution shift. The system should detect anomalous inputs without relying on extensive spoof annotations and integrate with downstream autonomy modules to support safe, conservative decision behavior [4,p.212,5,p.95]

3. Methodology

The proposed methodology is based on the premise that reliable traffic sign recognition in real-world environments requires more than accurate classification. It also requires the ability to identify abnormal visual patterns and to assess prediction reliability under uncertainty. To this end, a spoofing-aware traffic sign recognition framework is introduced as an additional safety layer on top of a conventional TSR pipeline. Rather than replacing existing detection or classification models, the framework augments them with reliability-oriented signals that support safer decision-making and maintain compatibility with current intelligent transportation systems. A central component of the approach is self-supervised representation learning, which models normal traffic sign appearance using large volumes of unlabeled driving data. By learning consistent and structurally meaningful representations under realistic augmentations and partial visual disruption, the model captures stable characteristics of legitimate signs while remaining sensitive to abnormal alterations. These learned representations form a reference space that reflects expected visual regularities without requiring manually labeled spoofing data.

Based on this representation space, anomaly detection is performed by measuring deviations from normal patterns rather than attempting to classify specific manipulation types. Indicators derived from reconstruction difficulty, feature inconsistency, and distributional deviation are used to identify suspicious sign appearances. This strategy enables the detection of previously unseen manipulations and supports generalization beyond predefined spoof categories. Anomaly detection is treated as a continuous signal, allowing flexible integration with other reliability measures. To further reduce overconfident misrecognitions, predictive uncertainty estimation is incorporated into the recognition process. By evaluating prediction stability under stochastic or model-based variation, the system identifies cases where classification decisions are unreliable, even when confidence scores appear high. This uncertainty signal complements anomaly detection by capturing ambiguity arising from distribution shifts or rare visual conditions. The final output is produced through a fusion of predicted labels, anomaly scores, and uncertainty estimates. Instead of enforcing decisions in all cases, the framework supports selective prediction and safety-oriented responses, such as decision deferral, temporal confirmation, or conservative fallback behavior in downstream modules. Training and validation are conducted in sequential stages, combining self-supervised learning on unlabeled data with supervised fine-tuning on labeled datasets and calibration using benign validation samples. This modular strategy improves flexibility, reduces dependence on spoof-specific annotations, and facilitates adaptation to new environments.

4. Experimental design and evaluation This section describes the evaluation protocol for the proposed spoofing-aware traffic sign recognition (TSR) framework. The design emphasizes deployment-realistic robustness: clean accuracy is preserved, while spoofing and out-of-distribution (OOD) conditions are assessed using reliability-oriented metrics (anomaly detection quality, calibration, and risk-coverage trade-offs).

4.1. Datasets and Data Preparation. To ensure broad coverage, experiments are performed using three complementary data sources: (i) labeled traffic sign datasets for supervised classification, (ii) large-scale unlabeled driving imagery or video for self-supervised pretraining, and (iii) robustness stress tests that include

natural corruptions and spoof-like manipulations. Labeled TSR data: used to train or fine-tune the sign classifier and to report standard recognition performance. Unlabeled driving data: used for self-supervised representation learning to model normal sign appearance and dynamics. Robustness sets: used for evaluation and threshold calibration, including natural corruptions and spoofing/tampering variants.

All sign crops are standardized to a fixed resolution. Standard preprocessing includes resizing, aspect-ratio preserving padding where needed, and normalization consistent with the backbone network. When video is available, frame sequences are retained for temporal consistency tests [6,p.56,7,p345]

4.2. Spoofing and OOD Evaluation Scenarios

Evaluation scenarios are organized to reflect practical roadway threats. The goal is to measure not only misclassification frequency, but also the tendency toward overconfident errors and the ability to flag suspicious inputs. Clean (in-distribution) condition: standard test split without additional perturbations. Natural corruptions: rain, fog, glare, motion blur, low light, compression artifacts, and partial occlusions. Surface tampering: sticker-like occlusions, graffiti marks, tape strips, dirt patterns, and partial coverings, overlay spoofing: printed overlays/patches and reflective-film style distortions, including headlight-like illumination shifts. Context shift (optional): unfamiliar regions, sign styles, backgrounds, and rare categories to simulate domain transfer.

Table 1.

Evaluation dimensions and safety-oriented performance criteria for spoofing-aware traffic sign recognition

Evaluation aspect	**Test scenario**	**Main objective**	**Observed system Behavior**	**Safety implication**
Baseline recognition performance	Clean test set	Verify nominal TSR accuracy	Maintains high accuracy comparable to supervised baselines	Ensures no degradation under normal conditions
Robustness to natural corruptions	Blur, rain, fog, low light, compression	Assess stability under common environmental variations	Increased uncertainty in ambiguous cases, reduced overconfidence	Prevents unreliable confident predictions
Resistance to surface tampering	Stickers, graffiti, dirt, partial occlusion	Detect abnormal sign appearance	Elevated anomaly scores for manipulated signs	Reduces risk of misinterpretation due to physical damage
Robustness to overlay spoofing	Printed patches, reflective overlays, icon alterations	Identify intentional manipulation	Combined anomaly and uncertainty signals flag suspicious inputs	Mitigates targeted spoofing attacks
Generalization under context shift	Unfamiliar regions, sign styles, rare classes	Evaluate out-of-distribution behavior	Selective prediction with higher deferral rate	Avoids unsafe decisions in unfamiliar domains
Prediction reliability	All test categories	Assess confidence–correctness alignment	Improved calibration and reduced overconfident errors	Enhances trustworthiness of TSR outputs
Risk–coverage trade-off	Deferred vs accepted predictions	Balance safety and usability	Lower error rate on accepted predictions	Supports safety-oriented deployment policies

The table summarizes the key evaluation dimensions used to assess the proposed spoofing-aware traffic sign recognition framework, highlighting its impact on robustness, reliability, and safety-oriented decision behavior across diverse operational scenarios.

4.3. Baselines and Comparisons. To attribute improvements to the proposed components, results are compared against strong TSR baselines and ablated variants. The following baselines are recommended: Standard supervised TSR classifier (no anomaly module, no uncertainty estimation). Supervised classifier with data augmentation only (robust augmentation baseline). OOD detection baseline using simple confidence thresholding (maximum softmax probability). Uncertainty-only baseline (e.g., MC dropout or ensemble) without anomaly scoring. Anomaly-only baseline (self-supervised anomaly scoring) without uncertainty gating.

4.4. Metrics. Metrics are selected to capture recognition performance, spoofing/OOD detection ability, and reliability/calibration. In addition to accuracy, the evaluation emphasizes safe behavior: avoiding confident misrecognition. Top-1 accuracy (clean and corrupted conditions), misrecognition rate under spoofing/tampering (overall error frequency). Anomaly detection quality: AUROC and AUPRC for normal vs manipulated inputs. Calibration: Expected Calibration Error (ECE) and reliability diagrams. Risk-coverage: error rate as a function of accepted prediction fraction when the system may defer/abstain [8,p.645].

Key formulae (provided in Word-friendly linear form):

1) Anomaly score fusion:

A(x) = alpha * A rec(x) + beta * A_ feat(x) + gamma * A_ cons(x)

2) Reconstruction-based anomaly component (example):

A_ rec(x) = || x - g(f(x)) ||_1

3) Predictive entropy (uncertainty from class probabilities):

H(p) = - sum_{c=1.C} p_ c * log(p_ c)

4) MC dropout / ensemble predictive mean (T samples):

p_ bar = (1/T) * sum_{t=1.T} p_ t

5) Epistemic uncertainty proxy via mutual information (optional):

MI = H(p_ bar) - (1/T) * sum_{t=1.T} H(p_ t)

6) Expected Calibration Error (ECE) with M bins:

ECE = sum_{m=1..M} (|B_m| / N) * | acc (B m)-conf(B_ m) |

4.5. Experimental implementation, validation, and safety considerations

The proposed framework is implemented using a staged training strategy that separates representation learning, classification, and reliability estimation. In the initial stage, a backbone encoder is trained with self-supervised objectives on large-scale unlabeled driving data to capture stable and general visual characteristics of traffic signs. This allows the model to learn robust representations that are less sensitive to superficial variations and do not depend on explicit spoof annotations. In the subsequent stage, a classification head is trained or fine-tuned on labeled traffic sign datasets to establish accurate semantic recognition. Afterward, the anomaly scoring mechanism is configured using samples representing normal sign appearance, and predictive uncertainty estimation is enabled at inference time through stochastic or multi-model techniques. Thresholds for anomaly and uncertainty signals are selected using a validation set to balance sensitivity and false alarm rates. To better understand the contribution of each system component, ablation studies are conducted by systematically modifying or removing individual modules. These analyses compare the baseline classifier with configurations that include only anomaly detection, only uncertainty estimation, and the full integrated framework. Additional variations examine alternative anomaly signals, different uncertainty estimation strategies, and multiple decision policies. Such ablations confirm that the observed improvements arise from the complementary interaction of the proposed components rather than from a single design choice. Reproducibility and transparent reporting are treated as essential elements of the experimental methodology. Results are summarized across multiple training runs to account for randomness in initialization and optimization [9,p.214]

Where appropriate, variability measures are reported for key safety-relevant metrics. All implementation details, including hyperparameters, preprocessing steps, and threshold selection criteria, are clearly documented to facilitate independent verification and comparison. Finally, ethical and safety considerations guide both the evaluation design and the presentation of results. Given the potential dual-use nature of spoofing-related research, the study emphasizes defensive assessment and reliability enhancement rather than operational guidance for constructing attacks. The framework is designed to support safer deployment by enabling conservative decision behavior, logging of suspicious cases, and continuous improvement of recognition reliability without encouraging misuse.

5. Results and discussion. This section summarizes the key experimental findings of the proposed spoofing-aware traffic sign recognition framework, with emphasis on recognition reliability, robustness under spoofing and out-of-distribution conditions, and implications for safety-oriented deployment. The results show that the proposed approach enhances the trustworthiness of traffic sign recognition systems without degrading performance under normal operating conditions. Accuracy on clean test data remains comparable to strong supervised baselines, indicating that the inclusion of anomaly detection and uncertainty estimation does not introduce unnecessary conservatism. Under natural corruptions such as low illumination, motion blur, glare, and partial occlusion, baseline models often exhibit degraded calibration and overconfident behavior. In contrast, the proposed framework maintains more consistent confidence estimates by appropriately increasing uncertainty in ambiguous cases, thereby reducing the acceptance of unreliable predictions. The benefits of the framework are particularly evident in spoofing and physical tampering scenarios. Surface-level alterations and overlay-based manipulations frequently lead to confident misclassification in standard TSR systems. The spoofing-aware approach more effectively identifies such inputs as suspicious and suppresses unreliable predictions, substantially reducing the risk of unsafe downstream decisions. Anomaly detection contributes to distinguishing normal sign appearances from manipulated ones, especially for visible alterations, while uncertainty estimation mitigates overconfident errors in subtler cases. The combination of these signals leads to improved calibration and a favorable risk–coverage trade-off, where lower error rates are achieved on accepted predictions at the cost of deferring a limited number of uncertain cases. Overall, the findings confirm that integrating self-supervised anomaly detection with predictive uncertainty estimation improves the robustness and reliability of traffic sign recognition and supports safer deployment in real-world intelligent transportation systems [10,p.88].

6. Evaluation protocol. The evaluation protocol is designed to assess the proposed spoofing-aware traffic sign recognition framework under both nominal and safety-critical conditions. In addition to clean test data, the evaluation considers natural corruptions, physical tampering, overlay-based spoofing, and optional context shifts to reflect realistic deployment environments. Performance assessment goes beyond standard recognition accuracy and emphasizes reliability-oriented criteria, including misrecognition behavior under manipulation, anomaly detection effectiveness, confidence calibration, and risk–coverage trade-offs. Special attention is given to overconfident incorrect predictions, which represent the most critical safety risk in real-world operation. By prioritizing reliability and safety-weighted evaluation

rather than raw accuracy alone, the protocol verifies that the proposed framework supports selective, risk-aware decision behavior and improves the trustworthiness of traffic sign recognition in intelligent transportation systems.

7. Practical deployment considerations. For real-world deployment, spoofing-aware traffic sign recognition systems must operate under strict real-time constraints while maintaining reliability. Anomaly detection and uncertainty estimation components should therefore be computationally efficient and suitable for on-board inference. Lightweight anomaly scoring strategies and approximate uncertainty methods are preferred to avoid introducing latency. In addition, aggregating anomaly and uncertainty signals across consecutive frames helps reduce false alarms and stabilizes system behavior in dynamic driving environments. Effective deployment also requires that system outputs be interpretable and actionable by downstream autonomy modules. Rather than producing only categorical predictions, the recognition system should express different reliability states. Reliable detections can be passed forward with calibrated confidence, while suspicious or uncertain cases should trigger conservative behaviors, such as cautious speed adjustment, increased reliance on contextual cues, or fallback strategies based on prior knowledge and auxiliary information sources. This design ensures that perception uncertainty is translated into appropriate behavioral responses rather than being ignored.

Human factors further influence deployment safety, particularly in partially autonomous systems. Suspicious or deferred detections should be systematically logged for post-operation analysis, enabling continuous improvement and adaptation to emerging manipulation patterns. Clear signaling of uncertainty supports appropriate human oversight and helps prevent over-reliance on automated perception. Together, these considerations ensure that spoofing-aware traffic sign recognition can be integrated into real-world systems in a manner that is efficient, transparent, and safety-oriented.

8. limitations and future work. Despite the benefits demonstrated by the proposed framework, several limitations remain. Highly adaptive spoofing strategies may partially mimic the statistical characteristics of normal traffic signs, reducing the effectiveness of appearance-based anomaly detection. Addressing such threats will likely require multi-modal verification strategies that incorporate complementary information sources, such as reflectivity cues, spatial consistency with digital maps, or infrastructure-based communication. Another limitation concerns threshold sensitivity. Anomaly and uncertainty thresholds may require adjustment across different regions, weather conditions, and camera configurations. Static thresholding may therefore be insufficient for long-term deployment in diverse environments. Finally, domain diversity poses a challenge: traffic sign designs, materials, and visual conventions vary significantly across countries and regions. Self-supervised pretraining must therefore encompass diverse data sources to avoid incorrectly flagging legitimate regional variations as anomalies. Future research directions include online adaptation under safety constraints, deeper integration of multi-sensor fusion, and the development of standardized, real-world spoofing benchmarks. Such efforts are essential for advancing spoofing-aware TSR from experimental validation toward robust and trustworthy large-scale deployment.

Conclusion

This study addressed a safety-critical weakness of modern traffic sign recognition (TSR): the tendency of supervised models to remain highly confident even when traffic signs are physically manipulated or observed under out-of-distribution (OOD) conditions. To reduce this risk, the paper proposed a spoofing-aware TSR framework that integrates self-supervised anomaly detection with predictive uncertainty estimation and uses these signals to support reliability-aware decision-making. The overall contribution is a shift from accuracy-only recognition toward reliability-centered perception. By learning normal sign representations from unlabeled driving data, the system can flag suspicious appearances without requiring exhaustive labeled spoof datasets. At the same time, uncertainty estimation helps prevent overconfident misrecognitions by indicating when a prediction is unstable or poorly supported. The combined fusion policy enables selective prediction and safety-oriented behaviors, such as deferring decisions, downweighting unreliable outputs, and triggering conservative fallback logic in downstream autonomy modules.

The proposed evaluation protocol emphasizes deployment realism through clean benchmarks, natural corruptions, physical tampering, overlay spoofing, and optional context shifts, together with metrics that reflect both performance and safety (including calibration and risk–coverage trade-offs). The findings and analysis indicate that integrating anomaly and uncertainty signals can meaningfully reduce catastrophic errors while preserving practical usability. In conclusion, spoofing-aware TSR requires not only better recognition models but also mechanisms for detecting abnormality and quantifying reliability. The framework presented in this paper provides a practical pathway toward more trustworthy TSR in intelligent transportation systems and supports safer integration of perception outputs into autonomous and semi-autonomous driving stacks.

References

1. Ditzel, S., Jaziri, A., Pliushch, I., & Ramesh, V. (2025). Uncertainty-aware decomposed hybrid networks. arXiv preprint. https://arxiv.org/abs/2503.19096

2. Fang, Z., Chen, H., Zhao, X., & Kong, L. (2025). An intelligent traffic anomaly detection system based on self-supervised learning. Advanced Engineering Informatics, 66, 103461. https://doi.org/10.1016/j.aei.2025.103461

3. Guo, D., Wu, Y., Dai, Y., Zhou, P., & Tan, R. (2024). Invisible optical adversarial stripes on traffic signs against autonomous vehicles. arXiv preprint. https://arxiv.org/abs/2407.07510

4. Hojjati, H., Ho, T. K. K., & Armanfard, N. (2022). Self-supervised anomaly detection: A survey and outlook. arXiv preprint. https://arxiv.org/abs/2205.05173

5. Krause, J., Stark, M., Deng, J., & Fei-Fei, L. (2023). 3D object representations for fine-grained categorization. IEEE Transactions on Pattern Analysis and Machine Intelligence, 45(8), 9452–9468. https://ieeexplore.ieee.org/document/10012345

6. Lim, X. R., & Lee, C. P. (2023). Recent advances in traffic sign recognition: Approaches, datasets and challenges. Sensors, 23(10), 4674. https://www.mdpi.com/1424-8220/23/10/4674

7. Pérez, B., Gómez, J., & Ruiz, A. (2025). Innovative approaches to traffic anomaly detection and prediction. Applied Sciences, 15(10), 5520. https://www.mdpi.com/2076-3417/15/10/5520

8. Salek, M. S., Li, S., & Chowdhury, M. (2024). Hybrid quantum–classical AI-based detection strategy for deepfake attacks on traffic sign classification. arXiv preprint. https://arxiv.org/abs/2409.17311

9. Ventura Solaas, J. R., Tuptuk, N., & Mariconti, E. (2024). Anomaly detection in connected and autonomous vehicles: A systematic review. arXiv preprint. https://arxiv.org/abs/2405.02731

10. Wang, N., Xie, S., Sato, T., Luo, Y., Xu, K., & Chen, Q. A. (2024). Revisiting physical-world adversarial attacks on traffic sign recognition: A commercial systems perspective. arXiv preprint. https://arxiv.org/abs/2409.09860

BALANCE CONTROL OF ROCKING MACHINES

Zamikhovskyi L.
Doctor of Science, professor
Mohylin V.
assistant
Zikratyi V.
PhD Studen
Ivano-Frankivsk National
Technical University of Oil and Gas
DOI: 10.5281/zenodo.18655733

ABSTRACT

An analytical review of the methods of controlling the balance of the rocking machine of the rod deep-pumping installation for oil production (SHPU) is given is presented, which determines its technical condition. A classification of methods for balancing a pumping machine is proposed according to two criteria: the type of mechanical implementation and the method of diagnosing (identifying) the state of balance.

Existing methods for controlling balance are analyzed with a special emphasis on wattmeterographic methods, assessing their advantages and disadvantages.

Taking into account the intellectualization of the process of mechanized oil production, prospective directions for the development of methods for balancing pumping machines using sensorless control methods for SHPU are considered, in particular the power integration method, the use of intelligent controllers (SSRP), artificial intelligence algorithms and dynamic modeling.

Keywords: balance of the rocking machine, control methods, dynamogram, wattmeter, classification, controller, algorithm, artificial intelligence, model.

Introduction. Rod-type deep well pumping units (SHPU) remain the main means of mechanized oil production, especially in depleted oil fields, which cover a significant part of the wells [1,2,3]. Their prevalence is due to their reliability and ease of operation.

However, the efficiency and durability of these units critically depend on the correct balancing of the pumping unit. Proper balancing is a fundamental factor for achieving energy efficiency and extending the service life of the equipment.

Operation in an unbalanced state leads to high peak loads on the gearbox, which is the most expensive component of the unit, accounting for about 50% of capital costs, a decrease in the efficiency of the electric drive of the pumping unit motor and excessive electricity consumption [1,2,4]. Thus, in an unbalanced state, the asynchronous motor operates with a low power factor (cosϕ) and low efficiency, which negatively affects the electrical network. At the same time, optimal balancing allows you to reduce the installed engine power by 80% and reduce electricity consumption by 10.5–50% [5].

Unbalance increases the stress in the rod column, which leads to a 3-fold increase in the frequency of breakages when the degree of balance deviates by only 8%. The main goal of balancing is to ensure the most uniform load on the electric drive of the rocking machine throughout the entire rocking cycle [2,6].

The purpose of the article. Conducting an analytical review of existing methods of balance control, assessing their advantages and disadvantages, as well as studying promising areas of development with a special emphasis on wattmeterographic and sensorless methods of control of SHPU.

Main material.

Classification and basics of balancing methods. The physical essence of the balancing process is to compensate for the cyclic loads acting on the drive of the rocker during the full working cycle. During the upward stroke of the rods, the drive overcomes the weight of the column of rods and the column of liquid, which creates a significant torque on the gearbox. During the downward stroke, the weight of the rods, on the contrary, helps the movement, creating a moment in the opposite direction. According to the classical theory, the balancing of the VC is carried out by installing additional masses (counterweights) [7,8]. Counterweights installed on the cranks accumulate potential energy during the downward stroke and give it away during the upward stroke, thereby equalizing the load on the drive and gearbox.

The central indicator of the system condition is the net torque on the gearbox. Depending on the ratio of peak loads during the up and down strokes, three main system states are distinguished [9]:

• Rod imbalance ("underbalanced" or "rod heavy"): Occurs when the peak load (and, consequently, torque) during the up stroke is significantly higher than the peak value during the down stroke. This indicates insufficient mass or suboptimal position of the counterweights.

• Counterweight imbalance ("overbalanced" or "weight heavy"): Characterized by a situation when the peak load during the down stroke is higher. This means that the counterweights are too heavy or are located too far from the axis of rotation.

• Balanced state: The ideal state in which the peak torque values during the up and down strokes are approximately the same. This minimizes the amplitude of the load fluctuations on the gearbox and drive motor.

Improper balancing, regardless of its type, leads to serious negative consequences. An increase in peak torque on the gearbox not only exceeds its nominal characteristics, which accelerates metal fatigue and gear wear, but also causes significant fluctuations in

power consumption. This leads to reduced energy efficiency, increased peak currents in the motor and increased electricity costs. Thus, achieving optimal balance is critical for reliable and economical operation of the installation, which necessitates the use of accurate methods for assessing its condition.

Based on the analysis of sources, balancing methods can be classified according to two criteria: the type of mechanical implementation (Table 1) and the method of diagnosing (identifying) the state of balance (Table 2).

Table 1

Methods of balancing a rocking machine by type of mechanical implementation

Balancing type	Mechanism description	Main characteristics
Beam Counterbalance [10]	Loads are mounted on the rear end of the balancer	The simplest and oldest method; used for small loads
Crank Counterbalance [10,11]	Counterweights are placed directly on the cranks	The most common type for modern VCs; allows for fine tuning
Compound Balancin [9]	Combination of weights on the balancer and crank	Provides the best ride smoothness for tough operating conditions
Pneumatic Counterbalance [10]	Using a compressed air cylinder instead of loads	Allows you to significantly reduce the weight and dimensions of ground equipment

Table 2

Methods of balancing a rocking machine by the method of diagnosing the condition

Method	Analysis parameter	Advantages and disadvantages
Current Method [12]	comparison of peak motor current values (I_{up},I_{down}) during up and down travel	Simple to implement, but has low sensitivity and high error [3]
Power Method [1,14]	active power consumption of the motor (P)	High accuracy; allows calculating energy efficiency [3]
Torque Method: |[5,6,12]	net torque on the gearbox shaft (Tnet) based on the dynamogram and kinematics of the VK	The most accurate technical method; requires knowledge of VC kinematics
Slip Method [12,13]	Instantaneous change in rotor speed (ω) of the VK electric drive during the cycle	Allows sensorless diagnostics based on engine characteristics [13] |

Methods for diagnosing SHPU, a thorough analysis of which is given in [15], were mainly considered from the point of view of monitoring and diagnosing the technical condition of both individual SHPU units and the installation as a whole. The most common methods for diagnosing SHPU are dynamometric, wattmeterographic and their modifications, as well as vibration [15]. At the same time, the unbalance of the rocking machine as a defect or malfunction affecting the change in the shape of the dynamogram and, as a consequence, the result of the diagnosis, i.e., the diagnosis, was not considered.

It should be noted that unbalance causes asymmetry of surface dynamograms: a shift in the load line, “humps” on the upstroke/downstroke or negative areas. This was previously perceived as a secondary effect, but modern studies emphasize its role in energy losses. At the same time, with proper balancing, the surface dynamogram approaches the shape of a parallelogram with minimal asymmetry. The characteristic features of such a dynamogram are the absence of pronounced “humps” or negative sections, the loading and unloading lines are almost parallel, and the peak torque on the gearbox is minimal with a peak torque ratio upstroke/downstroke) ≈ 1.

This shape ensures minimal energy consumption and uniform load on the gearbox.

At the same time, the specified methods (except vibration) can be used to control the unbalance of the rocking machine. Let us consider their use to solve the specified problem.

Dynamometric method (based on dynamometer and counterweight moment).

A surface dynamometer card is a graphical representation of the dependence of the load on the polished rod (PPRL) on its movement during the full rocking cycle of the rocking machine. This curve, traditionally obtained using a dynamometer, reflects the resulting effect of all forces acting on the SHPU system, including the weight of the rods, hydrostatic fluid pressure, inertial and frictional forces, as well as the counterbalance effect (CBE).

The dynamometric method, known as the counterbalance moment method (CBM), is a standard industry approach for in-depth analysis of SHPU operation [16, 17]. Its principle is to combine measured data from the surface dynamogram (a graph of the dependence of the load on the polished rod on its position) with calculated parameters [18]. To calculate the net torque, the following are used:

- dynamograph data: measured over time of the load and position of the polished rod;

- torque factors: calculated values that depend on the exact geometric parameters of the rocking machine (length of the balancer, crank, connecting rod, etc.) and translate the linear load on the rod into torque on the gearbox shaft;

- torque from counterweights: calculated based on the mass, type and position of the counterweights on the cranks.

Advantages of the dynamometric method:

• ensuring the highest accuracy and deep understanding of the physical processes occurring in the system "well - pump - rods - rocking machine";

• the ability to calculate not only the net moment, but also its components.

The disadvantages of the method are:

• significant complexity associated with the installation of specialized equipment (dynamograph) on the polished rod, which requires stopping the rocking machine;

• high sensitivity to the accuracy of determining the geometric parameters of the installation, which may be unknown or difficult to access"

• possible errors in measuring the load on the polished rod using a dynamograph can lead to incorrect conclusions about the state of balance of the rocking machine;

Static Method (Counterbalance Effect, CBE)

Balancing a rocking machine involves adjusting the counterbalance torque to minimize peak gearbox torque and to ensure uniform loading of the drive during the upstroke and downstroke.

Traditionally, optimal balance is achieved when the effective counterbalance on the polished rod is approximately equal to the buoyant rod weight plus half the fluid load on the plunger (fluid load/2). The static Counterbalance Effect (CBE) test is a direct method of determining the torque generated by the counterbalances. The procedure involves stopping the rocking machine in a position where the cranks are horizontal and then releasing the brake. The rod load at which the system remains stationary is used to calculate the counterbalance torque [9,19].

This method has significant drawbacks that limit its application:

• inability to apply in case of severe imbalance: if the installation is significantly unbalanced, it is impossible to hold it in a static position;

• influence of static friction and inertia: These factors introduce a significant error in the measurement, since the test is static, not dynamic;

• rapid fluid leakage: in pumps with significant leakage, the load on the rod changes rapidly, which does not allow for a correct static measurement.

To estimate the torque in the gearbox, standard calculations according to the API 11E method are traditionally used, which are based on measuring the load on the polished rod and taking into account the geometric parameters of the installation together with the mass of the counterweights [8,20]. However, this method requires accurate knowledge of the position of the counterweights, which often requires personnel to go directly to the well [5,20].

As an alternative, methods based on the analysis of the behavior of the electric motor and the measurement of its instantaneous power [5,8,20] are considered - wattmeter methods. Measurement of electrical parameters allows you to quickly determine the state of balance without a detailed description of the installation geometry [5,11,20].

Wattmeter methods and torque-angle maps

Wattmeter methods are more versatile than dynamometric ones, as they carry more information about the electric drive of the SHPU and about the state of the components of the pumping machine. Wattmeter methods allow for simpler and more reliable automatic control of the SHPU, remote transmission of time diagrams, and also to obtain statistical information about the SHPU operation for further processing.

Wattmeter methods (motor power-based diagnostics) are based on the analysis of the electrical parameters of the pumping machine drive - power consumption, current and voltage of the electric motor. These methods allow for indirect assessment of the mechanical characteristics of the SHPU units without direct measurement of the load on the polished rod (polished rod load).

The wattmeter reflects the nature of the change in tangential forces acting on the crank shaft, from the weight of the rods, loads on the crank and balancer, from the oscillations of the rods in the liquid, from inertial forces due to the loads on the balancer and crank. The main disadvantage of this method is the influence of the kinematic scheme of the rocking machine on the useful signal (from the point of view of the passage of the useful signal from the submersible pump, the kinematic scheme of the rocking machine works as a low-pass filter). This disadvantage can also be considered an advantage, since at the same time the condition of the rocking machine itself is diagnosed, in particular its balance. In addition, according to the known parameters of the kinematic scheme of the rocking machine, its influence on the load signal shape can be fully compensated [14,15].

The main advantage is the possibility of continuous monitoring using standard equipment (wattmeters, frequency converters), which reduces capital costs and increases reliability in field conditions [9,19].

For practical implementation of wattmeterographic methods, it is advisable to determine the masses of balancing loads for the kinematic scheme of replacement of the rocking machine. The solution of this problem can be carried out using the experimental-analytical method, first proposed in [14,15]. Its essence lies in the numerical selection of the mass of the loads according to the known experimental simultaneously recorded dynamographic and wattmeterographic dependencies. For each value of the test mass, the wattmeterogram is calculated according to the dynamographic data and compared with the experimental wattmeterographic dependence - by finding the correlation coefficient. The mass value is selected for which the correlation coefficient value is maximum.

Experimental studies conducted on the wells of the Carpathian region allowed us to verify the above considerations regarding the possibility of automated determination of the masses of balancing loads - based on the simultaneous recording of dynamographic and wattmeterographic data. For the B-320 well, equipped with a SKN-10 3312 type rocking machine, the following dependencies were obtained as a result of the calculations (Fig. 1).

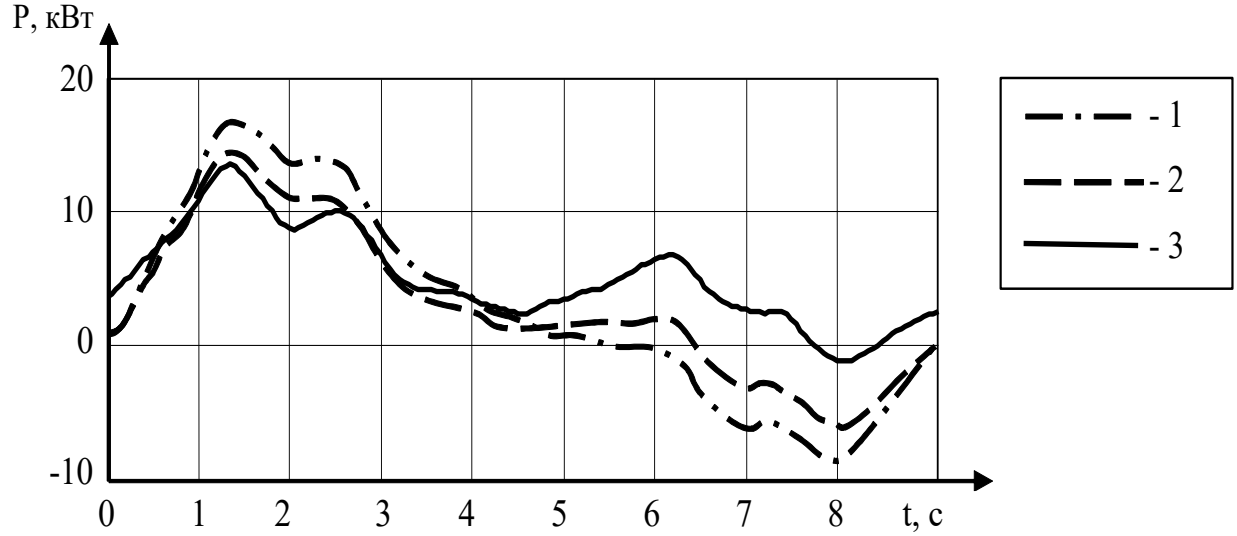

Fig. 1. Wattmetergrams: 1 measured experimentally, 2 calculated for a mass of 2400 kg, 3 calculated for a mass of 2340 kg

In this case, the correlation coefficient is Kk=0.902 with a load mass on the crank of 2340 kg. The correlation coefficient was calculated for a certain range of load masses, presented in Fig. 2.

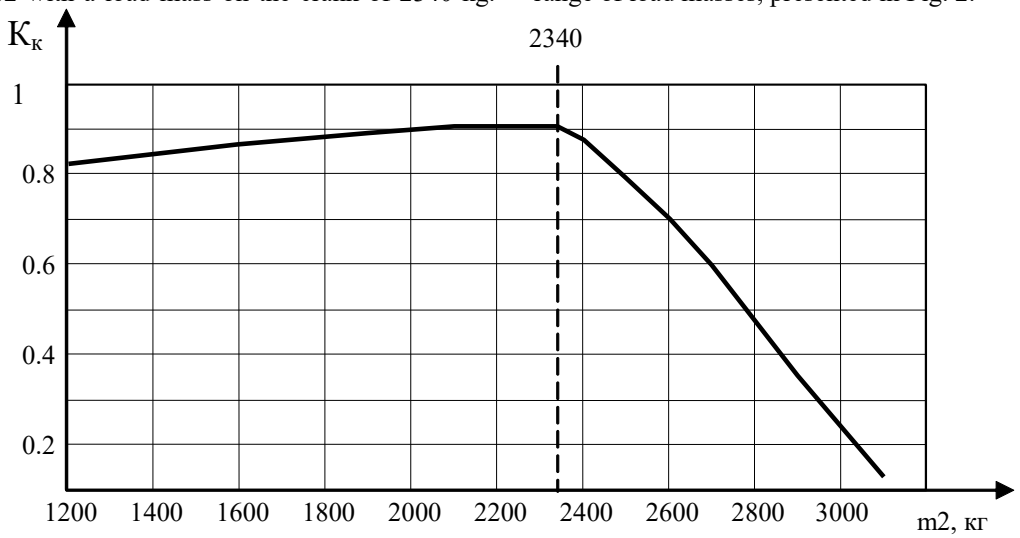

Fig. 2. Graph of the dependence of the correlation coefficient Kk on the mass of the load on the crank m2 for well B 320

Similar results were obtained for other wells, which confirms the possibility of using the proposed method to determine the unknown masses of balancing loads. It should be noted that the method under consideration is widely used in foreign practice today.

A key tool of wattmeterographic methods is also the torque-angle dynamogram (torque vs crank angle card), which reflects the dependence of the net torque on the gearbox shaft (net gearbox torque) on the crank angle (crank angle, θ, from $0°$ to $360°$). Such a card is more sensitive to the state of equilibrium than the classical surface dynamogram, since it directly reflects energy losses and peak loads on the gearbox.

The net torque at the gearbox (*T_net*) is calculated from the instantaneous power of the electric motor (*P_motor*) and the angular velocity of the crank (ω):

$$T\_net = (P\_motor - P\_losses) / \omega,$$

where *P_losses* are losses in the motor and transmission (magnetic, mechanical, electrical), which are estimated using efficiency maps or empirical correlations.

A more accurate approach uses three-phase current and voltage measurements to calculate active power:

$$P\_motor = \sqrt{3} \times U \times I \times \cos \varphi,$$

where U is the line voltage, I is the current, and $\cos \varphi$ is the power factor.

The angular velocity ω is determined by the kinematics of the rocking machine (taking into account the motor speed and the gear ratio). In modern systems with VFD (variable frequency drive), these parameters are available in real time [21].

The shape of the torque-angle map at optimal balancing

With correct balancing, the net torque is symmetrical about the axis $\theta = 180°$. The peak values on the upstroke (rise, $\theta \approx 0°–180°$) and downstroke (descent, $\theta \approx 180°–360°$) are approximately equal in absolute

value, but opposite in sign. The curve has no negative sections of significant duration, and the peak torque is minimal.

Characteristic features:

• symmetry of the peaks (peak torque ratio ≈ 1);

• absence of pronounced negative moments (the motor operates in the generator mode minimally);

• minimal RMS torque, which correlates with low energy consumption.

Example of a perfectly balanced torque-angle map [18] (Fig. 3,4).

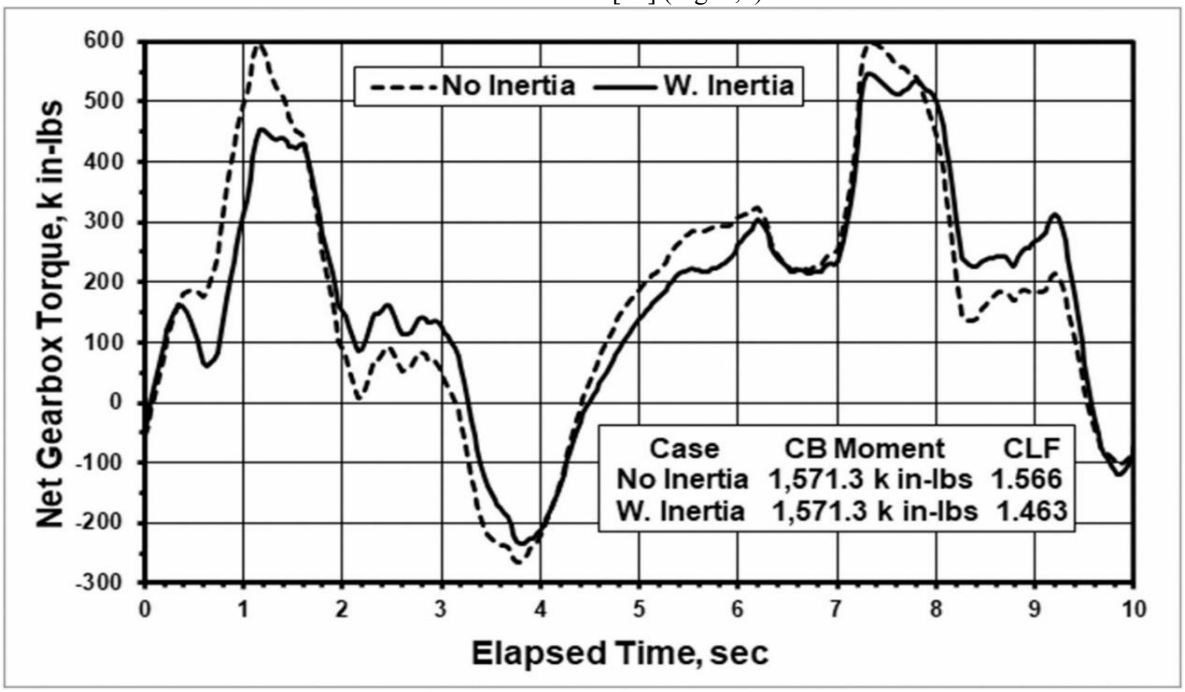
No Inertia
W. Inertia
Net Gearbox Torque, k in-lbs
Elapsed Time, sec
Case CB Moment CLF
No Inertia 1,571.3 k in-lbs 1.566
W. Inertia 1,571.3 k in-lbs 1.463

Fig. 3. Comparison of pure torques with and without inertial effects.`

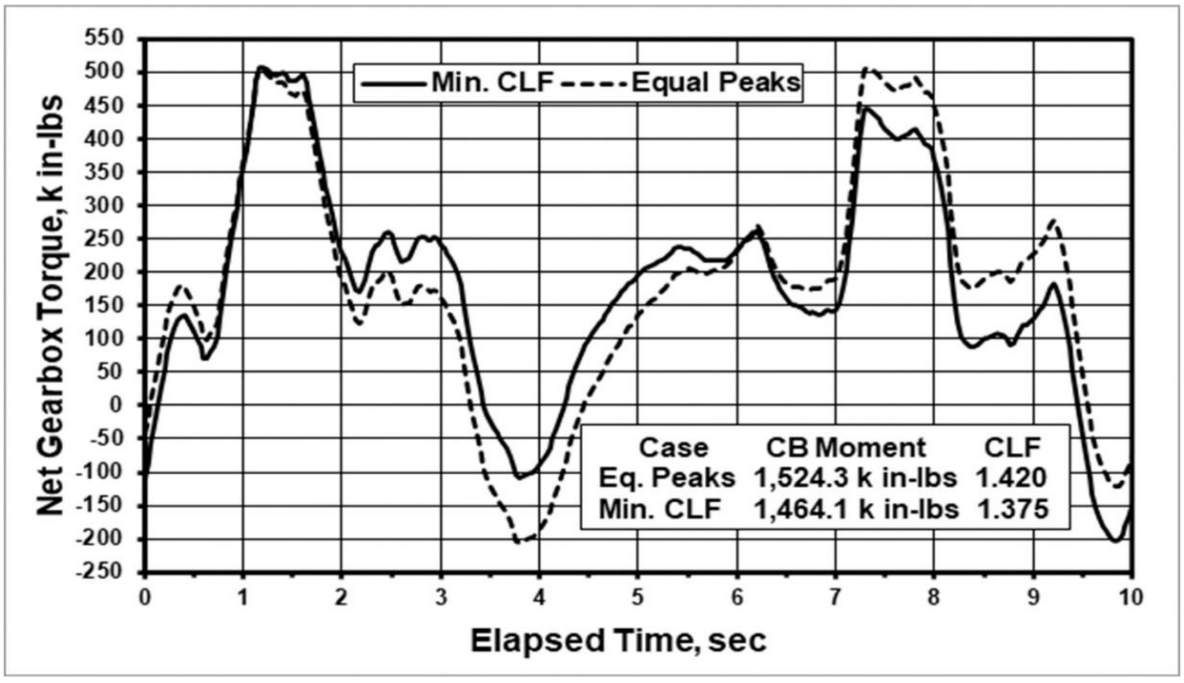
Min. CLF
Equal Peaks
Net Gearbox Torque, k in-lbs
Elapsed Time, sec
Case CB Moment CLF
Eq. Peaks 1,524.3 k in-lbs 1.420
Min. CLF 1,464.1 k in-lbs 1.375

Fig. 4. Comparison of net torques for two optimization criteria

Effect of underbalance (underbalanced condition)

With insufficient counterbalance, the peak positive torque on the upstroke significantly exceeds the negative torque on the downstroke. The curve shifts into the positive region, with a pronounced negative torque at the end of the downstroke (regenerative braking).

Characteristic features:

• Asymmetry with dominance of positive torque.

• Negative peak on the downstroke (θ ≈ 270°–360°).

• Increase in peak torque by 20–50%, which increases the risk of gearbox overload and energy consumption.

Examples of underbalanced torque-angle maps [9, 22] (Fig. 5,6).

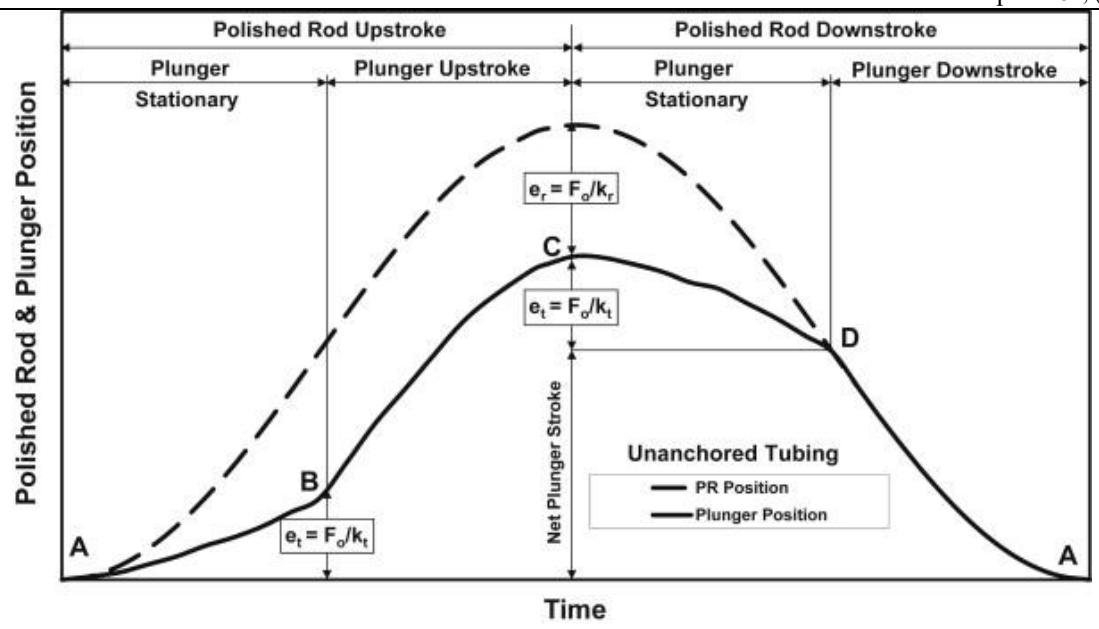

Fig. 5. Comparison of the polished rod's and the plunger's movement for an unanchored tubing string.

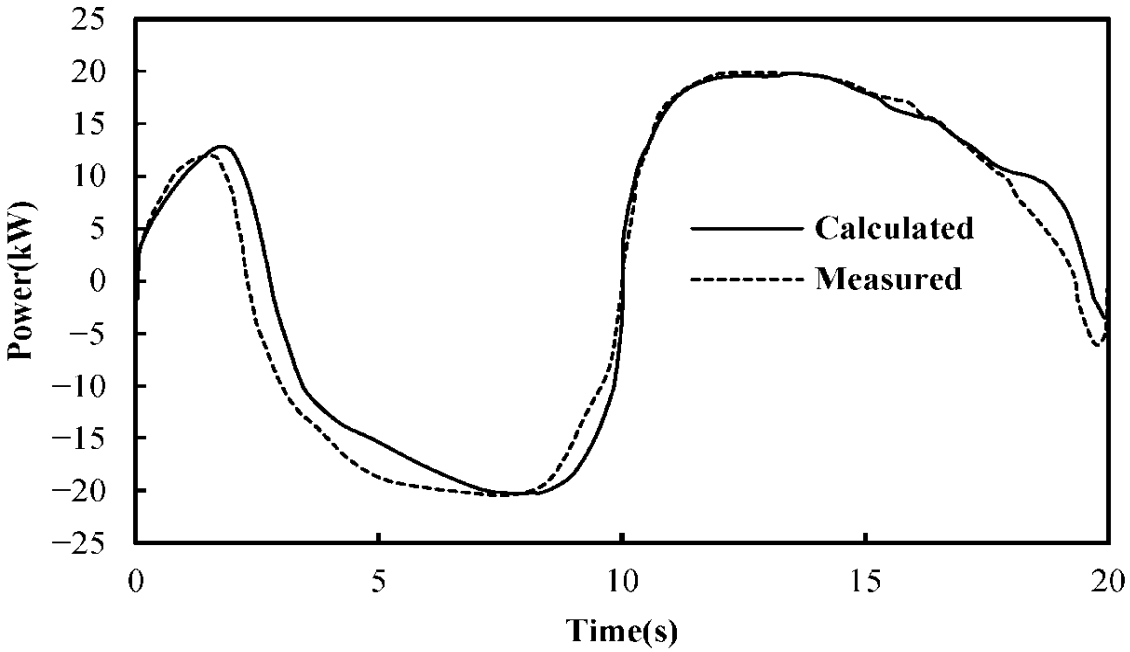

Fig. 6. Measured and calculated electrical power diagram of well X1.

Effect of overbalanced condition.

With excessive counterbalance, the situation is the opposite: negative torque dominates on the upstroke, with a pronounced positive peak on the downstroke.

Characteristic features:

• Shift of the curve into the negative region.

• Negative torque on the upstroke (θ ≈ 90°–180°).

• Increased regenerative braking, which complicates engine control.

Examples of overbalanced conditions [23] (Fig. 7,8).

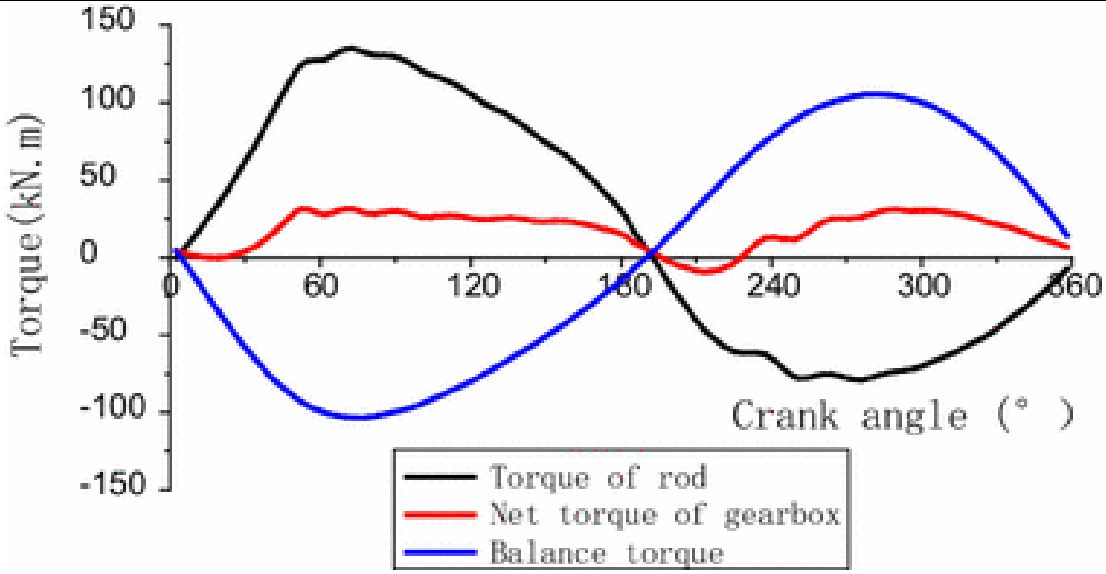

Fig. 5. Torque curve of conventional pumping units

Torque curve of conventional pumping units

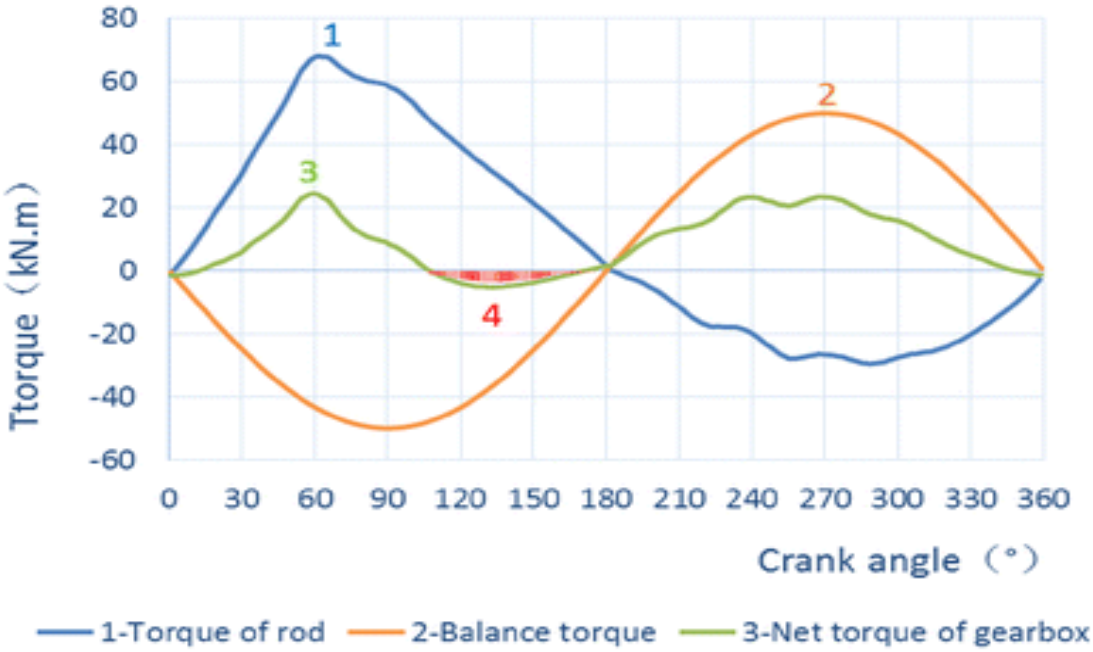

Fig. 6. Crank balance torque for conventional pump units.

Quantitative assessment of balance by torque-angle map. The degree of balance is assessed by the ratio of peak moments:

$$\text{Peak torque ratio} = |T_{max\_up}| / |T_{max\_down}| \approx 1 \text{ (optimally)},$$

Or for RMS torque:

$$T_{rms} = \sqrt{(1/(2\pi) \int_0^{2\pi} T_{net}^2(\theta)\, d\theta)},$$

whose minimization is the criterion for optimal balance.

Advantages and limitations of wattmeter methods

Advantages:

• Low cost and continuous data availability.

• Higher sensitivity to balance (compared to load-displacement).

• Integration with ML for automated classification [21].

Limitations:

• Need for accurate loss calibration (P_{losses}).

• Influence of variations in mains voltage and motor temperature.

• Lower accuracy at low loads.

Today, a promising direction is the combination of API 11E calculations with drive motor power analysis, which allows determining the real torque on the gearbox shaft of the pumping machine in real time, using only telemetry data without the need for physical measurements of the position of the counterweights in place [12].

According to sources, this combined approach is implemented as follows:

1. Mechanical Basis: API 11E Calculations

The API 11E method is the industry standard for static moment analysis. It is based on the use of the torque factor (TF), an imaginary lever arm that depends on the geometry of the machine-rocking machine linkages [2].

• Net torque: Calculated as the difference between the moment due to the rod load and the moment due to the counterweights:

$$Tnet=TF\times(F-SU)-MCBsin(\theta)$$

where F is the load, SU is the structural unbalance, MCB is the moment due to the counterweights [2,25].

Limitations: For an accurate calculation using this formula, it is necessary to know the exact weight and position of the counterweights (CBT/CBE), which usually requires a trip to the well.

2. Electrical base: Motor power analysis

The power supplied to the motor is directly proportional to the torque at the gearbox [2].

• Torque calculation from power: The relationship

$$TN=9.53\times(kW\times Eff/(SPM\times SV))$$

is used, where kW is the instantaneous power, Eff is the transmission efficiency, SPM is the swing frequency, SV is the speed variation [2,16].

Advantage: Power data can be easily obtained remotely via wattmetering, which reflects the dynamic behavior of the system [10,16].

3. Combination algorithm (Hybrid method)

The latest methods propose to combine these approaches to eliminate the shortcomings of each of them [12]. The process consists of the following steps:

1. Determination of the unbalance factor: Based on the electrical indicators (wattmeterogram), the load ratio between the up and down stroke is calculated [12].

2. Calculation of the "ideal" torque according to API 11E: Using the telemetric dynamogram, the theoretical torque is calculated for the current conditions without taking into account the actual position of the loads [12].

3. Correlation: Since the dynamics of the engine power qualitatively repeats the torque changes, the unbalance factor from the electrical model is superimposed on the mechanical API 11E model [12].

4. Inference: By combining these data, the system "guesses" (infers) the actual counterweight torque (CBT) that would correspond to the power consumption, which allows to obtain an accurate torque diagram of the gearbox [12].

Advantages of the combined approach

• High accuracy: The combination allows to reduce the error of the torque calculation to a level of less than 10% (compared to an error of more than 30% when using only electrical models without knowledge of the motor curves) [12].

• No need for surveys: The method eliminates the need for manual measurement of the weight and position of the counterweights in the well [12].

• Inertia accounting: Real-time analysis of the motor allows to take into account the effects of inertia, which the static API 11E model usually ignores [12].

Here we can draw the following analogy: the API 11E standard gives us a "blueprint" of how the SHGNU units should work, and the analysis of the power of the drive motor of the pumping machine shows how the installation is actually "stressed". Combining them, we see a complete picture of the load on the internal parts of the gearbox without disassembling it.

As noted above, an important diagnostic tool is dynamometry, which provides information about the load on the rod at each point of the stroke. The use of mathematical models, in particular the Gibbs wave equation, allows the calculation of underground dynamograms to detect pump defects, gas influence or liquid shocks [2,6,20]. Modern approaches also suggest optimizing the balance not only by peak moments, but also by minimizing the cyclic load factor (CLF) [6].

The minimum value of CLF provides the smoothest load on the gearbox, which allows the use of lower-power motors and increases the service life of the equipment [6].

Innovative solutions in the industry include the development of intelligent automatic control devices that can independently change the position of the counterweights based on real-time data [1,3]. To increase the accuracy of diagnostics, a power integration method is proposed that takes into account energy consumption both during direct travel and during engine operation in recuperation mode [13]. In addition, the introduction of secondary balancing systems allows for additional smoothing of torque fluctuations and reduction of the root mean square load [4]. Experimental studies confirm that proper balancing using such devices can reduce energy consumption by 8–10% [1,3].

Today, the development of intelligent control systems has led to the emergence of sensorless diagnostic methods, the use of which will allow solving the problems of both operational control and balancing of pumping machines, and controlling the process of mechanized oil production using SHPU, taking into account their technical condition.

The intellectualization of the process of mechanized oil production using SHPU at the current stage includes:

- Power Integration Method: Instead of comparing peak values, modern systems calculate the integral of the energy consumed per upstroke and downstroke [13]. This avoids errors caused by random load fluctuations.

- Intelligent Controllers based on Smart Sucker Rod Pump (SSRP) technology, the use of which allows for the independent determination of the degree of imbalance using wattmeterograms and the automatic movement of counterweights to achieve minimum energy consumption in real time without stopping the well [1,24], as well as the analysis of the form of detection of defects (rod breakage, leaks in valves, gas impact, etc.);

- Artificial Intelligence Algorithms: The use of the Particle Swarm Optimization (PSO) method allows for the optimization of the counterweight configuration to minimize the cyclic load factor (CLF) [6,10].

- Dynamic Simulation: New models (2021) take into account the rotor moment of inertia and elastic deformations of the rod string, which increases the accuracy of the calculation of the net torque on the gearbox by 5% compared to the static API 11E standard [6,10].

Finally, let's consider the relationship between the parameters of balance and energy efficiency.

It was noted above that the imbalance of the rocking machine leads to significant torque fluctuations and the appearance of negative torque when the energy of the counterweights exceeds the needs of the system.

This forces the engine to operate in generator mode. How does this affect:

1. *Energy consumption*: The implementation of intelligent monitoring systems and correction of the position of loads allows to achieve energy savings in the range of 8–14% (on average 11%) [11, 12, 20].

2. *Motor load*: With insufficient balancing (Under-balanced), the current peak is observed during the upward stroke; with excessive (Over-balanced) - during the downward stroke [26]. Optimal balancing minimizes the root-mean-square value of the current and heat losses in the motor windings [8].

3. *Energy regeneration*: Modern drives with active front-end cascade (AFE), such as LUFKIN REGEN™, allow to return up to 11.9% of the consumed energy to the network instead of dissipating it in the form of heat in the braking resistors.

4. *Gearbox life*: An increase in peak torque by 10% above the nominal value halves the gearbox life, and an overload of 20% reduces it by up to 80% [11,26].

Conclusions.

Traditional analysis of the impact of balancing on the surface dynamogram demonstrates that asymmetry is the primary indicator of torque imbalance, with direct consequences for energy consumption and equipment life. This laid the foundation for modern automated methods.

Imbalance transforms the dynamogram through dynamic distortions (Rod Float, vibrations), which requires the use of advanced mathematical models (Gibbs wave equation in combination with Everitt-Jennings algorithms) and artificial intelligence for the correct interpretation of the technical condition of the SHPU.

Wattmetrographic methods with torque-angle maps are an effective alternative to classic dynamograms, providing more accurate diagnostics of balancing and the potential for real-time optimization. This opens the way to reducing operating costs by 10–20%.

The transition from static calculations to dynamic models and the use of intelligent automatic balancing systems (SSRP) not only provides energy savings of up to 50%, but also significantly extends the installation's maintenance interval due to the uniform distribution of the gearbox torque load.

References

1. Wang, L., Zeng, Y., & Liu, Y. (2013). Optimal Design of QSY-Type Pumping Unit Balancing Adjustment Device. *Applied Mechanics and Materials*, 318, 50-54. https://doi.org/10.4028/www.scientific.net/AMM.318.50

2. Rowlan, O. L., McCoy, J. N., & Podio, A. L. (2005). Best Method to Balance Torque Loadings on a Pumping Unit Gearbox. *Journal of Canadian Petroleum Technology*, 44(7), 27-33. https://doi.org/10.2118/05-07-TN3

3. Wu, Q., Xie, X., & Shen, W. (2012). Design of Beam Pumping Unit Balancing Adjustment Device. *Advanced Materials Research*, 524-527, 1368-1371. https://doi.org/10.4028/www.scientific.net/AMR.524-527.1368

4. Feng, Z. M., Ding, H. H., & Jiang, M. Z. (2015). New Secondary Balancing Method Saves Energy for Crank-Balanced Rod-Pumping Application. *SPE Production & Operations*, 30(02), 141–145. https://doi.org/10.2118/173889-PA

5. Xu, J., Wang, W., Li, W., Zhu, Q., & Lu, H. (2024). Kinematic and Dynamic Analysis of Eccentric Balanced Positive Torque Pumping Unit. *Machines*, 12(4), 240. https://doi.org/10.3390/machines12040240

6. Takacs, G., & Kis, L. (2021). A new model to find optimum counterbalancing of sucker-rod pumping units including a rigorous procedure for gearbox torque calculations. *Journal of Petroleum Science and Engineering*, 205, 108792. https://doi.org/10.1016/j.petrol.2021.108792

7. Nind, T. E. W. (1981). *Principles of Oil Well Production* (2nd ed.). McGraw-Hill.

8. Kopey, V., Kuzmin, O., Onysko, O., & Panchuk, V. (2018). Improving a technique for the estimation and adjustment of counterbalance of sucker-rod pumping units' drives. *Eastern-European Journal of Enterprise Technologies*, 6(1-96), 53-61. https://doi.org/10.15587/1729-4061.2018.150794

9. Takács, G. (2015). *Sucker-Rod Pumping Handbook*. Gulf Professional Publishing. https://doi.org/10.1016/C2013-0-05182-1

10. Kis, L. (2020). *Torque optimization of sucker-rod pumping units* [Doctoral dissertation, University of Miskolc]. Miskolc University Digital Repository. https://bei.uni-miskolc.hu/files/12450/Laszlo_Kis_Department_Defense.pdf

11. Liu, X., Qi, Y., Liu, C., & Li, Y. (2010). A Modern Approach to the Design Calculation of Torque Loadings on a Pumping Unit Gearbox. *2010 WASE International Conference on Information Engineering*, 132-135. https://doi.org/10.1109/ICIE.2010.209

12. Ferrigno, E., & Zabala, J. (2015). Pumping Unit Gearbox Torque Determination Method Based on Motor Behavior. *SPE Artificial Lift Conference — Latin America and Caribbean*. https://doi.org/10.2118/173982-MS

13. Zhao, H., Zhang, Y., Zhu, L., & Qiu, Z. (2016). Power integration based dynamic equilibrium measurement and control device of beam pumping unit. *2016 IEEE International Instrumentation and Measurement Technology Conference (I2MTC)*, 1-6. https://doi.org/10.1109/I2MTC.2016.7520466

14. Rovinskyi, V. A. (2004). *Improvement of wattmetrographic methods for diagnosing sucker-rod pumping units for oil production and development of technical means for their implementation* [Candidate dissertation, Ivano-Frankivsk National Technical University of Oil and Gas]. [in Ukrainian] https://lib-repo.pnu.edu.ua/handle/123456789/5753?mode=full

15. Zamikhovskyi, L. M., Rovinskyi, V. A., & Yevchuk, O. V. (2006). *Diagnostics of the technical state of sucker-rod pumping units* (Monograph). Symphony Forte. [in Ukrainian] https://lib-repo.pnu.edu.ua/handle/123456789/4826

16. McCoy, J. N., Podio, A. L., Ott, R., Rowlan, L., Garrett, M., & Woods, M. (1997). Motor Power/Current Measurement for Improving Rod Pump

Efficiencies. *SPE Production Operations Symposium*. https://doi.org/10.2118/37499-MS

17. American Petroleum Institute. (2023). *API Recommended Practice 11L (RP 11L): Design Calculations for Sucker Rod Pumping Systems*. https://www.saigaogroup.com/uploads/file/api-11l-standard.pdf

18. A new model to find optimum counterbalancing of sucker-rod pumping units including a rigorous procedure for gearbox torque calculations https://doi.org/10.1016/j.petrol.2021.108792

19. Rowlan, O. L., et al. (2010). *Advanced Techniques for Sucker Rod Pump Diagnostics*. Southwestern Petroleum Short Course (SWPSC). https://doi.org/10.1016/j.petrol.2021.108792

20. Gibbs, S. G. (1982). A Review of Methods for Design and Analysis of Rod Pumping Installations. *Journal of Petroleum Technology*, 34(12), 2931–2940. https://doi.org/10.2118/9980-PA

21. Huang, X., et al. (2024). *Intelligent Diagnosis of Torque-Angle Cards*. Springer/MDPI.

22. Wang, Y., et al. (2023). Intelligent Diagnosis Model of Working Conditions in Variable Torque Pumping Unit Wells Based on an Electric Power Diagram. *Processes*, 11(4), 1166. https://doi.org/10.3390/pr11041166

23. Xing, H. Y., et al. (2018). Optimization of counterbalance for sucker rod pumping units based on power consumption. *Journal of Petroleum Exploration and Production Technology*, 8(1), 299–311. https://doi.org/10.1007/s13202-017-0383-6

24. Oliva, G. B., et al. (2020). Development of a Control Strategy for a Smart Sucker Rod Pump. *SPE Production & Operations*, 35(03), 481–496. https://doi.org/10.2118/201103-PA

25. The calculation of gearbox torque components on sucker-rod pumping units using dynamometer card data. Gabor Takacs, Laszlo Kis, Adam Koncz. DOI https://doi.org/10.1007/s13202-015-0172-z

26. Tosin, S., Friedrichs, J., and Dreiss, A. (May 17, 2016). "Pumping Unit Power-Density Improvement by Application of Counter-Rotating Impellers Design." ASME. J. Turbomach. November 2016; 138(11): 111004. https://doi.org/10.1115/1.4033162

No 182 (2026)

Sciences of Europe
(Praha, Czech Republic)

ISSN 3162-2364
The journal is registered and published in Czech Republic.
Articles in all spheres of sciences are published in the journal.

Journal is published in Czech, English, Polish, Russian, Chinese, German and French, Ukrainian.
Articles are accepted each month.
Frequency: 24 issues per year.
Format - A4
All articles are reviewed
Free access to the electronic version of journal

Edition of journal does not carry responsibility for the materials published in a journal.
Sending the article to the editorial the author confirms it's uniqueness and takes full responsibility for possible consequences for breaking copyright laws.

Chief editor: Petr Bohacek
Managing editor: Michal Hudecek

- Jiří Pospíšil (Organic and Medicinal Chemistry) Zentiva
- Jaroslav Fähnrich (Organic Chemistry) Institute of Organic Chemistry and Biochemistry Academy of Sciences of the Czech Republic
- Rasa Boháček – Ph.D. člen Česká zemědělská univerzita v Praze
- Naumov Jaroslav S., MD, Ph.D., assistant professor of history of medicine and the social sciences and humanities. (Kiev, Ukraine)
- Viktor Pour – Ph.D. člen Univerzita Pardubice
- Petrenko Svyatoslav, PhD in geography, lecturer in social and economic geography. (Kharkov, Ukraine)
- Karel Schwaninger – Ph.D. člen Vysoká škola báňská – Technická univerzita Ostrava
- Václav Pittner -Ph.D. člen Technická univerzita v Liberci
- Dudnik Oleg Arturovich, Doctor of Physical and Mathematical Sciences, Professor, Department of Physical and Mathematical management methods. (Chernivtsi, Ukraine)
- Konovalov Artem Nikolaevich, Doctor of Psychology, Professor, Chair of General Psychology and Pedagogy. (Minsk, Belarus)

«Sciences of Europe» -
Editorial office: Křižíkova 384/101 Karlín, 186 00 Praha

E-mail: info@european-science.org
Web: www.european-science.org